Development and Application of Analytical Techniques for Evaluating Function in Pancreatic Islets of Langerhans

by

Cynthia Marie Cipolla

A dissertation submitted in partial fulfillment
of the requirements for the degree of
Doctor of Philosophy
(Chemistry)
in the University of Michigan
2015

Doctoral Committee:

Professor Robert T. Kennedy, Chair
Professor Raoul Kopelman
Professor Mark E. Meyerhoff
Professor Leslie S. Satin

DEDICATION

To my family and friends for their love and support.

ACKNOWLEDGEMENTS

I would first and foremost like to thank my advisor, Dr. Robert Kennedy, for his support and guidance throughout my graduate career and for his contributions to this research. I would also like to thank my committee members, Dr. Raoul Kopelman, Dr. Mark Meyerhoff, and Dr. Leslie Satin for their feedback and suggestions for my project and for taking the time to serve on my committee.

I am grateful for the camaraderie and mentorship of all former and present Kennedy lab members, especially Dr. Ting Zhang for training me in islet isolation and microfabrication, Mahmoud El Azzouny for sharing his metabolomics expertise, Shusheng Lu for his assistance in insulin secretion measurements and for helpful discussions about islets, Erik Guetschow for his droplet microfluidics expertise and advice, and Thitaphat (Non) Ngernsutivorakul for taking over the fiber optic detector project and helping to push it to completion. I would also like to thank my collaborators at the University of Illinois at Chicago, Dr. David Eddington, Dr. José Oberholzer, and Elizabeth Ferraz-Samar for their work on the droplet microfluidic project, and Dr. Francis Esmonde-White for his work and guidance on the fiber optic detector project.

Finally, I would like to thank my family and friends for their support and encouragement throughout this endeavor.

TABLE OF CONTENTS

LIST OF FIGURES

LIST OF APPENDICES

LIST OF ABBREVIATIONS

General

Ab	antibody
ANOVA	analysis of variance
B/F	bound-to-free ratio
BCA	bicinchoninic acid
BSA	bovine serum albumin
BSS	balanced salt solution
CE	capillary electrophoresis
CE-IA	capillary electrophoresis- immunoassay
CMOS	complementary metal oxide semiconductor
DHEA	*trans*-dehydroepiandrosterone
DNA	deoxyribonucleic acid
EDTA	ethylenediaminetetraacetic acid
ELISA	enzyme-linked immunosorbent assay
EOF	electroosmotic flow
ESI	electrospray ionization
FDA	fluorescein diacetate
FITC	fluorescein isothiocyanate
FT-ICR	Fourier transform- ion cyclotron
GC-MS	gas chromatography-mass spectrometry
GLUT-2	glucose transporter- type 2
GPX1	glutathione peroxidase 1
GSIS	glucose-stimulated insulin secretion
HEPES	4-(2-hydroxyethyl)-1-piperazineethanesulfonic acid
HILIC	hydrophilic interaction chromatography
HPFA	high-purity perfluoroalkoxy
KRB	krebs ringer buffer
LC-MS	liquid chromatography-mass spectrometry
LIF	laser-induced fluorescence
LOD	limit of detection
MALDI	matrix-assisted laser desorption ionization
MCE	microchip electrophoresis
MS	mass spectrometry
NMB	nude mouse bioassay
NMR	nuclear magnetic resonance
OCR	oxygen consumption rate
PDMS	polydimethyl siloxane

PFD	perfluorodecalin
PFO	perfluorooctanoic acid
PI	propidium iodide
PMA	phorbol-12-myristate-13-acetate
PMT	photomultiplier tube
PPP	pentose phosphate pathway
RIA	radioimmunoassay
RIPA	radio-immunoprecipitation assay
ROS	reactive oxygen species
RPLC	reverse phase liquid chromatography
RPMI	Roswell Memorial Park Institute
RI	refractive index
RSD	relative standard deviation
RSE	relative standard error
SOD1	superoxide dismutase 1
SRM	selective reaction monitoring
TCA	tricarboxylic acid
TOF	time-of-flight
UHPLC	ultra high pressure liquid chromatography
UV	ultraviolet
QQQ	triple quadrupole

Metabolite/Enzyme

2PG	2-phosphoglycerate
3PG	3-phosphoglycerate
6PG	6-phosphogluconic acid
aCoA	acetyl coenzyme A
ADP	adenosine diphosphate
AKG	alpha-ketogluterate
AMP	adenosine monophosphate
AMPK	adenosine monophosphate-activated protein kinase
Asp	aspartate
ATP	adenosine triphosphate
CDP-choline	citicoline
CDP-EA	cytidine diphosphate ethanolamine
CIT	citrate
CPT-1	carnitine palmitoyltransferase I
DAG	diacylglycerol
F6P	fructose-6-phosphate
FAD	flavin adenine dinucleotide
FBP	fructose 1,6-bisphosphate
FFA	free fatty acid
G3P	glycerol-3-phosphate
G6P	glucose-6-phosphate
GAPDH	glyceraldehyde 3-phosphate dehydrogenase
GDP	guanosine diphosphate

GL	glycerolipid
Glu	glutamate
GMP	guanosine monophosphate
GSH	glutathione, reduced
GSSG	glutathione, oxidized
GTP	guanosine triphosphate
HMG-CoA	3-hydroxy-3-methylglutaryl-coenzyme A
ICIT	isocitrate
IMP	inosine monophosphate
LC-CoA	long chain acyl coenzyme A
LPA	lysophosphatidic acid
MAL	malate
mCoA	malonyl coenzyme-A
ME	malic enzyme
MG	monoacylglycerol
NAD^+	nicotinamide adenine dinucleotide
NADH	nicotinamide adenine dinucleotide, reduced
$NADP^+$	nicotinamide adenine dinucleotide phosphate
NADPH	nicotinamide adenine dinucleotide phosphate, reduced
PA	phosphatidic acid
PARP	poly (ADP-ribose) polymerase
PAN	pantothenic acid
PC	pyruvate carboxylase
PC	phosphatidylcholine
PE	phosphatidylethanolamine
PEP	phosphoenolpyruvate
PRPP	phosphoribosyl pyrophosphate
S7P	sedoheptulose-7-phosphate
SUC	succinate
TG	triacylglycerol
UDP-Gal	uridine diphosphate galactose
UDP-GalNAc	uridine diphosphate-N-acetylgalactosamine
UDP-Glc	uridine disphosphate glucose
UDP-GlcNAc	uridine diphosphate-N-acetylglycosamine
ZMP	5-aminoimidazole-4-carboxamide ribonucleotide

ABSTRACT

Type 1 diabetes is caused by autoimmune destruction of insulin-secreting beta-cells found in the islets of Langerhans of the pancreas. Severe cases can be treated in a minimally invasive way by islet transplantation; however, islet transplantation has been limited by an inability to measure islet viability and potency prior to transplant. To address this need, we have developed a microfluidic platform to measure both intracellular Ca^{2+} flux and insulin secretion, two important indicators of beta-cell function, at high temporal resolution during glucose treatment. Combining these measures on islets required methods for measuring fluorescence at two separate locations on a microfluidic system. To accomplish this objective, we used a 2-chip system in which perfusate was collected in fractions while $[Ca^{2+}]_i$ was measured using fluorescence imaging. The perfusate was subsequently analyzed for insulin by microchip electrophoresis with laser-induced fluorescence detection (MCE-LIF) using the same fluorescence microscope. We were able to distinguish first and second phase insulin secretion from batches of 8-10 islets with 80 s temporal resolution. Measured basal and peak first phase insulin secretion correlated well with previously reported results. Total analysis time using this system was <90 min.

For an alternative approach to islet evaluation, we developed a metabolomic method to identify potential biomarkers of islet health for transplant. Using a miniaturized sample preparation method and HPLC-TOF-MS, we were able to identify 62 metabolites reliably in whole islet samples. To mimic damage that can occur during islet transplant, we induced oxidative stress in islets using H_2O_2 and measured their immediate metabolomic response as well as their response 1-4 h following stress removal. Increased concentrations of pentose phosphates, glucose-6-phosphate, and fructose bisphosphate in the immediate response corresponded to glycolysis blockage and possibly increased flux through the pentose phosphate pathway. Post-stress responses

included increased levels of free fatty acids, phospholipids, long chain CoAs, and HMG-CoA as well blunted malonyl CoA concentrations, potentially relating to alterations in the glycerolipid/free fatty acid cycle and mevalonate pathway. These metabolites could comprise a metabolic signature of stressed cells for islet evaluation prior to transplantation.

CHAPTER 1
Introduction

The overall goal of this work was to develop analytical techniques for evaluating function in pancreatic islets of Langerhans, with the ultimate purpose of screening islet viability prior to clinical islet transplantation in type 1 diabetes patients. A secondary objective of islet evaluation was to study islet physiology and effects of stressors on islet function as they relate to mechanisms of diabetes pathogenesis. Although this work focused specifically on islets, the methods developed could potentially be used to study other cell systems as well.

Diabetes Background

The disease diabetes mellitus is characterized by a lack of proper blood glucose regulation. Diabetes is a serious concern in the United States, affecting 29.1 million people (9.3% of the population) and costing an estimated $245 billion annually (2014) (1). There are two distinct classes of this disease: type 1 diabetes, also known as insulin-dependent diabetes mellitus (IDDM), which involves autoimmune destruction of insulin-secreting β-cells, leading to insulin deficiency; and type 2 diabetes, or noninsulin-dependent diabetes mellitus (NIDDM), which occurs when tissues become resistant to insulin action, eventually leading to β-cell failure and a loss of β-cell mass (2). Type 2 diabetes is more prevalent than type 1, accounting for ~90-95% of Americans diagnosed with the disease (1).

Islets of Langerhans

Blood glucose levels are regulated in part by pancreatic endocrine tissue clustered into groups of cells called the islets of Langerhans. There are ~2 million islets in a human pancreas, with each islet containing ~2000-4000 cells. Islets can vary in size, with an

average diameter of ~150 μm, and they are comprised of 5 major cell types: glucagon-secreting α-cells, insulin-secreting β-cells, somatostatin-secreting δ-cells, pancreatic polypeptide-secreting PP cells, and grehlin-secreting ε-cells. The most prevalent cell types in an islet are β-cells (~50-80%) and α-cells (~15-20%) (3). Their associated hormones, insulin and glucagon, are important regulators of glucose homeostasis. Human blood glucose levels are maintained at a constant concentration of ~5 mM. When blood glucose concentration falls below 5 mM, glucagon is secreted from the pancreas, resulting in the breakdown of glycogen stores in the liver. When blood glucose concentration rises above 5 mM, insulin is secreted and carried through the bloodstream, where it interacts with insulin receptors on tissues, causing them to increase their blood glucose intake (4, 5). The release of insulin from healthy β-cells in response to a glucose challenge has been shown to be biphasic and pulsatile (6).

The first phase of glucose-stimulated insulin secretion (GSIS) is associated with the so-called K_{ATP}-dependent pathway of insulin secretion (Figure 1.1). In this pathway, an increase in extracellular glucose concentration causes increased glucose uptake across glucose transporter- type 1 (GLUT-1) in humans or type 2 (GLUT-2) in rodents (7). Once inside the β-cell, glucose undergoes glycolysis, and glycolytic products enter the citric acid cycle and undergo oxidative phosporylation, resulting in the production of adenosine triphosphate (ATP). The consequent increase in ATP/ADP ratio causes ATP-regulated K^+ channels to close, thus preventing K^+ from leaving the cell. The increased positive charge inside the cell due to increased intracellular [K^+] leads to membrane depolarization, resulting in the opening of voltage-gated L-type Ca^{2+} channels. Increased levels of Ca^{2+} induce vesicles containing insulin to fuse with the plasma membrane of the cell, releasing insulin into the extracellular space through exocytosis.

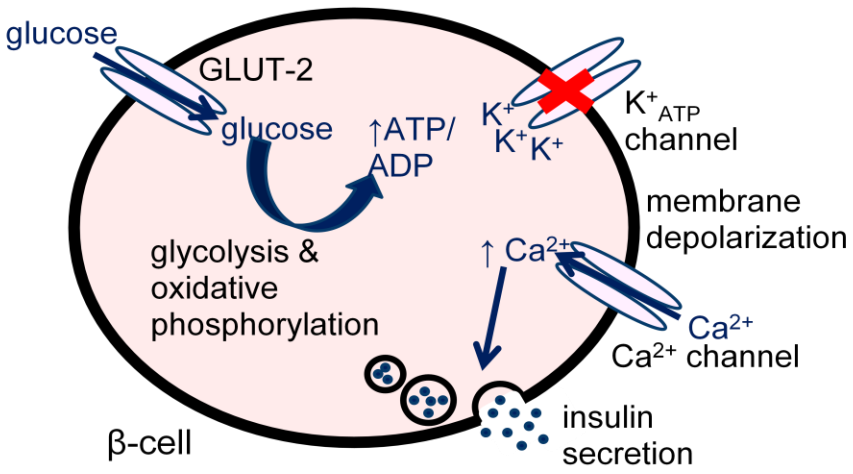

Figure 1.1. K_{ATP}-dependent pathway of GSIS. Abbreviations are: glucose transporter-2 (GLUT-2), adenosine triphosphate (ATP), adenosine diphosphate (ADP).

Although K_{ATP}-dependent GSIS has been well-characterized, investigations have determined that it cannot be solely responsible for all GSIS. When diazoxide is used to hold K_{ATP} channels open, glucose still is able to stimulate insulin release when β-cell membranes are depolarized using high $[K^+]$ (8). Additionally, when sulfonylureas are used to hold K_{ATP} channels closed, a glucose stimulus again increases insulin secretion (9). Taken together, these experiments provide evidence for a K_{ATP}-independent pathway of GSIS.

K_{ATP}-independent, or amplifying, pathways are thought to be associated with the second phase of GSIS, since these pathways serve only to amplify an existing insulin response and do not stimulate insulin secretion unless membrane depolarization and $[Ca^{2+}]_i$ influx have occurred (10). Several molecules have been implicated as possible amplifiers of insulin secretion, including glutamate (11), long chain acyl CoAs (10), mitochondrial GTP (12), AKG (13), and malonyl CoA (14, 15). Anaplerosis (replenishment of citric acid cycle metabolites) has been hypothesized to be involved in the K_{ATP}-independent pathways of GSIS; evidence for such a pathway includes high levels of expression of pyruvate carboxylase (PC) and malic enzyme (ME) in islets (16). It has been shown that ~50% of glucose carbon entering the mitochondria is metabolized by the anaplerotic enzyme PC in rat islet tissue, resulting in a net increase in citrate acid cycle metabolites in the mitochondria. These metabolites (e.g. citrate and malate) are then exported to the

cytosol, where they may be involved in insulin secretion signaling (13). This process is thought to occur through either a pyruvate/malate or pyruvate/citrate shuttle or through malonyl CoA formation and lipid esterification processes (16). Anaplerotic and cataplerotic reactions and products are summarized in Figure 1.2 (13).

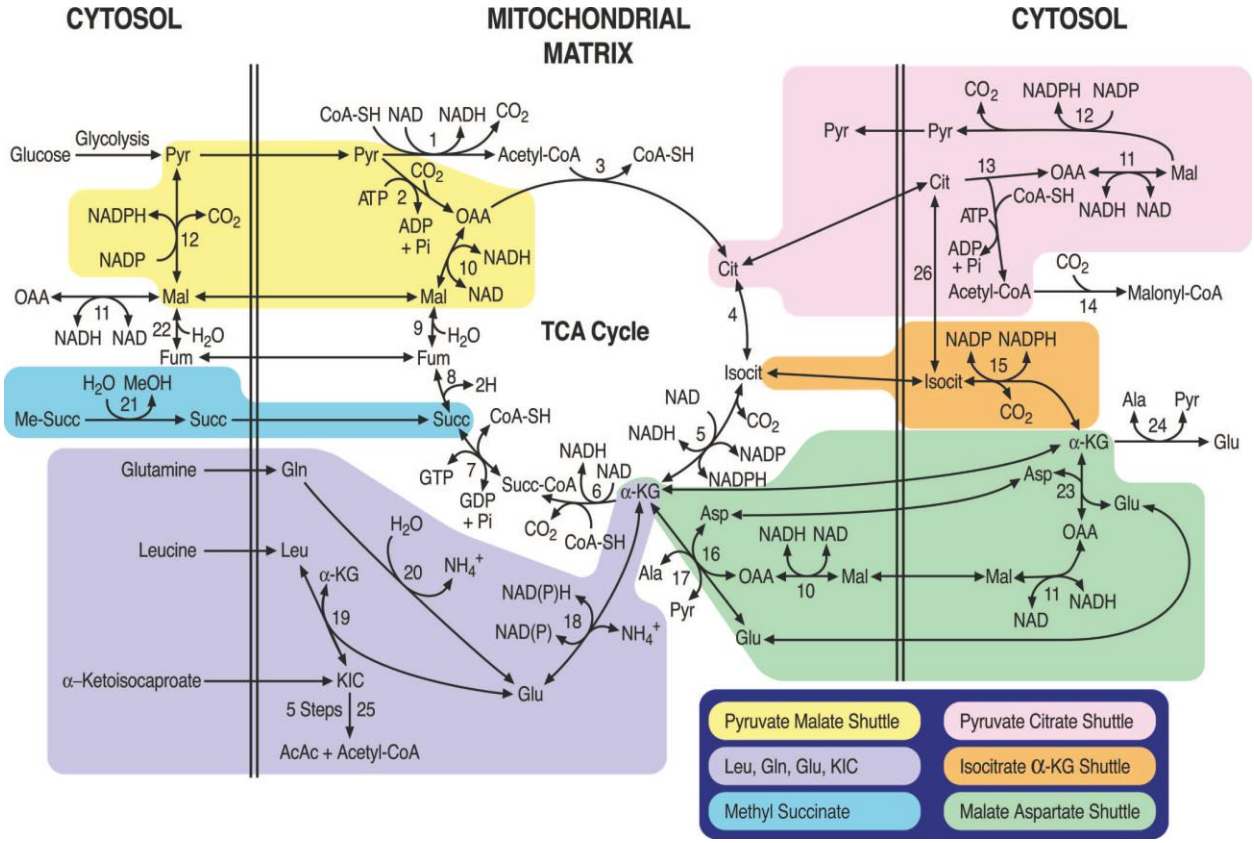

Figure 1.2. Anaplerotic and cataplerotic pathways. It is thought that K_{ATP}-independent pathways of GSIS are related to anaplerosis either through the pyruvate-malate or pyruvate-citrate shuttle. The pyruvate-citrate cycle involves cataplerosis of citrate (Cit) from the mitochondria to the cytosol, where it is converted to malonyl CoA through acetyl CoA. Malonyl CoA has been suggested as a metabolic coupling factor for GSIS. The pyruvate-malate shuttle involves cataplerosis of malate from the mitochondria to the cytosol, where it is converted to pyruvate or oxaloacetate, forming NADPH and NADH in the process, which also have been considered as possible coupling factors for GSIS. Reproduced with permission from reference 13.

Glucose and fatty acid metabolism interact through a glycerolipid/free fatty acid (GL/FFA) cycle, which consists of both anabolic and catabolic pathways (Figure 1.3). In the lipogenesis portion of the cycle, glycolysis-derived glycerol-3-phosphate (G3P) esterifies with fatty acyl CoA to form lysophosphatidic acid (LPA). LPA in turn is used to synthesize phosphatidic acid (PA), which is then hydrolyzed to diacylglycerol (DAG) and

finally culminates in triacylglycerol (TG). The lipolysis portion of the cycle reverses this pathway, hydrolyzing DAG from TG, which is further hydrolyzed to monoacylglycerol (MG). Glycerol and FFA are then formed from MG. This process is futile in terms of energy consumption/generation; however, altered flux through the GL/FFA cycle has been demonstrated in Zucker fatty rats and in models of type 2 diabetes (17). This signifies that flux through the GL/FFA cycle is important for regulation of GSIS.

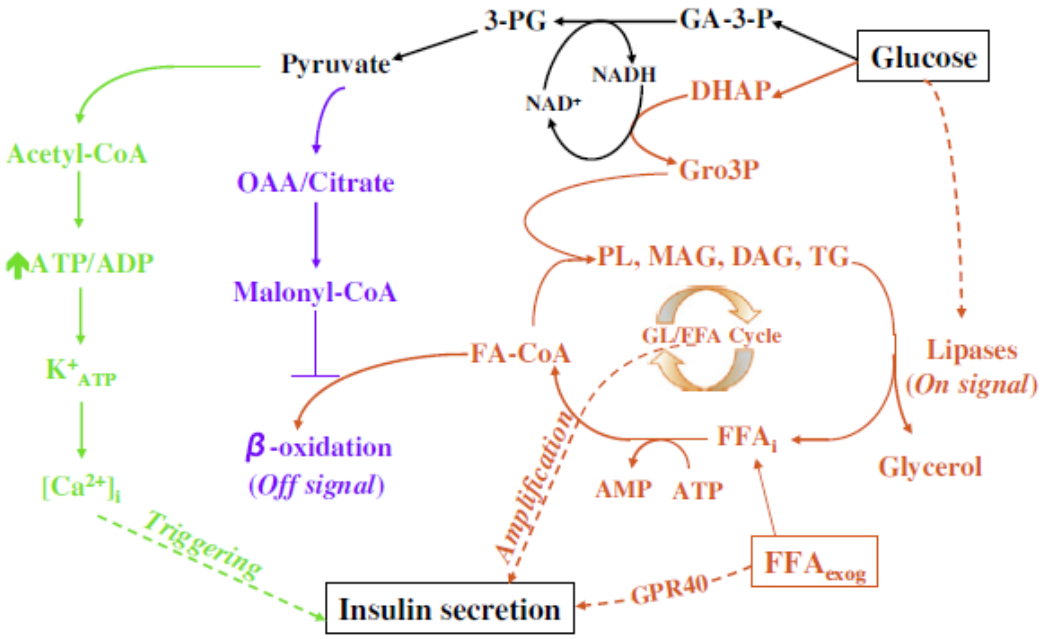

Figure 1.3. Interaction of glucose and fatty acid metabolism. Metabolites involved in the GL/FFA cycle pathway are shown in red, metabolites involved in the anaplerotic pathway are shown in blue, and metabolites involved in the K_{ATP}-dependent pathway are shown in green. Glucose-derived glycerol-3-phosphate (Gro3P) helps regenerate NAD^+ required for metabolism of glyceraldehyde-3-phosphate (GA-3-P) to 3-phosphoglycerate (3-PG). Pyruvate-derived citrate, formed via anaplerotic reactions, gives rise to malonyl-CoA, which inhibits β-oxidation of fatty acids. Fatty acyl CoAs (FA-CoA) are redirected towards formation of phospholipids, thus driving the GL/FFA cycle. Lipid molecules involved in this cycle can potentially act as signaling molecules for amplification of insulin secretion. Flux through the GL/FFA cycle has been shown to be altered in type 2 diabetes. Reproduced with permission from reference 17.

The pentose phosphate pathway (PPP) has also been found to be associated with insulin release. Although the PPP is not highly active in β-cells, increases in the PPP metabolites sedoheptulose-7-phosphate (S7P), pentose phosphates, 6-phosphogluconic acid (6PG), and phosphoribosyl pyrophosphate (PRPP) have been

observed in response to glucose stimulation in INS-1 cells (18) and in rat islets (19). Moreover, inhibition of the PPP through inhibition of glucose-6-phosphate dehydrogenase by *trans*-dehydroepiandrosterone (DHEA) reduces pentose phosphate levels and insulin secretion following glucose stimulation (19).

The K_{ATP}-independent pathway of GSIS has been shown to be impaired in β-cells derived from animal models of type 2 diabetes. Insulin release is blunted in diabetic rat islets, while $[Ca^{2+}]_i$ is normal compared to control. When high $[K^+]$ is used to depolarize plasma membranes in the presence of diazoxide, insulin release is significantly lower in diabetic rat islets as compared to control, indicating that the reduction in insulin secretion is not related to K_{ATP} channel function (20). Indirect evidence has shown the K_{ATP}-independent pathway to be impaired in diabetic human patients as well (10). Loss of K_{ATP}-dependent insulin secretion is observed in prediabetic type 1 diabetes patients (2). Although the mechanisms of disease progression differ, increasing loss of β-cell mass over time leads to an eventual inability to produce enough insulin in response to glucose to properly regulate blood glucose levels in both type 1 and type 2 diabetes.

Type 1 Diabetes Treatment

There are several treatment options available for type 1 diabetes. The most common method of treatment is the administration of exogenous insulin, either through injection or through an insulin pump. While blood glucose levels can often be regulated adequately with these methods, they are inconvenient for patients because blood glucose levels must be monitored regularly throughout the day through finger-pricking and patients must either inject themselves several times per day or wear a pump at all times, potentially restricting their daily activities. Additionally, exogenous insulin administration does not mimic the pulsatile patterns seen in endogenous insulin secretion. Some patients have difficulty achieving glycemic control with exogenous insulin and suffer life-threatening hypoglycemic episodes (1). For these patients, whole pancreas transplantation has been a successful method of treatment.

Pancreas transplantation is a major operation, and is most often performed in conjunction with a kidney transplant. While pancreas transplantation is quite successful, with ~85% of transplantation recipients remaining insulin-independent one year post-transplant, it has a high risk of complications and is thus only indicated for a small subset of diabetes sufferers (22). Another alternative, still in clinical trials, is islet transplantation. Islet transplantation, which involves infusion of donor islets into a vein in the recipient's liver (Figure 1.4), is minimally invasive and has a lower risk of complications compared to whole pancreas transplantation. However, islet transplantation has not been as successful. Many times, patients need several islet infusions to achieve insulin-independence, and the rates of long-term insulin-independence (~55%, sustained over 5 years) have been lower in comparison to whole pancreas transplantation (21).

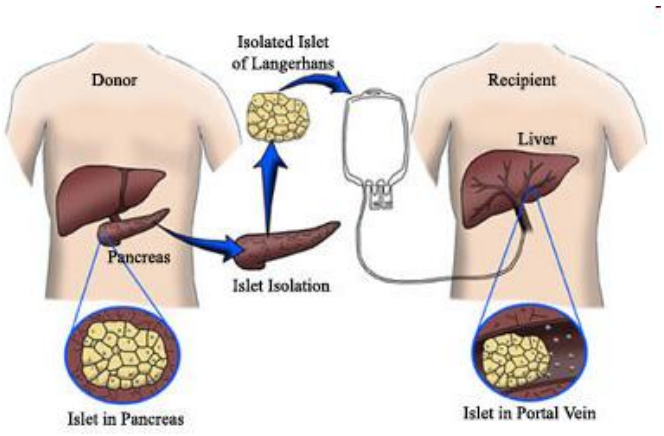

Figure 1.4. Schematic of islet transplantation. Islets are isolated from a donor pancreas and injected into the portal vein in the recipient's liver. This process is minimally invasive. Image (open-source) courtesy of the University of Alberta via the Clinical Islet Transplantation (CIT) Consortium (22).

Multiple reasons exist for islet failure in the context of islet transplantation. Islets lose vascularization during isolation and require the formation of new blood vessels for nutrient supply once transplanted. The current insertion site in the portal vein of the liver is not ideal for islet re-vascularization. Recent work has attempted to identify alternative locations for transplant that provide ease of surgical access, close proximity to blood supply, and capacity for a large transplant volume. Possible transplant sites include the

spleen, gastric submucosa, intramuscular, and subcutaneous (23). Because islets are allogeneic, immunosuppressants are required to prevent an immune response in transplant recipients. Encapsulation of islets is being investigated as a method to prevent immune rejection of transplanted islets. This method has the added benefit of allowing the xenotransplantation of islets, thus reducing the demand for human pancreata availability (24). Another potential source of β-cells for transplantation is through stem cell differentiation (25).

Islet Evaluation for Transplantation

There is currently no adequate way to determine the viability and potency of an islet preparation prior to transplantation, although such a method is necessary for regulatory reasons and to improve the success rate of clinical islet transplants. Requirements for any potential viability assay are that it is β-cell specific, correlates to transplantation outcome, and is fast. The median culture time for islets prior to human transplantation reported in a retrospective study is 20 h (26), so an assay would need to be able to be completed and analyzed within this timeframe to allow effective decisions about using a particular islet preparation.

Viability is currently measured using fluorescein diacetate/propidium iodide (FDA/PI) to assess membrane integrity (27). This test, however, does not account for early apoptotic cells, and does not correlate with clinical results. The current standard for determining potency is the diabetic nude mouse bioassay (NMB), in which islets are transplanted into a diabetic, immunodeficient mouse to determine whether they will reverse diabetes. The NMB correlates very well with islet transplantation success, but it can only be used retroactively, because several days to weeks are required to determine the outcome of the test. Static glucose-stimulated insulin secretion (GSIS), as measured through enzyme-linked immunosorbent assay (ELISA), has been used to evaluate islet potency prior to transplantation; however, the results have not correlated well with clinical outcomes (27). While the reason for this lack of correlation is unknown, there are several plausible explanations. Because the static GSIS test measures only bulk insulin release, it does not capture the dynamics of insulin secretion, which are

important to β-cell function (28). Additionally, stresses from isolation could temporarily impair insulin secretion from otherwise viable islets (29).

Many researchers have been working to develop assays that can successfully predict clinical outcomes prior to transplantation. Work has focused on cell membrane integrity tests (30), mitochondrial health assays, including oxygen consumption rate (OCR) (29, 31, 32) and ATP/ADP ratio (33, 34), and dynamic GSIS (27, 28, 35). A capillary electrophoresis (CE)-based microfluidic chip has previously been developed in our lab to measure dynamic GSIS from single islets (36), and was subsequently improved to allow parallel measurement of GSIS from single islets in four (37) or fifteen (38) channels. Using these devices, down to 6 s temporal resolution can be achieved (36). Such a system can record 300 electropherograms over a 30 minute timeframe in near real time, providing measurement of 1st and 2nd phase insulin secretion dynamics, including 3-5 min oscillations during 2nd phase release, that cannot be measured by static incubations.

Another microfluidic device has been developed for detection of multiple components of the GSIS pathway. Both calcium influx and mitochondrial membrane potential changes are measured from batches of 25-30 islets in response to glucose stimulation at established gradients. Perfusate from the chip is collected, and GSIS is determined by ELISA (28, 35). While this system is able to measure islet potency via several different parameters, ELISA is time-consuming, labor-intensive, requires large volumes (100-200 µL per assay), and is costly (over $5 per assay on average). One 30 min glucose stimulation experiment with fractions collected every minute would require 30 individual assays alone, and take several hours to complete following the experiment. One of the objectives of this dissertation was to develop a microfluidic chip that combines the multiparametric advantages of this device with the speed, temporal response, and cost advantages of on-chip GSIS measurements.

Microfluidic Monitoring of Cells

We elected to pursue a microfluidic approach to rapidly assay islet cell function. Microfluidic devices are useful for studying cellular systems because their dimensions (µm-scale) are compatible with cell size, and they allow precise control over the cellular environment. Using microfluidics, many processes (e.g. cell trapping, cell lysis, reagent addition, separation, and detection) can be incorporated onto a single device, resulting in a highly automated system. Reagent consumption is much lower in microfluidic devices than in conventional systems, resulting in lower costs and less waste. Because of these advantages, microfluidics has been adapted for a wide range of applications, including DNA analysis (39), *in vitro* fertilization (40), disease diagnostics (41), proteomics (42), high-throughput screening (43), and cell secretion studies (44).

CE -Based Immunoassay

One of the workhorse techniques in biochemical analyses is the immunoassay. ELISA and radioimmunoassay (RIA) are extremely sensitive techniques that are used to quantify molecules in a sample based on antibody-antigen interactions. However, these techniques suffer from long analysis times and high costs as described above. For time scale experiments, fractions must be collected for each desired measurement, which limits the temporal resolution that can be achieved due to sample size requirements. Temporal resolution is important in order to observe cellular secretion dynamics that can occur on a second-to-minute timescale. CE-based immunoassay (CE-IA) was thus developed to overcome some of these limitations.

CE-IA involves a solution-phase reaction of antigen with antibody prior to separation of antigen-antibody complexes from free molecules (45). Since its introduction, CE-IA has been described for the analysis of a wide array of molecules, including drugs (46), hormones (47), proteins (48), peptides (49), antibiotics (50), and toxins (51). CE-IA became a commonly used technique for detecting molecules secreted from cells (52), and was later adapted for use in an on-line microfluidic system (36, 44). Using microchip electrophoresis (MCE), separation times of 5-10 s can be routinely achieved, allowing detection to be completed in near-real time.

Despite its advantages, CE-IA typically exhibits higher concentration detection limits than ELISA. Most commercial ELISA kits report protein detection limits of 100 pg mL^{-1} (53), whereas insulin detection limits using MCE in our lab have been 2-5 ng mL^{-1} (38). Most typical detectors used with MCE are concentration-sensitive. Thus, in order to detect low concentrations of analytes that are secreted from cells in a continuous flow environment such as MCE, low perfusion flow rates are optimal to minimize sample dilution. This must be balanced with high enough perfusion rates to obtain fast temporal resolution. Temporal resolution can be improved using segmented flow, or droplet-based, microfluidics, in which small plugs of aqueous sample are separated by an immiscible oil phase to prevent diffusion (43). In this work, we explored continuous and segmented flow methods for collection of perfusate prior to MCE. Maintenance of temporal resolution under these conditions was critical for observing 1st and 2nd phase insulin secretion dynamics.

Detection on Microfluidic Chips

Multiple modes of detection exist for microfluidic chips, including electrochemical, mass spectrometry (MS)-based, and laser-induced fluorescence (LIF) detection. Electrochemical detection is advantageous because it is more compact than other methods, suggesting that it is more amenable to true "lab-on-a-chip" techniques. However, it is necessary to keep the high voltages used for electrophoretic separation on-chip distinct from the electrodes. Electrochemical detection on-chip usually involves either amperometry or conductimetry. In amperometry, oxidation and reduction currents are measured at a working electrode. Suppression of the separation voltage can be achieved by designing the channel cross-section to widen immediately in front of the detector electrode, resulting in a drop of resistance in the solution. Amperometry can only be used to measure electroactive species (54). Conductimetry involves applying AC voltage between two electrodes and measuring the electric current to determine solution conductivity (55). Contactless conductivity detectors, in which the electrodes are not in direct contact with the measured solution, have typically been used in MCE.

MCE has been coupled to mass spectrometry using matrix-assisted laser desorption ionization (MALDI) and electrospray ionization (ESI) interfaces. MS has the advantage of being able to detect a large number of unlabeled compounds and to give structural information. However, interfacing MCE to MS presents some challenges. MALDI detection is typically done off-line because the sample needs to be crystallized with matrix, which is not easily achieved in a continuous flow format (56). Although ESI is well-suited for continuous flow applications, few CE electrolytes are compatible with ESI. ESI can be coupled to a chip using spray generated directly on the planar side of the chip or using a nanospray emitter tip inserted into an on-chip channel. Spray generated on the side of the chip is subject to band broadening effects because fluid tends to spread over the surface prior to the onset of electrospray. Nanospray emitter tips result in less band broadening, although these effects can be variable from chip-to-chip due to differences in capillary alignment within the channel (57).

The most commonly used detection system with MCE is LIF due to its superior concentration detection limits in low volumes, down to the pM range (58). Materials used to fabricate microfluidic devices are typically transparent (e.g. glass or polydimethylsiloxane (PDMS)), so measuring fluorescence in a channel is straightforward. The downsides of this detection method are that it requires the sample to be fluorescent or labeled with a fluorescent tag, and most of the associated instrumentation (e.g. confocal microscopes and lasers) is large and bulky.

Recent work has focused on reducing the size of LIF systems so they can approach the "lab-on-a-chip" ideal. Typical optical arrangements for detection on a microfluidic channel are shown in Figure 1.5, including confocal (3a), bevel incident (3b-c), and orthogonal (3d-f). Confocal microscopy is the most commonly used configuration. Miniaturization of typical optical elements used in confocal microscopy has been demonstrated, although further miniaturization is limited by complicated material handling methods (59). Bevel incident configurations have suffered from high background signal due to reflection and refraction from the microchip surface (60). Orthogonal arrangements are amenable to insertion of an optical fiber into the chip for

excitation and/or emission, but LODs are higher than with a confocal arrangement, possibly due to poor focusing and collection capabilities of optical fibers (61). Alternatively, optical elements, including lenses and waveguides, have been fabricated directly into microfluidic devices (62–64). This approach allows for precise alignment of features with channels, but requires extensive fabrication processes. Additionally, optics must be designed individually for each new chip design. As such, miniaturization of LIF systems is an ongoing challenge.

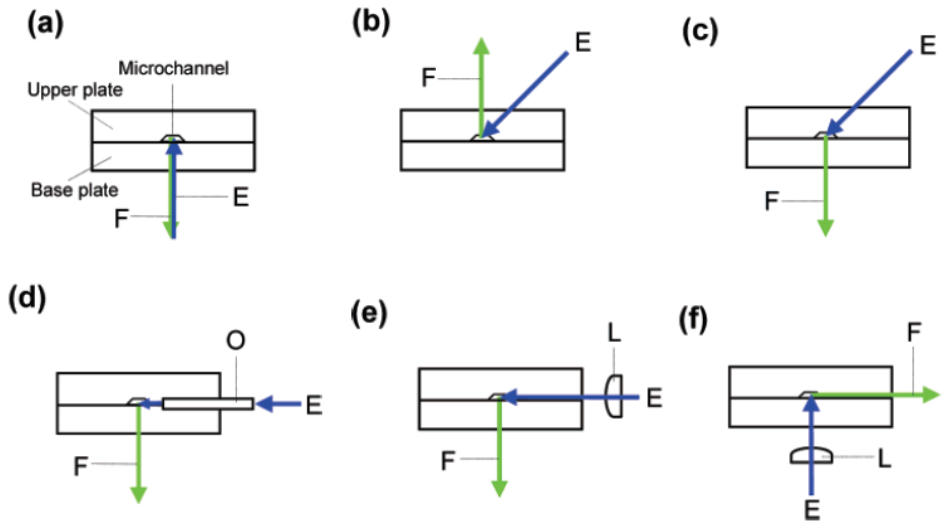

Figure 1.5. Optical configurations for detection on microfluidic chips. The confocal system (a) is the most commonly used for microchip detection, although options for miniaturization are limited. Introducing LIF at a bevel-incident angle and collecting fluorescence perpendicular to the microchip (b,c) results in high background due to reflection and refraction from the microchip surface. Orthogonal configurations have been employed by inserting an optical fiber into the side of the chip (d), by focusing laser light through the sidewall of the chip using an objective lens and measuring perpendicularly (e), or by focusing laser light along the perpendicular axis and collecting fluorescence through the sidewall of the chip (f). LOD of (d) and (e) are typically orders of magnitude higher than other configurations due to weak focusing of light in (d) or scattering of light at the chip sidewall in (e). LOD in (f) is comparable to traditional confocal systems, although alignment of the system is not trivial. E = excitation, F = fluorescent detection, O = optical fiber, L = lens. Reprinted with permission from reference 57. Copyright 2006 American Chemical Society.

Multi-Point Detection

One advantage of miniaturized LIF detectors is that they can afford the ability to optically detect compounds at multiple points on the same chip. This is important in our work because $[Ca^{2+}]_i$ requires fluorescent measurement in the islets, while MCE requires fluorescent measurement at a different point on the same chip. Previously, a

majority of multi-point detection systems on-chip employed electrochemical detection for one or both of the measurements. For example, characterization of red blood cells and circulating tumor cells consists of measuring differences in both cell morphology and cell electrical properties. Simultaneous detection of these properties on-chip has been accomplished by using electrodes to measure electrical properties via resistive pulse sensing while a complementary metal oxide semiconductor (CMOS) imaging sensor is used to image the cells (65). In another reported system, cardiac myocytes are perfused on-chip with test solutions. Integrated planar microelectrodes stimulate the cardiomyocytes and record the evoked action potential while $[Ca^{2+}]_i$ is monitored optically via imaging experiments using an epi-fluorescent microscope (66).

While multi-point detection using electrochemical detection for one or both of the measurements is relatively straightforward due to the small size requirements of electrodes, it is more difficult to achieve multi-point detection using optical detection for both of the measurements. Miniaturized detectors generally require extensive fabrication and/or complex instrumentation, as discussed above. Traditional optical equipment has been used for separation experiments in which multiple assays are performed on adjacent channels in parallel. Typically, single-point detection has been performed, either by moving the chip relative to the detector or by scanning the laser line relative to the channels (67). This method does not allow fast sampling rates. Alternatively, a radial design with all of the channels converging to one detection point has been employed (38). However, this is only useful for assays in which it is possible to design detection points close together; it would not be possible, for example, to visually monitor cells while measuring secreted products downstream. One study solves this problem by making sequential measurements and moving the objective. That study uses a microfluidic device to isolate and lyse single erythrocytes prior to CE separation and LIF detection of cellular GSH. Cell loading is observed with a confocal microscope, and then the chip is shifted to measure LIF detection of GSH with the same microscope (68). If both measurements need to be made temporally, decoupling the measurements in time so that they can be made sequentially is one strategy for successful analysis.

We explored this option for developing an islet evaluation system to achieve rapid multi-point detection of $[Ca^{2+}]_i$ and insulin release from islets.

Metabolomics

Our interest in β-cells and potency testing also led us to consider a metabolomics approach for islet analysis. Metabolomics aims to measure comprehensive metabolic responses to externally applied stimuli in an effort to characterize biochemical pathways and identify potential disease biomarkers (69). Metabolomics is complementary to genomics, transcriptomics, and proteomics. As metabolites are the end products of cellular systems, metabolomics data are most closely related to a cell's phenotype at a specific time (70). Eukaryotic organisms are estimated to contain 4000-20,000 different endogenous metabolites. Because the metabolome is so varied, consisting of molecules including lipids, cholesterols, amino acids, nucleic acids, and carbohydrates at concentrations ranging from the pM to mM range, detection of the entire metabolome using a single technique can be challenging (71).

Metabolomic Platforms

The platforms routinely used for metabolomics are mass spectrometry (MS) and nuclear magnetic resonance (NMR). NMR is fast, non-destructive, provides detailed structural information, and requires minimal sample preparation (72). Additionally, since NMR has routinely been used for metabolite analysis since the 1970s, analysis methods and associated chemometric software are readily available (71). ^{1}H-NMR is the most commonly used isotope due to its ubiquitous presence in compounds. However, NMR is not as sensitive as MS, with detection limits in the low µM range (73). Overlap of spectra in complex samples can complicate analyses (74). Typical ^{1}H-NMR metabolomics experiments can measure 25-75 metabolites in tissue samples and over 200 metabolites in urine samples. NMR suffers from high sensitivity to the chemical environment in that small differences in pH, protein content, or ionic strength can cause shifts in peak positions and line widths (74). This dependence on environment is especially important in biological samples such as urine or serum, which can vary significantly based on source.

MS can measure metabolites with high sensitivity and selectivity, although typically a sample preparation step is required, which can cause loss or degradation of metabolites (70). Direct injection of samples into the MS results in analysis times of less than 1 min. However, there any many disadvantages to a direct injection method: chemical isomers cannot be distinguished, and ion suppression is high since all compounds are introduced into the MS at the same time (70). These issues make it advantageous to add a separation step prior to MS analysis, resulting in longer analysis times and preference towards certain classes of metabolites based on the type of separation used.

Separation Methods

Separation methods can serve to reduce the amount of metabolites being introduced into the MS at one time, resulting in less ion suppression and improved sensitivity. They also add an additional parameter by which a compound can be identified, thus aiding in the certainty of feature identification. Separation techniques are utilized in both NMR and MS analyses.

In CE-MS, metabolites are separated by mass and charge before being introduced into the MS, typically using an electrospray ionization (ESI) interface. CE-MS has high resolution, high separation efficiency, and can separate metabolites over a wide m/z range (70-1027). Little sample pretreatment is required, and CE tends to be faster than liquid chromatography (LC). CE-MS has been used to detect 1692 compounds in *B. subtilis* cells (75). However, CE is not effective for separating uncharged compounds and macromolecules, such as sugars, lipids, cholesterols, and steroids. Also, due to poor concentration sensitivity, pre-concentration of samples is often required to improve detection limits (76). Finally, interfacing CE to MS is not trivial. Because of the low flow rates used in CE, the electrospray is not stable unless a sheath flow is used, which reduces the sensitivity of the method (77). Even so, detection limits of less than 50 nM have been reported with total ion electropherogram RSD of 5% for single-cell metabolomics (78).

Gas chromatography-mass spectrometry (GC-MS) has commonly been used in metabolomics studies. GC-MS typically exhibits greater chromatographic resolution than LC-MS, and because GC is typically coupled to MS using electron-impact ionization, it is not as susceptible as LC to ion suppression. This method offers good sensitivity, with detection limits in the pM to nM range (72). However, in order to be analyzed by GC-MS, compounds must either be volatile or be derivatized to be volatile. Derivatization can result in loss of thermally labile metabolites, and sample stability can be a concern. Additionally, derivatization can result in multiple peaks per analyte due to partial silylation, isomerization, or degradation, thus complicating the spectra and analysis (79).

Liquid chromatography-mass spectrometry (LC-MS) can provide complementary information to GC-MS data. LC-MS offers simpler sample preparation than GC-MS and can detect a wider range of metabolites. However, because it typically utilizes ESI, it is prone to ion suppression from co-eluting compounds and has lower retention time reproducibility than GC. Reverse phase C18 or C8 columns are commonly used to measure nonpolar and medium polarity analytes; however, polar analytes elute in the dead time and are not reliably quantified using reverse phase LC (RPLC). Ion-pairing agents have been used in RPLC to improve retention of polar compounds, but they can contaminate the column. Alternatively, polar compounds can be analyzed using hydrophilic interaction chromatography (HILIC). A HILIC method based on an amino-column and high mobile phase pH of 9.5 was developed for the analysis of central carbon metabolism (80). HILIC suffers from greater retention time variability than RPLC and shorter column life; however, it provides an orthogonal technique to RPLC for added metabolite coverage (81). The work presented in this dissertation utilizes both RPLC and HILIC for analysis of nonpolar and polar metabolites, respectively.

Mass Analyzers

Mass analyzers for metabolomics experiments include low resolution analyzers like the triple quadrupole (QQQ) and high resolution analyzers, like the time-of-flight (TOF), Fourier-transform ion cyclotron (FT-ICR), and Orbitrap analyzers (70, 82). The QQQ

has successfully been used to quantitate 90 metabolites with known fragmentation patterns when operated in selected reaction monitoring (SRM) mode (83). When the analytes of interest are unknown, a high resolution analyzer is preferable. TOF analyzers can provide resolution of compounds with the same nominal mass but different monoisotopic mass and have mass accuracy down to 5 ppm (72). Orbitrap and FT-ICR instruments provide even greater resolving power and mass accuracy (<1 ppm for FT-ICR) and don't require chromatographic separation. However, without separation, isomers cannot be distinguished (71). Also, the scan rate for these high resolution analyzers is slow (up to 1600 s/spectra, compared to 1 s/spectra for TOF analyzers) (82). These disadvantages, coupled with the high cost of these instruments, have limited their use in metabolomics studies (72).

Directed vs. Undirected Metabolomics

Directed, or targeted, analysis involves the analysis of a subset of metabolites, such as those associated with a specific pathway of interest. Directed analysis is fairly straightforward, requiring identification of metabolites by comparison of retention time and m/z to standard compounds. Undirected, or untargeted, analysis involves the identification of as many metabolites as possible. This approach is often referred to as "hypothesis-generating", since the goal is typically to identify possible compounds of interest based on differences between treatment groups (84). Undirected analysis requires a high resolution mass analyzer for accurate peak identifications, as well as advanced data analysis techniques.

Data Analysis

Data analysis for directed metabolomics is fairly straightforward and can be accomplished using conventional MS software. Undirected metabolomics is more challenging due to the large number of "features" (ions with unique m/z and retention time) that must be found and subsequently identified. Several software programs have been developed to process metabolomics data, including MetaboMiner for NMR data (85) and MetAlign, MZmine, and XCMS for LC-MS data (86). Software is also available from MS vendors, such as Mass Profile Pro (Agilent) or Metabolic Profile (Bruker). Raw

data is pre-processed and filtered, features with signal above a specified signal-to-noise threshold are selected based on m/z and retention time, peaks are aligned using specified m/z and retention time windows to account for nonlinear drift in the instrument, and ions/adducts are identified through comparison to metabolite databases, such as the Kyoto encyclopedia of genes and genomes (KEGG), the Human Metabolome Database (HMDB), and the Metabolite Link (METLIN) database (87, 88). Compounds preliminarily identified through undirected analysis should be confirmed by injecting standards of the identified compounds onto the MS for direct comparison. Pre-processed data can be visually interpreted with either the previously mentioned software or MetaboAnalyst (89) to determine compounds of interest that differ between sample groups based on multivariate statistical analysis.

Metabolomics in Diabetes Research

Metabolomics has been widely employed for the identification of possible biomarkers of disease, and has been applied to clinical studies involving the onset of type 1 diabetes. Increased levels of glutamic and aspartic acids and branched chain amino acids are observed in mice at high risk of developing type 1 diabetes (90). Another study corroborated these findings; serum samples from children who later developed type 1 diabetes were shown to exhibit lower levels of phosphatidylcholines (PC) from birth, as well as increased levels of proinflammatory lysophosphatidylcholine, glutamate, and branched chain amino acids and decreased levels of several TCA cycle metabolites prior to the development of islet autoantibodies (91). This research demonstrates a phenotype that could be used for identifying those at risk of identifying type 1 diabetes and for identifying possible targets for intervention in disease progression.

In addition to clinical studies, isolated islets and clonal β-cells have also been studied in order to gain insights into islet function and diabetes progression. One study has used NMR-based metabolomics in clonal β-cells to try to identify possible biomarkers of β-cell health for the purpose of islet transplantation (92). Clonal β-cells have typically been preferred for metabolomics studies due to their ease of access and specificity for β-cell metabolism (18, 19, 93–96). Several different clonal lines exist, including rat-derived

INS-1 and BRIN-BD11 cells and mouse-derived MIN-6 cells (97–99). However, because clonal cells are proliferative and may exhibit different metabolic regulation than non-proliferative native islets, it is unclear whether findings made in clonal cells can be extrapolated to whole islets. Several recent metabolomics studies have been conducted using islets; however, the large number of islets used per sample (240-500) limits the scope of experiments that can be performed (19, 100). Thus, sample preparation methods for the reproducible analysis of smaller amounts of tissue are required so that more comprehensive studies of islet function can be performed. In this work, we aimed to develop a sample preparation method for islet metabolomics that could be applied to studies of islet viability.

Dissertation Overview

The main objective of this research was to develop analytical techniques to evaluate the viability and potency of pancreatic islets for clinical islet transplantation. Chapter 2 describes the development of two analogous techniques for measuring Ca^{2+} flux and insulin secretion from the same group of islets. Both techniques involve fluorescent imaging of islets in a microfluidic chamber to measure $[Ca^{2+}]_i$ while collecting perfusate to later assay for insulin via a microchip-based electrophoretic competitive immunoassay. The first method involves continuous collection of perfusate in a capillary, while the second method involves fraction collection in a well plate followed by segmentation with oil in tubing for infusion into an electrophoresis chip. The second method was completed in collaboration with Dr. José Oberholzer and Dr. David Eddington at the University of Illinois at Chicago. This work is currently in preparation for submission to *Analytical Methods*.

Chapter 3 describes the development of a sample preparation method for extraction and LC-MS analysis of intracellular metabolites in whole islets. This method was used in Chapter 4 to study the effects of oxidative stress on islet metabolism. Metabolites and pathways that were altered by these treatments were identified; these metabolites could comprise a metabolic signature of stressed cells for the purpose of islet evaluation prior to transplantation. These results are currently in preparation for submission to *Islets*.

References

1. Centers for Disease Control and Prevention (2014) *National Diabetes Statistics Report: Estimates of Diabetes and Its Burden in the United States, 2014*, U.S. Department of Health and Human Services, Atlanta, GA, [online] http://www.cdc.gov/diabetes/pubs/statsreport14/national-diabetes-report-web.pdf (Accessed January 19, 2015)
2. Cnop, M., Welsh, N., Jonas, J. C., Jorns, A., Lenzen, S., and Eizirik, D. L. (2005) Mechanisms of pancreatic beta-cell death in type 1 and type 2 diabetes- Many differences, few similarities, pp. S97–S107, Diabetes, St Jean Cap Ferrat, France, **54**, S97–S107
3. In't Veld, P., and Marichal, M. (2010) Microscopic Anatomy of the Human Islet of Langerhans. in *The Islets of Langerhans* (Islam, M. S. ed), pp. 1–19, Springer Netherlands, Dordrecht, **654**, 1–19
4. Newsholme, P., Gaudel, C., and McClenaghan, N. H. (2010) Nutrient Regulation of Insulin Secretion and β-Cell Functional Integrity. in *The Islets of Langerhans* (Islam, M. S. ed), pp. 91–114, Springer Netherlands, Dordrecht, **654**, 91–114
5. Rutter, G. A. (2001) Nutrient-secretion coupling in the pancreatic islet beta-cell: Recent advances. *Mol. Aspects Med.* **22**, 247–284
6. Pørksen, N., Hollingdal, M., Juhl, C., Butler, P., Veldhuis, J. D., and Schmitz, O. (2002) Pulsatile insulin secretion: detection, regulation, and role in diabetes. *Diabetes*. **51**, S245–S254
7. Cabrera, O., Jacques-Silva, M. C., Berman, D. M., Fachado, A., Echeverri, F., Poo, R., Khan, A., Kenyon, N. S., Ricordi, C., Berggren, P.-O., and Caicedo, A. (2007) Automated, High-Throughput Assays for Evaluation of Human Pancreatic Islet Function. *Cell Transplant.* **16**, 1039–1048
8. Gembal, M., Gilon, P., and Henquin, J. C. (1992) Evidence that glucose can control insulin release independently from its action on ATP-sensitive K+ channels in mouse B cells. *J. Clin. Invest.* **89**, 1288–1295
9. Panten, U., Schwanstecher, M., Wallasch, A., and Lenzen, S. (1988) Glucose both inhibits and stimulates insulin secretion from isolated pancreatic islets exposed to maximally effective concentrations of sulfonylureas. *Naunyn. Schmiedebergs Arch. Pharmacol.* **338**, 459–462
10. Henquin, J.-C. (2000) Triggering and amplifying pathways of regulation of insulin secretion by glucose. *Diabetes*. **49**, 1751–1760
11. Gheni, G., Ogura, M., Iwasaki, M., Yokoi, N., Minami, K., Nakayama, Y., Harada, K., Hastoy, B., Wu, X., Takahashi, H., Kimura, K., Matsubara, T., Hoshikawa, R., Hatano, N., Sugawara, K., Shibasaki, T., Inagaki, N., Bamba, T., Mizoguchi, A., Fukusaki, E., Rorsman, P., and Seino, S. (2014) Glutamate Acts as a Key Signal Linking Glucose Metabolism to Incretin/cAMP Action to Amplify Insulin Secretion. *Cell Rep.* **9**, 661–673
12. Kibbey, R. G., Pongratz, R. L., Romanelli, A. J., Wollheim, C. B., Cline, G. W., and Shulman, G. I. (2007) Mitochondrial GTP Regulates Glucose-Stimulated Insulin Secretion. *Cell Metab.* **5**, 253–264
13. MacDonald, M. J. (2004) Perspective: emerging evidence for signaling roles of mitochondrial anaplerotic products in insulin secretion. *AJP Endocrinol. Metab.* **288**, E1–E15

14. Prentki, M., Vischer, S., Glennon, M. C., Regazzi, R., Deeney, J. T., and Corkey, B. E. (1992) Malonyl-CoA and long chain acyl-CoA esters as metabolic coupling factors in nutrient-induced insulin secretion. *J. Biol. Chem.* **267**, 5802–5810
15. Roduit, R., Nolan, C., Alarcon, C., Moore, P., Barbeau, A., Delghingaro-Augusto, V., Przybykowski, E., Morin, J., Massé, F., Massie, B., Ruderman, N., Rhodes, C., Poitout, V., and Prentki, M. (2004) A role for the malonyl-CoA/long-chain acyl-CoA pathway of lipid signaling in the regulation of insulin secretion in response to both fuel and nonfuel stimuli. *Diabetes*. **53**, 1007–1019
16. Farfari, S., Schulz, V., Corkey, B., and Prentki, M. (2000) Glucose-regulated anaplerosis and cataplerosis in pancreatic beta-cells: possible implication of a pyruvate/citrate shuttle in insulin secretion. *Diabetes*. **49**, 718–726
17. Prentki, M., and Madiraju, S. R. M. (2012) Glycerolipid/free fatty acid cycle and islet β-cell function in health, obesity and diabetes. *Mol. Cell. Endocrinol.* **353**, 88–100
18. Lorenz, M. A., El Azzouny, M. A., Kennedy, R. T., and Burant, C. F. (2013) Metabolome Response to Glucose in the β-Cell Line INS-1 832/13. *J. Biol. Chem.* **288**, 10923–10935
19. Spégel, P., Sharoyko, V. V., Goehring, I., Danielsson, A. P. H., Malmgren, S., Nagorny, C. L. F., Andersson, L. E., Koeck, T., Sharp, G. W. G., Straub, S. G., Wollheim, C. B., and Mulder, H. (2013) Time-resolved metabolomics analysis of β-cells implicates the pentose phosphate pathway in the control of insulin release. *Biochem. J.* **450**, 595–605
20. Hughes, S. J., Faehling, M., Thorneley, C. W., Proks, P., Ashcroft, F. M., and Smith, P. A. (1998) Electrophysiological and metabolic characterization of single β-cells and islets from diabetic GK rats. *Diabetes*. **47**, 73–81
21. CITR Coordinating Center Scientific Summary of the Collaborative Islet Transplant Registry (CITR) 2012 (Eighth) Annual Report. [online] https://web.emmes.com/study/isl/reports/20150218_CITR_2012EighthAnnualReportScientificSummary.pdf (Accessed February 18, 2015)
22. Clinical Islet Transplantation Consortium [online] http://www.citisletstudy.org/islet.html (Accessed April 12, 2015)
23. Pepper, A. R., Gala-Lopez, B., Pawlick, R., Merani, S., Kin, T., and Shapiro, A. M. J. (2015) A prevascularized subcutaneous device-less site for islet and cellular transplantation. *Nat. Biotechnol.* 10.1038/nbt.3211
24. Wiedemeier, S., Ehrhart, F., Mettler, E., Gastrock, G., Forst, T., Weber, M. M., Zimmermann, H., and Metze, J. (2011) Encapsulation of Langerhans' islets: Microtechnological developments for transplantation. *Eng. Life Sci.* **11**, 165–173
25. Kroon, E., Martinson, L. A., Kadoya, K., Bang, A. G., Kelly, O. G., Eliazer, S., Young, H., Richardson, M., Smart, N. G., Cunningham, J., Agulnick, A. D., D'Amour, K. A., Carpenter, M. K., and Baetge, E. E. (2008) Pancreatic endoderm derived from human embryonic stem cells generates glucose-responsive insulin-secreting cells in vivo. *Nat. Biotechnol.* **26**, 443–452
26. Kin, T. (2010) Islet Isolation for Clinical Transplantation. in *The Islets of Langerhans* (Islam, M. S. ed), pp. 683–710, Springer Netherlands, Dordrecht, **654**, 683–710
27. Papas, K. K., Suszynski, T. M., and Colton, C. K. (2009) Islet assessment for transplantation: *Curr. Opin. Organ Transplant.* **14**, 674–682

28. Mohammed, J. S., Wang, Y., Harvat, T. A., Oberholzer, J., and Eddington, D. T. (2009) Microfluidic device for multimodal characterization of pancreatic islets. *Lab. Chip*. **9**, 97
29. Papas, K. K., Colton, C. K., Nelson, R. A., Rozak, P. R., Avgoustiniatos, E. S., Scott, W. E., Wildey, G. M., Pisania, A., Weir, G. C., and Hering, B. J. (2007) Human Islet Oxygen Consumption Rate and DNA Measurements Predict Diabetes Reversal in Nude Mice. *Am. J. Transplant.* **7**, 707–713
30. Barnett, M. J., McGhee-Wilson, D., Shapiro, A. M. J., and Lakey, J. R. T. Variation in human islet viability based on different membrane integrity stains. *Cell Transplant.* **13**, 481–488
31. Fraker, C., Timmins, M. R., Guarino, R. D., Haaland, P. D., Ichii, H., Molano, D., and Pileggi, A. The use of the BD oxygen biosensor system to assess isolated human islets of Langerhans: Oxygen consumption as a potential measure of islet potency. *Cell Transplant.* **15**, 745–758
32. Sweet, I. R., Gilbert, M., Scott, S., Todorov, I., Jensen, R., Nair, I., Al-Abdullah, I., Rawson, J., Kandeel, F., and Ferreri, K. (2008) Glucose-Stimulated Increment in Oxygen Consumption Rate as a Standardized Test of Human Islet Quality. *Am. J. Transplant.* **8**, 183–192
33. Goto, M., Holgersson, J., Kumagai-Braesch, M., and Korsgren, O. (2006) The ADP/ATP Ratio: A Novel Predictive Assay for Quality Assessment of Isolated Pancreatic Islets. *Am. J. Transplant.* **6**, 2483–2487
34. Suszynski, T. M., Wildey, G. M., Falde, E. J., Cline, G. W., Maynard, K. S., Ko, N., Sotiris, J., Naji, A., Hering, B. J., and Papas, K. K. (2008) The ATP/DNA Ratio Is a Better Indicator of Islet Cell Viability Than the ADP/ATP Ratio. *Transplant. Proc.* **40**, 346–350
35. Adewola, A. F., Lee, D., Harvat, T., Mohammed, J., Eddington, D. T., Oberholzer, J., and Wang, Y. (2010) Microfluidic perifusion and imaging device for multi-parametric islet function assessment. *Biomed. Microdevices*. **12**, 409–417
36. Shackman, J. G., Dahlgren, G. M., Peters, J. L., and Kennedy, R. T. (2005) Perfusion and chemical monitoring of living cells on a microfluidic chip. *Lab. Chip*. **5**, 56
37. Dishinger, J. F., and Kennedy, R. T. (2007) Serial Immunoassays in Parallel on a Microfluidic Chip for Monitoring Hormone Secretion from Living Cells. *Anal. Chem.* **79**, 947–954
38. Dishinger, J. F., Reid, K. R., and Kennedy, R. T. (2009) Quantitative Monitoring of Insulin Secretion from Single Islets of Langerhans in Parallel on a Microfluidic Chip. *Anal. Chem.* **81**, 3119–3127
39. Dongre, C., van Weerd, J., van Weeghel, R., Martinez Vazquez, R., Osellame, R., Ramponi, R., Cerullo, G., Dekker, R., Besselink, G. A. J., van den Vlekkert, H. H., Hoekstra, H. J. W. M., and Pollnau, M. (2009) Multi-point, multi-wavelength fluorescence monitoring of DNA separation in a lab-on-a-chip with monolithically integrated femtosecond-laser-written waveguides. [online] http://doc.utwente.nl/70142/ (Accessed March 29, 2015)
40. Suh, R. S. (2005) IVF within microfluidic channels requires lower total numbers and lower concentrations of sperm. *Hum. Reprod.* **21**, 477–483

41. Yager, P., Edwards, T., Fu, E., Helton, K., Nelson, K., Tam, M. R., and Weigl, B. H. (2006) Microfluidic diagnostic technologies for global public health. *Nature*. **442**, 412–418
42. Lion, N., Rohner, T. C., Dayon, L., Arnaud, I. L., Damoc, E., Youhnovski, N., Wu, Z.-Y., Roussel, C., Josserand, J., Jensen, H., Rossier, J. S., Przybylski, M., and Girault, H. H. (2003) Microfluidic systems in proteomics. *Electrophoresis*. **24**, 3533–3562
43. Guetschow, E. D., Steyer, D. J., and Kennedy, R. T. (2014) Subsecond Electrophoretic Separations from Droplet Samples for Screening of Enzyme Modulators. *Anal. Chem.* **86**, 10373–10379
44. Roper, M. G., Shackman, J. G., Dahlgren, G. M., and Kennedy, R. T. (2003) Microfluidic Chip for Continuous Monitoring of Hormone Secretion from Live Cells Using an Electrophoresis-Based Immunoassay. *Anal. Chem.* **75**, 4711–4717
45. Taylor, J., Picelli, G., and Harrison, D. J. (2001) An evaluation of the detection limits possible for competitive capillary electrophoretic immunoassays. *Electrophoresis*. **22**, 3699
46. Huang, Y., Zhao, S., Shi, M., and Liang, H. (2011) One-way multiplexed immunoassay strategy for simultaneous determination of multi-analytes by microchip electrophoresis. *The Analyst*. **136**, 2119
47. Schultz, N. M., Huang, L., and Kennedy, R. T. (1995) Capillary electrophoresis-based immunoassay to determine insulin content and insulin secretion from single islets of Langerhans. *Anal. Chem.* **67**, 924–929
48. Deng, Y.-H., Zhang, Z.-X., Zhang, H.-S., and Wang, H. (2010) Development of an N-hydroxysuccinimidyl fluorescein-O-acetate-labeled probe for competitive capillary electrophoretic immunoassay of bovine serum albumin. *Talanta*. **81**, 1806–1809
49. Guillo, C., and Roper, M. G. (2011) Simultaneous capillary electrophoresis competitive immunoassay for insulin, glucagon, and islet amyloid polypeptide secretion from mouse islets of Langerhans. *J. Chromatogr. A*. **1218**, 4059–4064
50. Wan, Q.-H., and Le, X. C. (1999) Capillary electrophoretic immunoassays for digoxin and gentamicin with laser-induced fluorescence polarization detection. *J. Chromatogr. B. Biomed. Sci. App.* **734**, 31–38
51. Lam, M. T., Wan, Q. H., Boulet, C. A., and Le, X. C. (1999) Competitive immunoassay for staphylococcal enterotoxin A using capillary electrophoresis with laser-induced fluorescence detection. *J. Chromatogr. A*. **853**, 545–553
52. Schultz, N. M., and Kennedy, R. T. (1993) Rapid immunoassays using capillary electrophoresis with fluorescence detection. *Anal. Chem.* **65**, 3161–3165
53. Zhang, S., Garcia-D'Angeli, A., Brennan, J. P., and Huo, Q. (2014) Predicting detection limits of enzyme-linked immunosorbent assay (ELISA) and bioanalytical techniques in general. *The Analyst*. **139**, 439–445
54. Schwarz, M. A., and Hauser, P. C. (2001) Recent developments in detection methods for microfabricated analytical devices. *Lab. Chip*. **1**, 1
55. Šolínová, V., and Kašička, V. (2006) Recent applications of conductivity detection in capillary and chip electrophoresis. *J. Sep. Sci.* **29**, 1743–1762
56. Gustafsson, M., Hirschberg, D., Palmberg, C., Jörnvall, H., and Bergman, T. (2004) Integrated Sample Preparation and MALDI Mass Spectrometry on a Microfluidic Compact Disk. *Anal. Chem.* **76**, 345–350

57. Mellors, J. S., Jorabchi, K., Smith, L. M., and Ramsey, J. M. (2010) Integrated Microfluidic Device for Automated Single Cell Analysis Using Electrophoretic Separation and Electrospray Ionization Mass Spectrometry. *Anal. Chem.* **82**, 967–973
58. Ocvirk, G., Tang, T.; and Harrison, D. J. (1998) Optimization of confocal epifluorescence microscopy for microchip-based miniaturized total analysis systems. *Analyst*. **123**, 1429–1434
59. Benhabib, M., Chiesl, T. N., Stockton, A. M., Scherer, J. R., and Mathies, R. A. (2010) Multichannel Capillary Electrophoresis Microdevice and Instrumentation for in Situ Planetary Analysis of Organic Molecules and Biomarkers. *Anal. Chem.* **82**, 2372–2379
60. Fu, J.-L., Fang, Q., Zhang, T., Jin, X.-H., and Fang, Z.-L. (2006) Laser-Induced Fluorescence Detection System for Microfluidic Chips Based on an Orthogonal Optical Arrangement. *Anal. Chem.* **78**, 3827–3834
61. Li, H.-F., Lin, J.-M., Su, R.-G., Uchiyama, K., and Hobo, T. (2004) A compactly integrated laser-induced fluorescence detector for microchip electrophoresis. *Electrophoresis*. **25**, 1907–1915
62. Bliss, C. L., McMullin, J. N., and Backhouse, C. J. (2007) Rapid fabrication of a microfluidic device with integrated optical waveguides for DNA fragment analysis. *Lab. Chip*. **7**, 1280
63. Hsiung, S.-K., Lee, C.-H., and Lee, G.-B. (2008) Microcapillary electrophoresis chips utilizing controllable micro-lens structures and buried optical fibers for on-line optical detection. *Electrophoresis*. **29**, 1866–1873
64. Washburn, A. L., and Bailey, R. C. (2011) Photonics-on-a-chip: recent advances in integrated waveguides as enabling detection elements for real-world, lab-on-a-chip biosensing applications. *The Analyst*. **136**, 227–236
65. Guo, J., Chen, L., Huang, X., Li, C. M., Ai, Y., and Kang, Y. (2015) Dual characterization of biological cells by optofluidic microscope and resistive pulse sensor: Microfluidics and Miniaturization. *Electrophoresis*. **36**, 420–423
66. Klauke, N., Smith, G. L., and Cooper, J. M. (2007) Microfluidic Partitioning of the Extracellular Space around Single Cardiac Myocytes. *Anal. Chem.* **79**, 1205–1212
67. Xu, B., Yang, M., Wang, H., Zhang, H., Jin, Q., Zhao, J., and Wang, H. (2009) Line laser beam based laser-induced fluorescence detection system for microfluidic chip electrophoresis analysis. *Sens. Actuators Phys.* **152**, 168–175
68. Gao, J., Yin, X.-F., and Fang, Z.-L. (2004) Integration of single cell injection, cell lysis, separation and detection of intracellular constituents on a microfluidic chip. *Lab. Chip*. **4**, 47
69. Zhao, Y.-Y., and Lin, R.-C. (2014) UPLC–MSE application in disease biomarker discovery: The discoveries in proteomics to metabolomics. *Chem. Biol. Interact.* **215**, 7–16
70. Dettmer, K., Aronov, P. A., and Hammock, B. D. (2007) Mass spectrometry-based metabolomics. *Mass Spectrom. Rev.* **26**, 51–78
71. Fernie, A. R., Trethewey, R. N., Krotzky, A. J., and Willmitzer, L. (2004) Metabolite profiling: from diagnostics to systems biology. *Nat. Rev. Mol. Cell Biol.* **5**, 763–769
72. Dunn, W. B., and Ellis, David I. (2005) Metabolomics: Current analytical platforms and methodologies. *TrAC Trends Anal. Chem.* **24**, 285–294

73. Martineau, E., Tea, I., Loaëc, G., Giraudeau, P., and Akoka, S. (2011) Strategy for choosing extraction procedures for NMR-based metabolomic analysis of mammalian cells. *Anal. Bioanal. Chem.* **401**, 2133–2142
74. Weljie, A. M., Newton, J., Mercier, P., Carlson, E., and Slupsky, C. M. (2006) Targeted Profiling: Quantitative Analysis of ^{1}H NMR Metabolomics Data. *Anal. Chem.* **78**, 4430–4442
75. Soga, T., Ohashi, Y., Ueno, Y., Naraoka, H., Tomita, M., and Nishioka, T. (2003) Quantitative Metabolome Analysis Using Capillary Electrophoresis Mass Spectrometry. *J. Proteome Res.* **2**, 488–494
76. Hirayama, A., Kami, K., Sugimoto, M., Sugawara, M., Toki, N., Onozuka, H., Kinoshita, T., Saito, N., Ochiai, A., Tomita, M., Esumi, H., and Soga, T. (2009) Quantitative Metabolome Profiling of Colon and Stomach Cancer Microenvironment by Capillary Electrophoresis Time-of-Flight Mass Spectrometry. *Cancer Res.* **69**, 4918–4925
77. Ramautar, R., Demirci, A., and Jong, G. J. de (2006) Capillary electrophoresis in metabolomics. *TrAC Trends Anal. Chem.* **25**, 455–466
78. Lapainis, T., Rubakhin, S. S., and Sweedler, J. V. (2009) Capillary Electrophoresis with Electrospray Ionization Mass Spectrometric Detection for Single-Cell Metabolomics. *Anal. Chem.* **81**, 5858–5864
79. Lisec, J., Schauer, N., Kopka, J., Willmitzer, L., and Fernie, A. R. (2006) Gas chromatography mass spectrometry–based metabolite profiling in plants. *Nat. Protoc.* **1**, 387–396
80. Bajad, S. U., Lu, W., Kimball, E. H., Yuan, J., Peterson, C., and Rabinowitz, J. D. (2006) Separation and quantitation of water soluble cellular metabolites by hydrophilic interaction chromatography-tandem mass spectrometry. *J. Chromatogr. A*. **1125**, 76–88
81. Ivanisevic, J., Zhu, Z.-J., Plate, L., Tautenhahn, R., Chen, S., O'Brien, P. J., Johnson, C. H., Marletta, M. A., Patti, G. J., and Siuzdak, G. (2013) Toward 'Omic Scale Metabolite Profiling: A Dual Separation–Mass Spectrometry Approach for Coverage of Lipid and Central Carbon Metabolism. *Anal. Chem.* **85**, 6876–6884
82. Hu, Q., Noll, R. J., Li, H., Makarov, A., Hardman, M., and Graham Cooks, R. (2005) The Orbitrap: a new mass spectrometer. *J. Mass Spectrom.* **40**, 430–443
83. Lu, W., Kimball, E., and Rabinowitz, J. D. (2006) A high-performance liquid chromatography-tandem mass spectrometry method for quantitation of nitrogen-containing intracellular metabolites. *J. Am. Soc. Mass Spectrom.* **17**, 37–50
84. Goodacre, R., Vaidyanathan, S., Dunn, W. B., Harrigan, G. G., and Kell, D. B. (2004) Metabolomics by numbers: acquiring and understanding global metabolite data. *Trends Biotechnol.* **22**, 245–252
85. Xia, J., Bjorndahl, T. C., Tang, P., and Wishart, D. S. (2008) MetaboMiner – semi-automated identification of metabolites from 2D NMR spectra of complex biofluids. *BMC Bioinformatics*. **9**, 507
86. Tautenhahn, R., Patti, G. J., Rinehart, D., and Siuzdak, G. (2012) XCMS Online: A Web-Based Platform to Process Untargeted Metabolomic Data. *Anal. Chem.* **84**, 5035–5039
87. Katajamaa, M., and Orešič, M. (2007) Data processing for mass spectrometry-based metabolomics. *J. Chromatogr. A*. **1158**, 318–328

88. Smith, C. A., O'Maille, G., Want, E. J., Qin, C., Trauger, S. A., Brandon, T. R., Custodio, D. E., Abagyan, R., and Siuzdak, G. (2005) METLIN: a metabolite mass spectral database. *Ther. Drug Monit.* **27**, 747–751
89. Xia, J., Psychogios, N., Young, N., and Wishart, D. S. (2009) MetaboAnalyst: a web server for metabolomic data analysis and interpretation. *Nucleic Acids Res.* **37**, W652–W660
90. Sysi-Aho, M., Ermolov, A., Gopalacharyulu, P. V., Tripathi, A., Seppänen-Laakso, T., Maukonen, J., Mattila, I., Ruohonen, S. T., Vähätalo, L., Yetukuri, L., Härkönen, T., Lindfors, E., Nikkilä, J., Ilonen, J., Simell, O., Saarela, M., Knip, M., Kaski, S., Savontaus, E., and Orešič, M. (2011) Metabolic Regulation in Progression to Autoimmune Diabetes. *PLoS Comput. Biol.* **7**, e1002257
91. Oresic, M. (2012) Metabolomics in the Studies of Islet Autoimmunity and Type 1 Diabetes. *Rev. Diabet. Stud.* **9**, 236–247
92. Tian, L., Kim, H. S., Kim, H., Jin, X., Jung, H. S., Park, K. S., Cho, K. W., Park, S., and Moon, W. K. (2013) Changes in Metabolic Markers in Insulin-Producing β-Cells during Hypoxia-Induced Cell Death As Studied by NMR Metabolomics. *J. Proteome Res.* **12**, 3738–3745
93. Lorenz, M. A., Burant, C. F., and Kennedy, R. T. (2011) Reducing Time and Increasing Sensitivity in Sample Preparation for Adherent Mammalian Cell Metabolomics. *Anal. Chem.* **83**, 3406–3414
94. Huang, M., and Joseph, J. W. (2012) Metabolomic analysis of pancreatic β-cell insulin release in response to glucose. *Islets*. **4**, 210–222
95. Huang, M., and Joseph, J. W. (2014) Assessment of the Metabolic Pathways Associated With Glucose-Stimulated Biphasic Insulin Secretion. *Endocrinology*. **155**, 1653–1666
96. Wallace, M., Whelan, H., and Brennan, L. (2013) Metabolomic analysis of pancreatic beta cells following exposure to high glucose. *Biochim. Biophys. Acta BBA - Gen. Subj.* **1830**, 2583–2590
97. Dixon, G., Nolan, J., McClenaghan, N., Flatt, P. R., and Newsholme, P. (2003) A comparative study of amino acid consumption by rat islet cells and the clonal beta-cell line BRIN-BD11-the functional significance of L-alanine. *J. Endocrinol.* **179**, 447–454
98. Iwasaki, M., Minami, K., Shibasaki, T., Miki, T., Miyazaki, J., and Seino, S. (2010) Establishment of new clonal pancreatic β-cell lines (MIN6-K) useful for study of incretin/cyclic adenosine monophosphate signaling: Novel pancreatic β-cell lines. *J. Diabetes Investig.* 10.1111/j.2040-1124.2010.00026.x
99. Hohmeier, H. E., Mulder, H., Chen, G., Henkel-Rieger, R., Prentki, M., and Newgard, C. B. (2000) Isolation of INS-1-derived cell lines with robust ATP-sensitive K+ channel-dependent and-independent glucose-stimulated insulin secretion. *Diabetes*. **49**, 424–430
100. Li, C., Liu, C., Nissim, I., Chen, J., Chen, P., Doliba, N., Zhang, T., Nissim, I., Daikhin, Y., Stokes, D., Yudkoff, M., Bennett, M. J., Stanley, C. A., Matschinsky, F. M., and Naji, A. (2013) Regulation of Glucagon Secretion in Normal and Diabetic Human Islets by γ-Hydroxybutyrate and Glycine. *J. Biol. Chem.* **288**, 3938–3951

CHAPTER 2
Sequential Detection of $[Ca^{2+}]_i$ and Insulin Secretion On-Chip

Introduction

Type 1 diabetes, a disease characterized by an inability to properly regulate blood glucose levels, is caused by autoimmune destruction of insulin-secreting β-cells found in the islets of Langerhans of the pancreas. A promising treatment for type 1 diabetes (currently in stage 3 clinical trials) is islet transplantation, which involves infusion of donor islets into the portal vein in the recipient's liver. More recently, alternate insertion sites, such as a subcutaneous, pre-vascularized site, have shown potential in animal studies (1). Islet transplantation is minimally invasive and has a lower risk of complications than current treatments, such as whole pancreas transplantation. However, islet transplantation has not been as successful as anticipated. Many times, patients need several islet infusions to obtain insulin-independence, and the rates of long-term insulin-independence (~55%, sustained over 5 years) have been low in comparison to whole pancreas transplantation (2).

One possible contribution to this low success rate is inadequacy of current methods in determining the viability and potency of an islet preparation prior to transplantation. Viability is currently measured using fluorescein diacetate/propidium iodide (FDA/PI) to assess membrane integrity (3). This test, however, does not account for early apoptotic cells, and does not correlate with clinical results. The current standard for determining potency is the diabetic nude mouse bioassay (NMB), in which islets are transplanted into a diabetic, immunodeficient mouse to determine whether they will reverse diabetes. The NMB correlates well with islet transplantation success, but it can only be used retroactively, because several days to weeks are required to determine the outcome of the test. Static glucose-stimulated insulin secretion (GSIS), as measured through

enzyme-linked immunosorbent assay (ELISA), has been used to evaluate islet potency prior to transplantation; however, the results have not correlated well with clinical outcome (3). The reason for this lack of correlation is unknown, though there are several plausible explanations. For example, the static GSIS test measures only bulk insulin release and does not capture the dynamics of insulin secretion, such as first and second phase and oscillations that may be better indicators of β-cell function (4). Additionally, stresses from isolation could temporarily impair insulin secretion from otherwise viable islets (5).

Researchers have been working to develop assays that can successfully predict clinical outcomes prior to transplantation. Work has focused on measuring cell membrane integrity (6), oxygen consumption rate (OCR) (5, 7, 8), ATP/ADP ratio (9, 10), and dynamic GSIS (3). Several of these tests have shown promise in predicting islet transplant outcome. One study that screened human islet preparations via GSIS, ATP/ADP ratio, and mitochondrial membrane potential prior to transplantation in mice showed that each of these measures demonstrates some predictive power for transplant outcome, but a combination of all three provides the highest success rate (85.7%) in islet classification (11). However, because this study measured each component separately, the total time required to run such an evaluation is not conducive to islet transplant requirements. Incorporating simultaneous measurements of several predictors of islet health and function in a single microfluidic system could allow more rapid analysis.

To address multimodal detection of islet function on-chip, a device dubbed the chemistrode has been devised to measure $[Ca^{2+}]_i$, insulin, and glucose. In this method, the chemistrode is brought into contact with a single islet. Stimulus plugs are introduced to the islet surface, and response plugs containing perfusate are collected for later analysis (12). However, this method can only measure single islets, and total analysis time is >24 h. Alternatively, a microfluidic device has been developed to measure calcium influx and mitochondrial membrane potential changes from batches of 25-30 islets in response to glucose stimulation at established gradients. Perfusate from the

chip is collected, and GSIS is determined by ELISA (4, 13). While this system is able to measure islet potency via several different parameters, ELISA is time-consuming, labor-intensive, high volume (100-200 µL per assay), costly (over $5 per assay on average), and slow. One 30 min glucose stimulation experiment with fractions collected every minute would require 30 individual assays alone, and take several hours following the experiment to complete.

An alternative to ELISA is microchip electrophoresis immunoassay (MCE-IA), which involves solution-phase reaction of antigen with antibody prior to separation of the antigen-antibody complex from the free molecules and detection. A chip has previously been developed to measure dynamic GSIS from single islets. Using this device, down to 6 s temporal resolution and 0.8 nM insulin detection limits are achieved, allowing rapid measurements of insulin secretion dynamics (14). We aimed to couple MCE with $[Ca^{2+}]_i$ measurements to achieve rapid multimodal evaluation of islets.

A difficulty with multimodal detection is that $[Ca^{2+}]_i$ requires fluorescent measurements in the islets, while MCE requires fluorescent measurement at a different point on the same chip. Placing two standard microscope objectives in close proximity is impractical, thus an alternative strategy is required. Several methods of performing multi-point fluorescence measurements have been described; however, they require extensive fabrication and/or complex instrumentation (15, 16). One study solves this problem by making sequential measurements and moving the objective. In that study, a microfluidic device is used to isolate and lyse single erythrocytes prior to CE separation and LIF detection of cellular GSH. Cell loading is observed with a confocal microscope, and then the chip is shifted to measure LIF detection of GSH with the same microscope (17).

In our work, both measurements needed to be made simultaneously ($[Ca^{2+}]_i$ flux and insulin secretion). To use the same microscope for both measurements, we had to decouple the events in time so that they could be measured sequentially. We thus developed a facile method for collecting perfusate during glucose stimulation to be analyzed following the completion of the $[Ca^{2+}]_i$ measurements. We compared the

sensitivity and temporal resolution of perfusate collected in a capillary (continuous flow collection) to perfusate collected in a well plate and converted into plugs segmented with oil for introduction of small volumes into a CE chip (segmented flow collection). Both methods achieved faster analysis times and were less expensive to operate than existing multimodal microfluidic devices for islet evaluation. This system demonstrates a simple and cost-effective method for rapid detection of multiple analytes in a microfluidic system.

Experimental Procedures

Materials

Electrophoresis buffers were: balanced salt solution (BSS), consisting of 125 mM NaCl, 5.9 mM KCl, 1.2 mM $MgCl_2$, 2.4 mM $CaCl_2$, 25 mM tricine, and 0.7 mg mL^{-1} BSA; immunoassay buffer, consisting of 60 mM NaCl, 1 mM EDTA, 20 mM tricine, 0.1% (w/v) Tween-20, and 0.7 mg mL^{-1} BSA; and electrophoresis buffer, consisting of 20 mM NaCl and 150 mM tricine. All buffers were adjusted to pH 7.4.

Roswell Park Memorial Institute (RPMI) culture medium, fetal bovine serum, penicillin-streptomycin, collagenase, fura-2 dye, and anti-insulin antibody were purchased from Life Technologies (Carlsbad, CA). Fluorescein isothiocyanate-labeled insulin (FITC-insulin) was purchased from Sigma-Aldrich (St. Louis, MO). All other chemicals were purchased from Thermo Fisher Scientific (Waltham, MA).

Cell Culture

Pancreatic islets were isolated from 20-30 g male CD-1 mice as previously described (18). Islets were cultured in RPMI-1640 media supplemented with 11 mM glucose, 10% fetal bovine serum, and 1% penicillin/streptomycin at 37 ºC and 5% CO_2 for 2-5 days prior to experimentation.

Glass Microfluidic Chip Fabrication

Glass microfluidic chips were fabricated as previously described (19). Briefly, blank 2.5 cm x 7.6 cm x 1.1 mm glass slides coated with a 530 nm thick layer of AZ1518 positive

photoresist over a 120 nm chrome layer (Telic Co., Santa Monica, CA) were exposed to collimated UV light through patterned photomasks for 5 s. The exposed slides were developed in AZ726 MIF Developer (Microchemicals) for 30 s, and the underlying chrome was removed using CEP-200 Chrome Etchant (Microchrome Technologies, Inc., San Jose, CA). The exposed glass was etched in a solution of 14:20:66 (v/v/v) HNO_3/HF/H_2O for variable times depending on desired channel depth. Multiple channel depths were formed on a single chip by protecting desired channels with HF-resistant tape for a portion of the etching time. Carbide drill bits (Kyocera Precision Tools, Inc., Hendersonville, NC) were used to drill 360 µm diameter access holes and 750 µm diameter islet chambers. The remaining photoresist and chrome were then removed using acetone and CEP-200 chrome etchant, respectively, and the etched glass plates were cleaned in piranha solution (3:1 v/v H_2SO_4/H_2O_2) for 20 min followed by heated RCA solution (5:1:1 v/v/v H_2O/NH_4/H_2O_2) for 40 min. Chips were aligned under water (taking care to align any features etched into both halves of the chip under a microscope), dried, and annealed at 640 ºC for 8 h. Microfluidic reservoirs (Upchurch Scientific, Oak Harbor, WA) were applied over access holes after bonding. Capillaries (40 µm i.d. x 150 µm o.d.) were inserted into capillary channels and glued in place by wicking heat-sensitive epoxy into the channel over a hot plate and then rapidly cooling. Care was taken to ensure epoxy did not flow into the microfluidic channels. Capillaries were then cut to size, and if necessary, a sheath capillary (185 µm i.d. x 360 µm o.d.) was epoxied over the inserted capillary to allow connections to other capillaries to be made.

PDMS Microfluidic Chip Fabrication

Multilayer PDMS microfluidic devices were fabricated using soft photolithography as previously described (20). Degassed PDMS (10:1 polymer base/curing agent) was poured into three master molds, taking care to keep thickness of the bottom layer <1 mm to be compatible with the working distance of the microscope. After the PDMS was cured, access holes were created using a 14 gauge hole punch and the layers were bonded together using plasma treatment. Novec 1720 (3M, St. Paul, MN) was perfused through the device to coat the channel walls and prevent absorption of analyte

molecules into the PDMS during experimentation. After all visible bubbles had disappeared and the channel walls were entirely wet, the device was heated to 130 ºC on a hot plate for 15 min. Once cooled, microbore tubing (Cole-Palmer, Vernon Hills, IL) was inserted into the outlet and "glued" into place using tacky PDMS that was then cured. The completed device consisted of three layers: the top layer contained perfusion channels; the middle layer consisted of a 2.5 mm diameter x 1 mm depth islet chamber and the reagent mixing channels; and the bottom layer contained an array of 500 µm diameter x 150 µm depth wells to immobilize the islets. An image of the assembled device is shown in Figure 2.1.

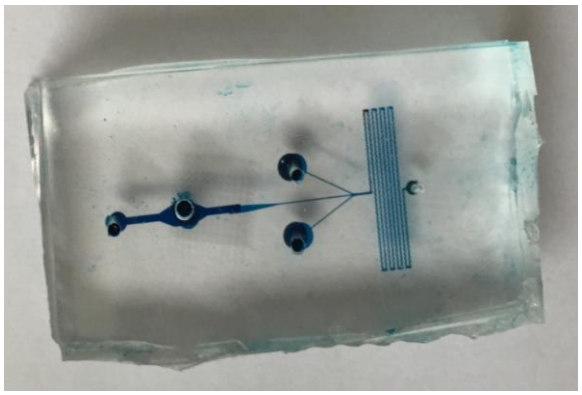

Figure 2.1. Image of PDMS chip for fraction collection, filled with food dye for visualization of channels.

PDMS Extraction Device Fabrication

PDMS tees used to align droplet tubing with glass electrophoresis chips were formed using a pour over method as previously described (21).

Calcium Flux Measurements

$[Ca^{2+}]_i$ was measured using fura-2 dye as previously described (22). Briefly, islets were loaded with 2 µM fura-2-AM via a 45 min incubation. They were then rinsed briefly with BSS and loaded into a microfluidic chamber, where they were perfused with BSS containing basal (3 mM) and stimulatory (11-14 mM) levels of glucose. The dye was excited alternately with 340 nm (Ca^{2+}-complexed dye) and 380 nm (free dye) light and emission was collected at 510 nm. The ratio of complexed to free dye was calculated

and converted to Ca^{2+} concentrations using calibration standards as described before (22).

Insulin Secretion Measurements

Insulin secretion was measured by microchip electrophoretic competitive immunoassay as previously reported (14, 23). Briefly, electrophoresis chips were conditioned with 0.1 mM NaOH using a vacuum pump attached to the waste reservoir, followed by ddH_2O, followed by electrophoresis buffers. Secreted insulin, FITC-insulin, and anti-insulin antibody were sampled by electroosmotic flow (EOF) and mixed, after which they were injected onto a separation channel in 5 or 8 s intervals using a flow-gated injection. Laser-induced fluorescence at the end of the separation channel was detected using a photomultiplier tube (PMT). Instrument control and data collection were regulated by a LabVIEW program (National Instruments, Austin, TX) (23). High throughput peak analysis of the collected electropherograms was accomplished using Cutter software (24). The ratio of FITC-insulin bound to antibody to FITC-insulin free in solution (B/F) was calculated and converted to insulin concentrations using calibration standards.

Sequential Detection of $[Ca^{2+}]_i$ and Insulin Secretion with Continuous Flow Collection

Groups of 7-10 islets were loaded into a 0.44 mm^2 cell chamber on a glass microfluidic chip. A schematic of the chip design is shown in Figure 2.2. The chamber was plugged with a piece of PDMS that had been punched out of a larger slab using a 17 gauge hypo tube (Small Parts, Inc., Logansport, IN) and cut to size. The plug naturally flared out, so when it was inserted into the chamber, the edge of the plug remained above the surface of the hole, making removal of the plug straightforward so that the chip could be re-used. Islets were perfused at a rate of 1.3 µL min^{-1} with basal (3 mM) and stimulatory (11 mM) levels of glucose using helium pressure. Channels were designed to fan out leading into and from the islet chamber; this design improved the flow through the chamber as compared to a single inlet and outlet, thus allowing all islets to be stimulated simultaneously regardless of their position in the chamber (Figure 2.2a and Figure 2.3a). A thin film resistor taped to the bottom of the chip maintained the cell chamber at 37 ºC.

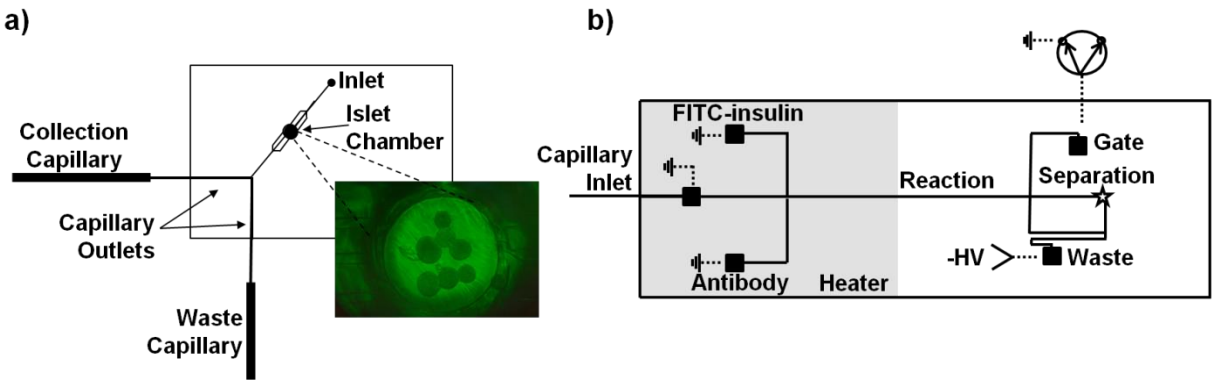

Figure 2.2. Schematic of capillary collection chips. a) Islets were placed in a chamber (inset) and perfused with basal and stimulatory levels of glucose at 1.3 µL min^{-1}. Perfusate was collected in a 75 µm i.d. capillary attached via one capillary outlet, while a 2nd capillary acted as a flow split. b) The collection capillary was detached from the perfusion chip and attached to the inlet of an electrophoretic chip. Perfusate and reagents were sampled by EOF. Secreted insulin, FITC-insulin, and anti-insulin antibody mixed and reacted, after which they were injected onto a separation channel (0.5 s injection, 8 s interval). FITC-insulin-antibody complex and free FITC-insulin were separated based on size and charge and were detected by LIF at the end of the separation channel.

$[Ca^{2+}]_i$ was measured via fluorescence imaging while perfusate was collected in a 75 µm i.d. x 360 µm o.d. capillary. A second, waste capillary was also attached to the chip to reduce the flow rate into the collection capillary and allow for longer collection time. Sample could be collected for 25-30 min in a 330 cm long capillary. Following collection, the capillary was transferred to a glass electrophoresis chip. Typically, perfusion reservoirs are used to introduce fluid into a chip; however, commercially available reservoirs introduce a void volume that can result in band broadening. In order to maintain as high temporal resolution as possible, capillaries were inserted directly into inlet and outlet channels etched on the perfusion and electrophoresis chips (Figure 2.2). The perfusate was pumped into an open reservoir on the electrophoresis chip at a rate of ~0.9 µL min^{-1}, from which it was then sampled by electroosmotic flow. Insulin was detected by electrophoretic competitive immunoassay as described above.

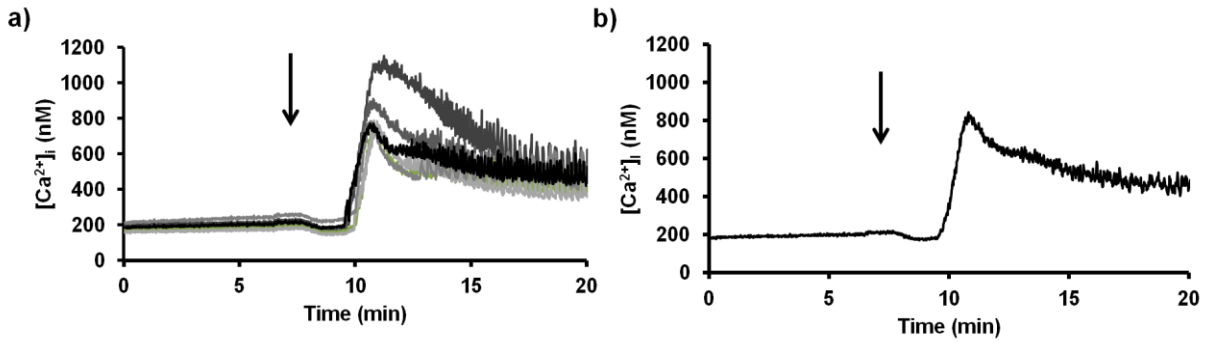

Figure 2.3. $[Ca^{2+}]_i$ measurements on-chip. a) Individual islets (plotted as separate traces) responded to glucose stimulation simultaneously in a 0.75 mm diameter chamber with fanned chamber inlet/outlet design. Following an initial abrupt influx of Ca^{2+}, $[Ca^{2+}]_i$ oscillated rapidly in individual islets. b) The averaged $[Ca^{2+}]_i$ response from the individual traces in (a) did not exhibit oscillations because of varying oscillation frequencies in individual islets. Arrows indicate time of glucose stimulation. Basal and stimulatory glucose concentrations were 3 and 11 mM, respectively.

Sequential Detection of $[Ca^{2+}]_i$ and Insulin Secretion with Segmented Flow Collection

Prior to each use, the PDMS-based perfusion chamber was conditioned with ethanol for 15 min followed by KRB supplemented with 3 mM glucose. Groups of 20 islets were loaded into the chamber and the chamber was plugged with a closed-tipped connector. A thin film resistor was taped to the bottom of the device to maintain the cell chamber at 37 ºC. Islets were then perfused with basal (3 mM) and stimulatory (14 mM) levels of glucose at a flow rate of 2.5 µL min^{-1} using a syringe pump. FITC-labeled insulin and anti-insulin antibody were pumped into the chip at flow rates of 1 µL min^{-1} each, where they mixed with the perfusate from the islets. The mixed insulin, FITC-insulin, and antibody flowed from the outlet of the microfluidic device into a low-volume 384-well plate. Samples were collected in 2.5 min intervals. Insulin standards (1-500 nM) were added to the adjacent wells.

Perfluorinated oil (100:1 PFD/PFO) was added on top of the wells (the well plate had previously been built-up with epoxy and derivatized using Teflon spray to allow the oil phase to remain on top of the less-dense aqueous phase). The well plate was placed on an xyz stage, which was controlled by a computerized program. A syringe pump operated in reverse mode was used to pull alternating plugs of oil and sample into a 150

μm i.d. x 360 μm o.d. HPFA+ tube (Idex Health & Science, Oak Harbor, WA). Each well was sampled 10 times, creating 10 droplets from each well.

To then separate the aqueous droplets from the oil for insulin detection, the tube containing the droplets was inserted into a PDMS extraction device, shown in Figure 2.4, as previously described (21). An electrophoresis chip with a 40 μm i.d. x 150 μm o.d. x 4 mm length inlet capillary was inserted into the extraction device perpendicular to the droplet tube, so that the outlet of the tube and the inlet of the capillary were in close proximity. A second capillary filled with food dye was inserted into the extraction device in the waste channel to provide some additional back pressure. When droplets were pumped into the device at a flow rate of 0.3 μL min^{-1}, aqueous sample droplets were extracted across the hydrophilic capillary into the electrophoresis chip. Oil was excluded from the capillary, and continued down the PDMS waste channel. Insulin was then detected by electrophoretic competitive immunoassay.

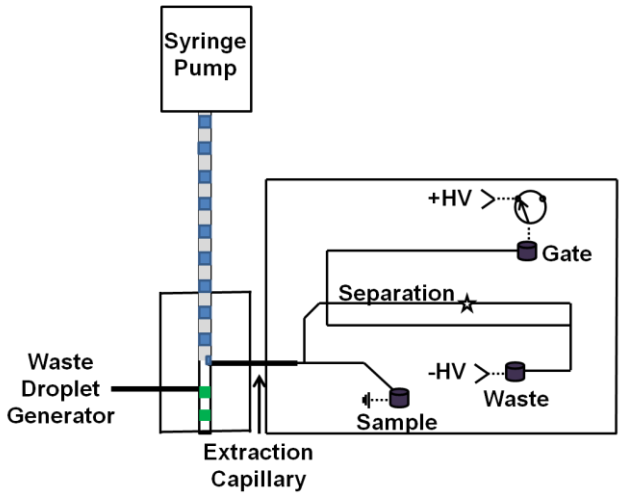

Figure 2.4. Schematic of microfluidic devices for aqueous droplet extraction and analysis. Droplets containing secreted insulin, FITC-insulin, and anti-insulin antibody were pumped into a PDMS device (left) at 0.3 μL min^{-1}. Aqueous sample was extracted across the hydrophilic capillary into an electrophoresis chip while oil continued to waste. A waste droplet generator added back pressure to improve extraction efficiency. Extracted aqueous solution was sampled by EOF, and then injected onto a separation channel (0.2 s injection, 5 s interval). FITC-insulin-antibody complex and free FITC-insulin were separated based on size and charge and were detected by LIF at the indicated location in the separation channel. Adapted with permission from reference 21. Copyright 2014 ACS.

Alignment of Sequentially Collected Data

Because $[Ca^{2+}]_i$ data was collected in real time and insulin data was collected from stored samples, it was necessary to report insulin data based on its collection time instead of its analysis time. To align the peaks from each measurement, we added a fluorescent tracer to the perfusion solution (either fluorescein or rhodamine) to indicate when a step change from basal to stimulatory glucose concentration was made. We also accounted for differences in flow rates between measurements for the continuous flow collection method. For the segmented flow collection method, 10 droplets were collected from each well; the measurements from replicate droplets were averaged together for each time point.

Statistical Analysis

Error bars are expressed as means ± 1 standard deviation unless otherwise specified.

Results

In this work, we explored the possibility of collecting samples from islets while $[Ca^{2+}]_i$ was measured, and then assaying the collected samples for secreted insulin by electrophoresis. Samples were collected and analyzed in a way that preserved the temporal insulin secretion profile and therefore allowed both time-resolved $[Ca^{2+}]_i$ and secreted insulin to be measured. We developed two methods for collection and electrophoretic analysis. In the first, depicted in Figure 2.2, perfusate from an islet chip was collected in a narrow bore (75 µm i.d.) capillary and infused into an electrophoresis chip for insulin detection. In the second, shown in Figure 2.4, perfusate from an islet chip was collected as fractions in a 96-well plate. Fractions were sampled into tubing as aqueous droplets segmented with oil. The droplets were de-segmented immediately prior to infusion into an electrophoresis chip for insulin measurement. Our results showed that detection limits and electropherogram stability were similar for both methods, but the continuous flow collection method was less manually intensive and simpler to implement.

Electropherogram Reproducibility

Electropherogram reproducibility over the time span of a typical experiment (30 min) was ~10% RSD in B/F for both electrophoresis chip designs with no added insulin. To measure day-to-day electropherogram reproducibility of a single chip, calibrations were recorded on 3-5 separate days. Average RSD in B/F for standard insulin concentrations was 10 ± 3% for the continuous flow collection method (Figure 2.5a) and 25 ± 12% for the segmented flow collection method (Figure 2.5b). This drift in signal could be due to possible differences in conditioning or clogging in the channels. Chips were calibrated daily to account for this drift. Average RSD in B/F for three separate calibrations taken on a single day (n = 3 days) was 11 ± 3% for the segmented flow chip, which was similar to electropherogram stability throughout a single experiment. This indicated that calibrating daily should be sufficient for accurately measuring insulin concentrations.

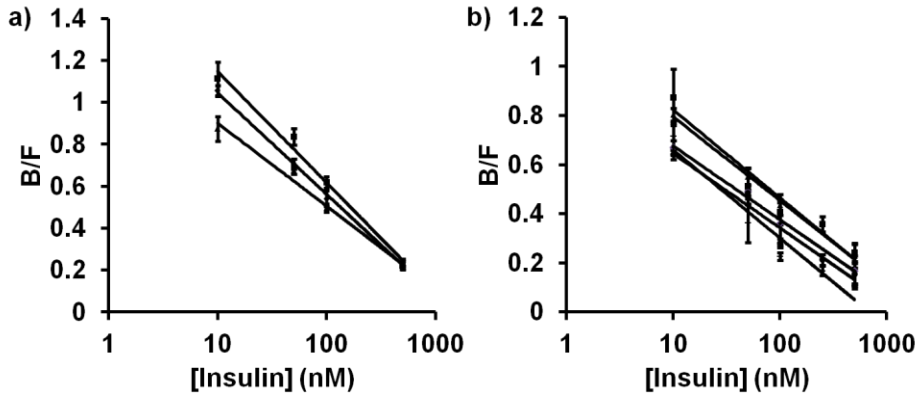

Figure 2.5. Insulin immunoassay reproducibility. Day-to-day variations in insulin calibrations using a) continuous flow collection b) segmented flow collection. Error bars represent 1 standard deviation.

Continuous Flow Collection Method

The insulin secretion assay was calibrated by flowing insulin standards through the perfusion chip, collecting them in the capillary, and then pumping them into the electrophoresis chip. A plot of B/F against time during infusion of the capillary is shown in Figure 2.6a. An overlay of the insulin concentrations, corrected to reflect the time points at which they were collected instead of the times at which they were analyzed, shows the correlation between the B/F and the concentration input. The average LOD,

calculated as the concentration required to give a B/F lower than 3x the standard deviation of the blank, was 19 ± 10 nM (n = 3). This was below the expected basal concentrations of insulin secretion from groups of 7-10 islets, so it was adequate for our islet experiments. A representative calibration plot obtained from this data is shown in Figure 2.6b, with good fit (R^2 = 0.987) to a logarithmic curve.

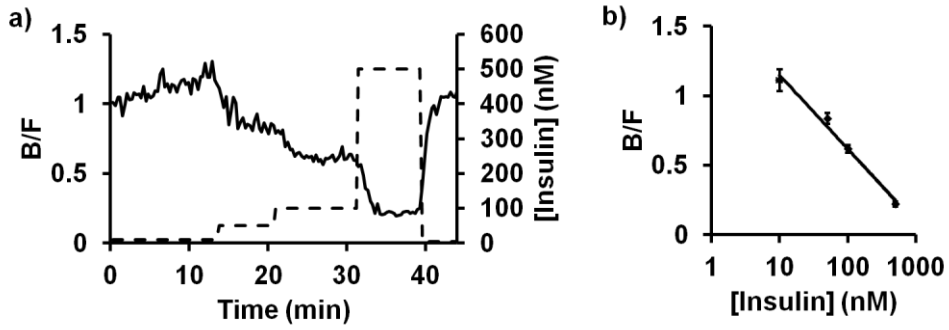

Figure 2.6. Representative calibration of standard insulin using continuous flow collection method. a) Temporal trace, with resolution of 84 ± 15 s. B/F (solid line) corresponding to standard insulin concentrations of 10, 50, 100, and 500 nM (dashed line) was measured. b) Calibration showed good fit to a logarithmic curve (R^2 = 0.987). Error bars represent 1 standard deviation.

We then evaluated the temporal resolution of this collection method. The fall time, measured as the amount of time it required the signal to drop from 90% average intensity of one concentration to 110% average intensity of the following concentration, was calculated to be 84 ± 15 s (n = 4). Insulin secretion dynamics are on the order of minutes (1st phase insulin secretion typically lasts for 2-5 min following glucose stimulation, with slow changes in second phase). Based on these dynamics, 84 s temporal resolution should be adequate for recording first and second phase insulin secretion dynamics. Insulin secretion in single islets can oscillate in 2nd phase with periods of 3-5 min. Islets in groups can be entrained to all oscillate with the same frequency under some conditions (25), but in most cases, oscillation frequencies differ between individual islets and tend to offset each other. Consequently, we were not concerned with having sufficient temporal resolution for oscillations at this stage.

To test the method, we measured $[Ca^{2+}]_i$ and insulin secretion from groups of 7-10 islets. Islets were perfused with basal levels of glucose for 60 min followed by

stimulatory levels of glucose for 15 min. Fluorescein was spiked into the stimulatory glucose to act as a tracer to determine when the change from basal to stimulatory glucose levels was made in the insulin plot. This facilitated temporal matching of the different traces. Fluorescein migrated slower than the bound and free peaks, so it did not interfere with detection of insulin secretion (Figure 2.7). Representative averaged $[Ca^{2+}]_i$ data is shown in Figure 2.8a, and representative time-corrected insulin data is shown in Figure 2.8b, demonstrating measurement of 1st phase and 2nd phase secretion dynamics. The average basal insulin concentration measured was 25 ± 10 pg min^{-1} $islet^{-1}$, and the average maximum insulin release during 1st phase secretion was 195 ± 91 pg min^{-1} $islet^{-1}$ (n = 5). Typical values reported in islets are 30-50 pg min^{-1} $islet^{-1}$ and 100-200 pg min^{-1} $islet^{-1}$ for basal and 1st phase secretion, respectively, so our results were comparable (23, 26). The average first phase peak width was 3.0 ± 0.9 min; this was comparable to $[Ca^{2+}]_i$ data and similar to expected first phase peaks of 2-5 min (27). Second phase secretion was elevated above basal levels, but oscillations in insulin secretion were skewed or not present, probably due to varying oscillation frequencies between individual islets, as demonstrated in Figure 2.3b with $[Ca^{2+}]_i$ oscillations.

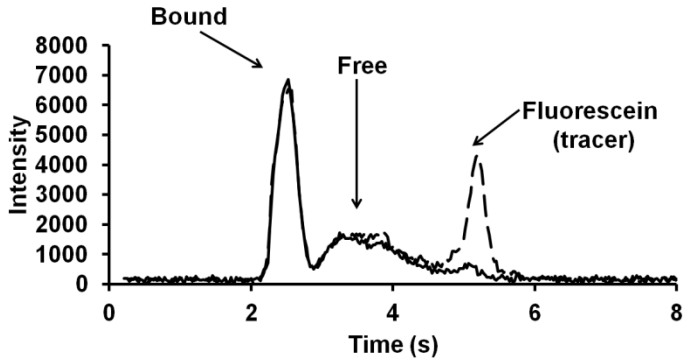

Figure 2.7. Electropherogram with fluorescein tracer. Fluorescein migrated following the bound and free peaks, and thus could be added to perfusion solutions to act as a tracer without interfere with insulin measurements. Dashed and solid lines represent traces with and without added fluorescein, respectively.

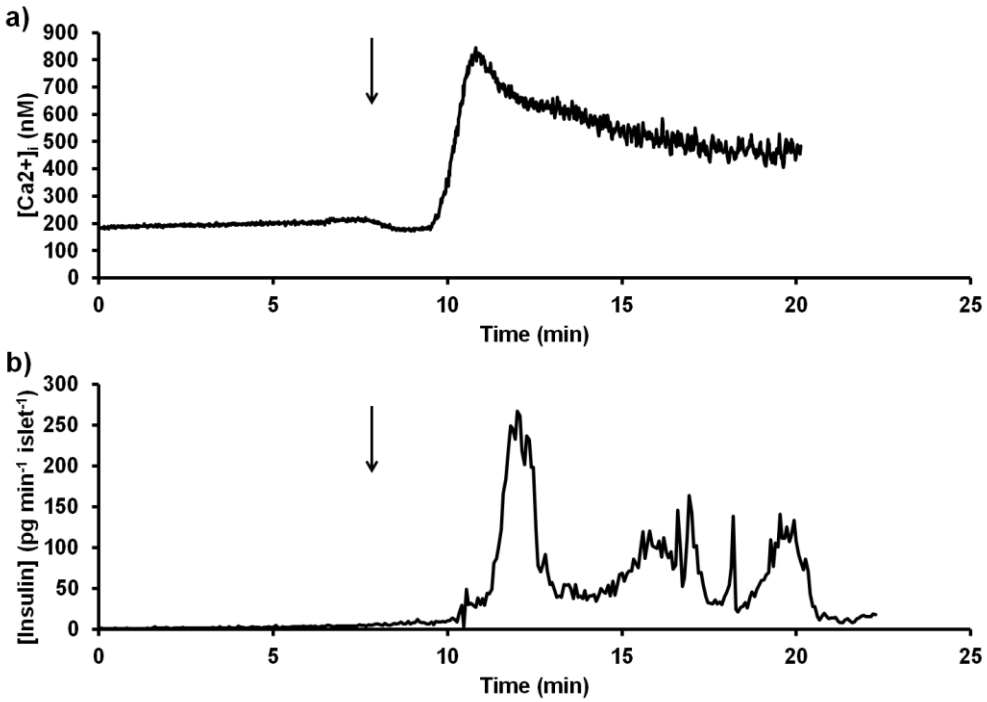

Figure 2.8. Measurement of $[Ca^{2+}]_i$ and insulin secretion from a representative group of 8 islets using continuous flow collection method. Traces shown for a) averaged $[Ca^{2+}]_i$ and b) secreted insulin. Arrows indicate time of stimulation with 11 mM glucose. Basal glucose concentration was 3 mM.

Segmented Flow Collection Method

As an alternative method for perfusate collection, we tested a segmented flow collection strategy. We calibrated the insulin immunoassay using insulin standards, as shown in Figure 2.9. The LOD was calculated to be 2.4 ± 1.0 nM insulin (n = 4). By injecting sample onto the separation channel every 5 s, we were able to measure ~10 electropherograms per insulin concentration; since 10 droplets were collected at each concentration, this corresponded to ~1 electropherogram per droplet. It took 3 droplets to wash the previous droplet from the sampling channel, so these "carry-over" droplets between concentrations were not included in averaged concentration data.

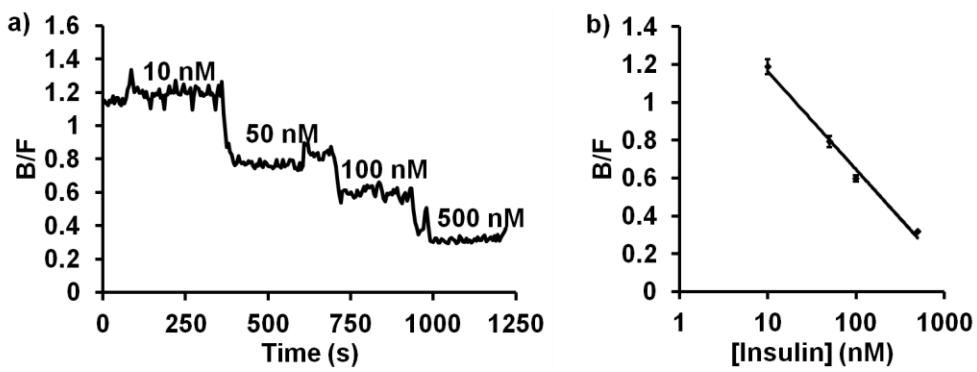

Figure 2.9. Representative calibration of standard insulin using droplets generated from a 96-well plate. a) Temporal trace of experiment. B/F corresponding to standard insulin concentrations of 10, 50, 100, and 500 nM was measured. Three injections (15 s), corresponding to 3 droplets, were required to completely wash out the sampling channel. b) Calibration showed good fit to a logarithmic curve, with R^2 = 0.9897. Error bars represent 1 standard deviation.

We then measured $[Ca^{2+}]_i$ and insulin secretion from a group of 25 islets. Rhodamine 110 was spiked into the stimulatory glucose to act as a tracer for when the switch from basal to stimulatory levels of glucose occurred. Rhodamine was selected instead of fluorescein, which we used in the prior experiments, because the peak migrated earlier in the electropherograms than the analyte peaks instead of later (Figure 2.10). Therefore, no sacrifices needed to be made in injection time. Averaged $[Ca^{2+}]_i$ data from the 7 islets imaged is shown in Figure 2.11a, and the corresponding insulin data for the experiment is shown in Figure 2.11b. The basal insulin secretion was 11 ± 1 pg min^{-1} $islet^{-1}$, and the maximum 1st phase insulin secretion was 108 ± 33 pg min^{-1} $islet^{-1}$ (n = 1). These results were similar to those previously reported (14, 22) as well as those obtained using the capillary collection method, and demonstrated the ability of the sequential detection method to distinguish 1st and 2nd phase insulin secretion dynamics.

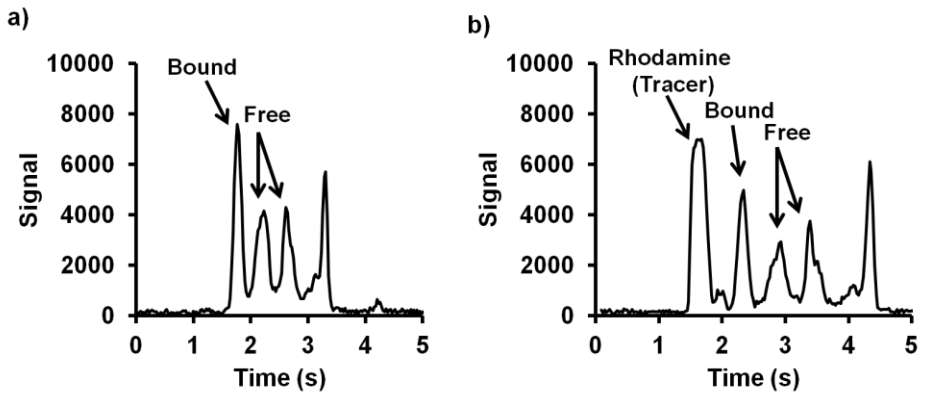

Figure 2.10. Electropherograms with and without rhodamine tracer. Rhodamine eluted before bound and free peaks, allowing maintenance of fast separation times without interfering with insulin detection.

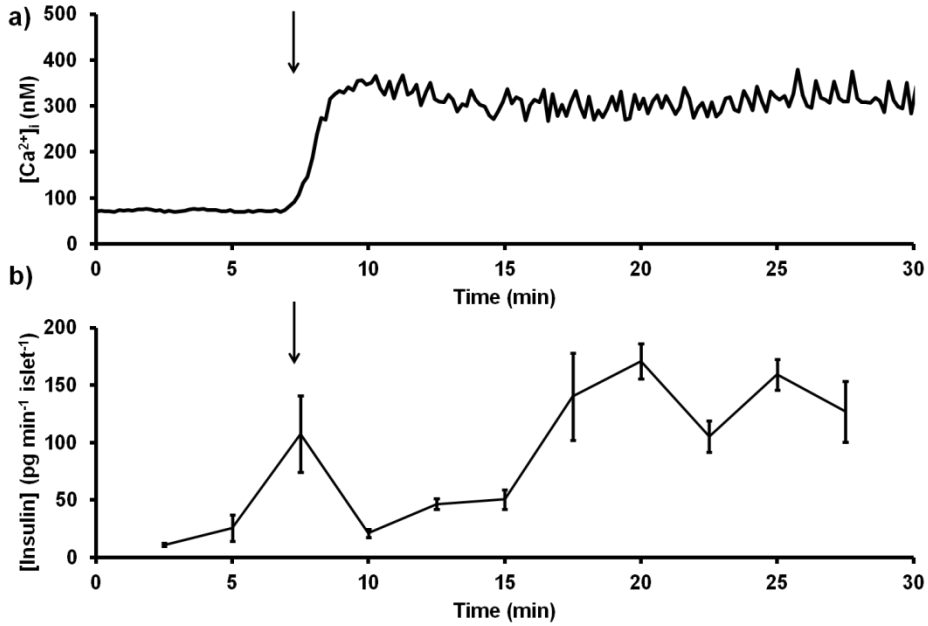

Figure 2.11. $[Ca^{2+}]_i$ and insulin secretion measured from 20 islets with segmented flow collection method. Representative traces shown of a) averaged $[Ca^{2+}]_i$ from 7 islets (those in the microscopic field of view) and b) insulin secretion. Each time point corresponded to averaged insulin concentrations measured from 9 injections of replicate samples. Arrows indicate time of stimulation with 14 mM glucose. Basal glucose was 3 mM. Error bars represent SEM.

Discussion

We have developed a simple, cost-effective method for collecting cellular secretions from microfluidic devices while retaining temporal information. This method provided the ability to monitor cells optically on-chip and later measure cellular secretions via LIF

using the same microscope; by decoupling the two measurements, no specialized optical equipment was required. We applied this system to measuring $[Ca^{2+}]_i$ and insulin secretion from islets. By using a multimodal method, we aimed to achieve a more holistic view of islet health than by using either of these measures alone. Because the measurements were made on a microfluidic chip, the analytes could be measured and analyzed more rapidly than with traditional methods, making this method compatible with requirements of islet evaluation prior to transplantation.

Insulin Limits of Detection

Insulin detection limits were in the low nM range (2-20 nM) for both the continuous flow and segmented flow collection methods. Previous studies using similar chip-based immunoassays for insulin have reported detection limits below 1 nM (23, 24, 26). A possible reason for this loss in sensitivity could be due to differences in the fluorescently-labeled insulin used for the studies. While previous studies reported only one peak due to FITC-insulin free in solution, we detected two separate free peaks. This is likely due to a difference in labeling. FITC is functionalized with an isothiocyanate reactive group, which can react with amine and sulfhydryl groups. Insulin contains two reactive amine groups, so it is possible for each molecule of insulin to be either singly or doubly labeled (28). While the FITC-insulin used in previous studies was likely all doubly labeled, the FITC-insulin used here contained both types of labels, resulting in differences in electrophoretic mobility and thus 2 separate peaks. This difference in labeling could contribute to differences in B/F determination or interactions with antibody that may have resulted in higher detection limits. Nonetheless, the detection limits were low enough to detect basal levels of insulin secretion from groups of islets as required for this study.

Temporal Resolution of Insulin Detection

When collecting continuous perfusate in a capillary, one concern was that diffusion in the capillary would greatly reduce the temporal resolution of the system. Reducing the inner diameter of the capillary can limit diffusion; however, narrow capillary sizes also limit the collection time possible because the increased back pressure could cause the

chip to leak at the point of connection and/or the cell chamber could feel this pressure. Additionally, narrower bore capillaries can clog easily, affecting the flow rate through the capillary and interfering with accurate timescale analysis of insulin secretion. We found that 75 µm i.d. capillaries were the smallest we could use without leaking when used in conjunction with a second, waste capillary. With this capillary size, the temporal resolution of the system was 84 ± 15 s (n = 4). By comparison, the temporal resolution on a single-chip system was measured to be 53 ± 10 s (n = 2) using similar perfusion flow rates (1.35 µL min^{-1}), so we obtained 1.6-fold worse resolution due to diffusion in the capillary (Figure 2.12).

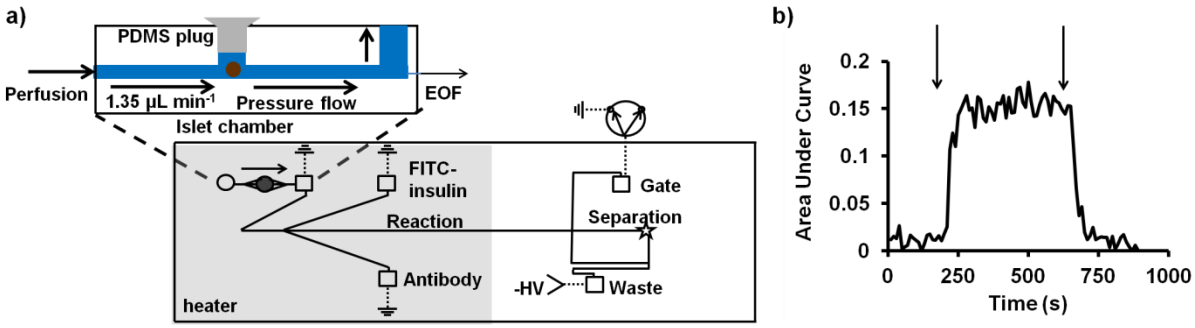

Figure 2.12. Design and performance of single channel electrophoresis chip. a) Islets were inserted into the islet chamber, which was then plugged with a PDMS plug (illustrated in inset). Islets were perfused with basal and stimulatory levels of glucose at a rate of 1.35 µL min^{-1}. The sample flowed into an open reservoir, which was sampled by EOF. b) By adding or removing fluorescein from the perfusion solution (as indicated by arrows), the temporal resolution of the system was measured to be 53 ± 10 s.

Using segmented flow, we could prevent diffusion during sample collection and maintain high temporal resolution. In order to segment the perfusate, we collected fractions in a well plate that were then sampled alternately with oil using a syringe pump operated in reverse-flow mode. In this instance, the temporal resolution was limited by the fraction size. Because we were using low-volume 384-well plates (50 µL volume), we needed to collect 10 µL per well to ensure sampling of the aqueous solution. At the flow rates used, this translated to 2.5 min collection times. Speeding up the flow rates to achieve higher temporal resolution was not an option, because the insulin concentrations would have been diluted below the limit of detection.

Because the fraction volume was limited by the well plate and not the assay, there are several methods that can be used to easily reduce the temporal resolution. One option is to collect fractions in a 1536-well plate (2 µL volume). Using smaller wells, we could reduce the collection time to 5-10 s per well. Another advantage of reducing the well sizes is that it would increase the surface-to-volume ratio in the wells. Although the wells were derivatized with a Teflon spray prior to use to maintain the perfluorinated oil phase on top of the less dense aqueous phase, we found that the phases would sometimes flip mid-experiment. This was especially prevalent in islet perfusate samples, since the BSA and tween-20 present in the samples (necessary to block adsorption of proteins and reagents to microchannel walls) reduced the surface tension as compared to other samples without these additives. By maintaining a higher surface-to-volume ratio in the wells, a higher ratio of the oil would be in contact with the derivatized well walls, and the samples would be less likely to flip.

While there are advantages to collecting fractions in smaller wells, one must consider that the trade-off for improved temporal resolution is that instead of collecting 10 wells in 25 min, we would be collecting 150-300 wells in the same time frame. In doing so, both the time spent forming droplets and the time spent analyzing droplets would be greatly increased. Another option for reducing the temporal resolution is to form droplets continuously directly on-chip. This method eliminates the need for an added droplet formation step, thus reducing the time and labor required for analysis. However, the length of tubing required to collect droplets directly from the chip for 20-30 min is prohibitive. When collecting such large quantities of droplets, the backpressure that builds up in the collection tube can cause droplets to merge or to split. When droplet size varies, then the droplets will move at different rates, thus impeding the ability to relate the droplets' measurements back to the times that they were taken.

Comparison of Methods

Both of these methods exhibited similar electrophoretic reproducibility, with slightly lower limits of insulin detection for the segmented flow chip. The continuous flow collection method obtained better temporal resolution; however, both were capable of

measuring first phase and second phase insulin secretion dynamics. Importantly, the continuous flow collection method required less time and less labor to run (because it did not include the added steps of droplet formation and droplet extraction). Operation of the continuous flow system was comparatively simple, only requiring a capillary to be transferred from one chip to another. Compared to a single-chip system, which would require expensive and/or complicated optical systems to analyze both analytes, the temporal resolution was only 1.6-fold worse, which was an acceptable trade-off. Based on these characteristics, the continuous flow collection method was better suited for islet evaluation. However, the continuous flow collection method was limited in further advancements by backpressure experienced in the capillary and potentially the cell chamber, whereas the segmented flow collection method can be vastly improved in temporal resolution and analysis time, making the segmented flow collection method more attractive for future developments.

Applicability to Islet Evaluation for Transplantation

The main requirement for applicability of this method to islet evaluation for transplantation was that the measurement could be completed quickly. The median culture time for islets prior to human transplantation, reported in a retrospective study, is 20 h (29). Previously developed evaluation methods using ELISA for insulin detection are labor-intensive and time-consuming, taking a half day to run. Our sequential detection method, comparatively, took <90 min for measurement and analysis of $[Ca^{2+}]_i$ and secreted insulin, making it compatible with the time requirements necessary for transplantation.

Previous work has indicated that a combination of $[Ca^{2+}]_i$, insulin, and mitochondrial membrane potential measurements should better predict the outcome of a transplant than any of these measures alone (13). Mitochondrial membrane potential imaging measurements could easily be incorporated into our system by adding another excitation wavelength to the filter wheel.

Conclusion

In this work, we have developed two proof-of-concept methods for the rapid sequential detection of $[Ca^{2+}]_i$ and insulin secretion in glucose-stimulated islets. These methods demonstrated a simple way to detect analytes in solution on-chip via LIF while monitoring cells or a reaction at a different point on the chip. Further improvements to temporal resolution could broaden the applicability of these methods to measuring other cellular phenomena. If temporal resolution is not a great concern for a specific application, continuous flow collection offers a simple method with minimal manual manipulation for conducting multi-point detection. Other options, like second detectors, are discussed in Appendix A.

Rapid sequential detection of $[Ca^{2+}]_i$ and secreted insulin is worth exploring for use as a regulatory standard to indicate whether islets are suitable for clinical transplantation. Before this would be possible, issues in chip reliability need to be addressed- for example, chip clogging, occasional leaking at capillary connections to the chip, and electropherogram variability. To test the validity of the method, we would need to transplant islets into mice and develop an islet health scoring system relating the dynamics of the measures to the outcomes of the transplantations. We could then determine the suitability of the scoring system for predicting the viability of future islet transplants.

References

1. Pepper, A. R., Gala-Lopez, B., Pawlick, R., Merani, S., Kin, T., and Shapiro, A. M. J. (2015) A prevascularized subcutaneous device-less site for islet and cellular transplantation. *Nat. Biotechnol.* 10.1038/nbt.3211
2. CITR Coordinating Center Scientific Summary of the Collaborative Islet Transplant Registry (CITR) 2012 (Eighth) Annual Report. [online] https://web.emmes.com/study/isl/reports/20150218_CITR_2012EighthAnnualReportScientificSummary.pdf (Accessed February 18, 2015)
3. Papas, K. K., Suszynski, T. M., and Colton, C. K. (2009) Islet assessment for transplantation: *Curr. Opin. Organ Transplant.* **14**, 674–682
4. Mohammed, J. S., Wang, Y., Harvat, T. A., Oberholzer, J., and Eddington, D. T. (2009) Microfluidic device for multimodal characterization of pancreatic islets. *Lab. Chip*. **9**, 97
5. Papas, K. K., Colton, C. K., Nelson, R. A., Rozak, P. R., Avgoustiniatos, E. S., Scott, W. E., Wildey, G. M., Pisania, A., Weir, G. C., and Hering, B. J. (2007) Human Islet Oxygen Consumption Rate and DNA Measurements Predict Diabetes Reversal in Nude Mice. *Am. J. Transplant.* **7**, 707–713
6. Barnett, M. J., McGhee-Wilson, D., Shapiro, A. M. J., and Lakey, J. R. T. Variation in human islet viability based on different membrane integrity stains. *Cell Transplant.* **13**, 481–488
7. Sweet, I. R., Gilbert, M., Scott, S., Todorov, I., Jensen, R., Nair, I., Al-Abdullah, I., Rawson, J., Kandeel, F., and Ferreri, K. (2008) Glucose-Stimulated Increment in Oxygen Consumption Rate as a Standardized Test of Human Islet Quality. *Am. J. Transplant.* **8**, 183–192
8. Fraker, C., Timmins, M. R., Guarino, R. D., Haaland, P. D., Ichii, H., Molano, D., and Pileggi, A. The use of the BD oxygen biosensor system to assess isolated human islets of Langerhans: Oxygen consumption as a potential measure of islet potency. *Cell Transplant.* **15**, 745–758
9. Goto, M., Holgersson, J., Kumagai-Braesch, M., and Korsgren, O. (2006) The ADP/ATP Ratio: A Novel Predictive Assay for Quality Assessment of Isolated Pancreatic Islets. *Am. J. Transplant.* **6**, 2483–2487
10. Suszynski, T. M., Wildey, G. M., Falde, E. J., Cline, G. W., Maynard, K. S., Ko, N., Sotiris, J., Naji, A., Hering, B. J., and Papas, K. K. (2008) The ATP/DNA Ratio Is a Better Indicator of Islet Cell Viability Than the ADP/ATP Ratio. *Transplant. Proc.* **40**, 346–350
11. Hanson, M. S., Park, E. E., Sears, M. L., Greenwood, K. K., Danobeitia, J. S., Hullett, D. A., and Fernandez, L. A. (2010) A Simplified Approach to Human Islet Quality Assessment: *Transplantation*. **89**, 1178–1188
12. Chen, D., Du, W., Liu, Y., Liu, W., Kuznetsov, A., Mendez, F. E., Philipson, L. H., and Ismagilov, R. F. (2008) The chemistrode: a droplet-based microfluidic device for stimulation and recording with high temporal, spatial, and chemical resolution. *Proc. Natl. Acad. Sci.* **105**, 16843–16848
13. Adewola, A. F., Lee, D., Harvat, T., Mohammed, J., Eddington, D. T., Oberholzer, J., and Wang, Y. (2010) Microfluidic perifusion and imaging device for multi-parametric islet function assessment. *Biomed. Microdevices*. **12**, 409–417

14. Shackman, J. G., Dahlgren, G. M., Peters, J. L., and Kennedy, R. T. (2005) Perfusion and chemical monitoring of living cells on a microfluidic chip. *Lab. Chip*. **5**, 56
15. Wu, D., Xu, J., Niu, L.-G., Wu, S.-Z., Midorikawa, K., and Sugioka, K. (2015) In-channel integration of designable microoptical devices using flat scaffold-supported femtosecond-laser microfabrication for coupling-free optofluidic cell counting. *Light Sci. Appl.* **4**, e228
16. Yu, L., Shen, Z., Mo, J., Dong, X., Qin, J., and Lin, B. (2007) Microfluidic chip-based cell electrophoresis with multipoint laser-induced fluorescence detection system. *Electrophoresis*. **28**, 4741–4747
17. Gao, J., Yin, X.-F., and Fang, Z.-L. (2004) Integration of single cell injection, cell lysis, separation and detection of intracellular constituents on a microfluidic chip. *Lab. Chip*. **4**, 47
18. Pralong, W. F., Bartley, C., and Wollheim, C. B. (1990) Single islet beta-cell stimulation by nutrients: relationship between pyridine nucleotides, cytosolic Ca2+ and secretion. *EMBO J.* **9**, 53
19. Roper, M. G., Shackman, J. G., Dahlgren, G. M., and Kennedy, R. T. (2003) Microfluidic Chip for Continuous Monitoring of Hormone Secretion from Live Cells Using an Electrophoresis-Based Immunoassay. *Anal. Chem.* **75**, 4711–4717
20. Duffy, D. C., McDonald, J. C., Schueller, O. J. A., and Whitesides, G. M. (1998) Rapid Prototyping of Microfluidic Systems in Poly(dimethylsiloxane). *Anal. Chem.* **70**, 4974–4984
21. Guetschow, E. D., Steyer, D. J., and Kennedy, R. T. (2014) Subsecond Electrophoretic Separations from Droplet Samples for Screening of Enzyme Modulators. *Anal. Chem.* **86**, 10373–10379
22. Grynkiewicz, G., Poenie, M., and Tsien, R. Y. (1985) A New Generation of Ca2+ Indicators with Greatly Improved Fluorescence Properties. *J. Biol. Chem.* **260**, 3440–3450
23. Reid, K. R., and Kennedy, R. T. (2009) Continuous Operation of Microfabricated Electrophoresis Devices for 24 Hours and Application to Chemical Monitoring of Living Cells. *Anal. Chem.* **81**, 6837–6842
24. Shackman, J. G., Watson, C. J., and Kennedy, R. T. (2004) High-throughput automated post-processing of separation data. *J. Chromatogr. A*. **1040**, 273–282
25. Zhang, X., Daou, A., Truong, T. M., Bertram, R., and Roper, M. G. (2011) Synchronization of mouse islets of Langerhans by glucose waveforms. *AJP Endocrinol. Metab.* **301**, E742–E747
26. Dishinger, J. F., Reid, K. R., and Kennedy, R. T. (2009) Quantitative Monitoring of Insulin Secretion from Single Islets of Langerhans in Parallel on a Microfluidic Chip. *Anal. Chem.* **81**, 3119–3127
27. Kasai, H., Hatakeyama, H., Ohno, M., and Takahashi, N. (2010) Exocytosis in Islet β-Cells. in *The Islets of Langerhans* (Islam, M. S. ed), pp. 305–338, Springer Netherlands, Dordrecht, **654**, 305–338
28. Schultz, N. M., Huang, L., and Kennedy, R. T. (1995) Capillary electrophoresis-based immunoassay to determine insulin content and insulin secretion from single islets of Langerhans. *Anal. Chem.* **67**, 924–929

29. Kin, T. (2010) Islet Isolation for Clinical Transplantation. in *The Islets of Langerhans* (Islam, M. S. ed), pp. 683–710, Springer Netherlands, Dordrecht, **654**, 683–710

CHAPTER 3
Development and Optimization of a Sample Preparation Method for Islet Metabolomics

Introduction

Insulin-secreting pancreatic β-cells regulate glucose homeostasis through a triggering (K_{ATP}-dependent) and an amplifying (K_{ATP}-independent) pathway (1–3). While the mechanism of action of the triggering pathway is well-characterized, less is known about the amplifying pathway, which is thought to involve anaplerosis through either malonyl CoA formation and lipid esterification processes or through a pyruvate/malate or pyruvate/citrate shuttle (4). Investigation into these pathways is imperative for understanding the mechanics of glucose-stimulated insulin secretion (GSIS), which could provide insights into the development of diabetes mellitus and provide potential targets for therapeutic development.

Metabolomic analysis is a powerful tool for investigating alterations in cellular response to various stimuli. A desirable metabolomic method is able to quantify a wide range and amount of metabolites with good reproducibility. Nuclear magnetic resonance (NMR), gas chromatography-mass spectrometry (GC-MS), and liquid chromatography-mass spectrometry (LC-MS) have all been employed successfully for mammalian cell metabolomics (5–8); we chose to use high performance liquid chromatography-time-of-flight mass spectrometry (HPLC-TOF-MS) here because it is highly sensitivity compared to NMR and avoids the need to derivatize samples as in GC-MS, thus simplifying the experiment and metabolite identification.

Previous β-cell metabolomic studies have typically been conducted with clonal β-cells rather than primary islets because clonal cells are easily obtained in large quantities, do

not require animal sacrifice, and consist purely of β-cells (9–14). Clonal lines such as rat-derived INS-1 and BRIN-BD11 cells and mouse-derived MIN-6 cells (15–17) have proven to be valuable models of β-cell function. Certain strains secrete insulin in response to a variety of secretagogues, including glucose, amino acids (15, 18), incretins (16), tolbutamide (17), forskolin (19, 20), and phorbol-12-myristate-13-acetate (PMA) (19, 20). However, underlying metabolic differences could still exist, resulting in discordant metabolic responses in clonal cells as compared to native islets. For example, it has been reported that suppression of either the cytosolic or mitochondrial form of malic enzyme reduces GSIS in glucose-responsive INS-1 832/13 cells but not in isolated rat islets (21). Additionally, while it has been widely reported that lipotoxicity is glucose-dependent (so-called glucolipotoxicity), this effect may be dependent on β-cell source. While glucolipotoxicity is present in INS-1 cells, studies did not replicate these findings in MIN6 cells or in isolated human islets (22).

Because of these potential differences in metabolic activity, it is important to corroborate data obtained from clonal cells with data derived from native islets. However, such work requires overcoming challenges of islet analysis. Islets are not as easily obtained or manipulated as clonal cells and they vary widely in size. Murine islets from an eight-week-old NOD mouse were found to range in volume from ~20,000 to 3,600,000 μm^3 (23), meaning that a sample of a set number of islets could contain widely ranging numbers of cells. Size variation creates potential differences in islet metabolite content when normalizing to islet numbers. More subtle is the fact that islet size can affect nutrient availability. Islets in culture rely on diffusion for stimulants to reach the center of the cell cluster; therefore, the steady-state stimulant concentration at the center of the islet is influenced by outer cell stimulant consumption, thus creating an intra-islet stimulant concentration gradient (24). As such, the metabolic profile of islets with varying size is inherently more variable than in dissociated cells, potentially leading to lower reproducibility of results.

One way to combat this is to use a large number of islets per sample to average out the effect of size. Recent studies have used 240-500 islets per sample (11, 25). Increasing

islet number also in principle increases number of metabolites covered, signals, and reproducibility. However, large sample sizes are not practical for large-scale experiments due to the availability of primary islets. Only 100-200 islets can be routinely isolated from a single mouse, so 2-3 animals would need to be sacrificed for a single sample. Not only is this wasteful and ethically problematic, but it also limits the amount and scope of experiments that can be performed due to time constraints involved in obtaining the required number of islets. We thus aimed to determine the minimum number of islets that could be used while still obtaining similar metabolite coverage and reproducibility as previous reports using conventional columns and sample preparation methods.

In this work, we developed a sample preparation method for the reproducible analysis of 62 metabolites from groups of 50 murine islets of Langerhans. We then compared metabolite changes in response to glucose stimulation in islets to those reported in INS-1 832/13 cells. Several key differences were discovered, indicating possible differences in metabolic regulation between primary islets and clonal cell lines.

Experimental Procedures

Materials

Kreb's Ringer Buffer consisted of 20 mM HEPES, 118 mM NaCl, 5.4 mM KCl, 1.2 mM $MgSO_4 \bullet 7H_2O$, 1.2 mM KH_2PO_4, and 2.4 mM $CaCl_2$ and was adjusted to pH 7.4.

Roswell Park Memorial Institute (RPMI) culture medium, fetal bovine serum, penicillin-streptomycin, and collagenase were purchased from Life Technologies (Carlsbad, CA). Acetonitrile, ammonium acetate, methanol, and chloroform were purchased from Sigma-Aldrich (St. Louis, MO). All other chemicals were purchased from Thermo Fisher Scientific (Waltham, MA).

Islet Isolation and Culture

Pancreatic islets were isolated from 20-30 g male CD-1 mice as previously described (26). Typically 100-200 islets were isolated per mouse, and the islets from 3-4 mice

were pooled together. Islets were cultured in RPMI-1640 media supplemented with 11 mM glucose, 10% fetal bovine serum, and 1% penicillin/streptomycin at 37 ºC and 5% CO_2 for 2-3 days prior to experimentation. Islets selected for experimentation were 100-300 µm in diameter, oblong to spherical in shape, had an intact membrane, and lacked a hypoxic (darkened) center. When aliquoting islets for various conditions, we handpicked 10-15 islets per condition at a time instead of picking a whole group at once to reduce the chance of introducing investigator bias by preferentially selecting a certain size or shape of islet for the conditions aliquoted first. Islets were transferred to KRB 1 h prior to metabolism quenching to replicate conditions present in insulin secretion studies. For optimization experiments, islets were incubated in KRB supplemented with 11 mM glucose for 1 h prior to metabolism quenching, while for glucose stimulation experiments, islets were transferred to KRB with 2.8 mM glucose for 1 h, after which 1 M glucose was spiked in to a final concentration of 16.7 mM glucose. Metabolism was quenched either 5 or 15 min following stimulation, roughly corresponding to 1st phase and 2nd phase secretion.

Metabolite Quenching Method

Islets were transferred by pipette to a 1.5 mL Eppendorf tube and centrifuged for 30 s, after which the supernatant was aspirated from the islet pellet. Islet metabolism was then quenched either by dropping the tube into liquid nitrogen or by adding 100-200 µL of extraction solvent at -75 ºC (kept on dry ice) directly to the pellet. Samples were stored at -80 ºC for up to 8 days, after which extraction solvent was added to the tubes that had been snap frozen in liquid nitrogen. All samples were then extracted by probe sonication and LC-TOF-MS was performed on the resulting supernatant.

Extraction Solvent Screen

Groups of 75 islets were quenched with liquid nitrogen and extracted with either 75% 9:1 MeOH:$CHCl_3$/25% H_2O, 80% MeOH/20% H_2O, or 90% 9:1 MeOH:$CHCl_3$/10% H_2O. Extraction solvents were compared based on metabolite coverage, peak heights, and peak shapes. Experiments were performed in triplicate.

Internal Standard Metabolite Quantification

^{13}C-labeled internal standards (adenosine monophosphate (AMP), adenosine diphosphate (ADP), adenosine triphosphate (ATP), citrate (CIT), succinate (SUC), malate (MAL), and acetyl CoA (aCoA)) were spiked into the extraction solvent in approximately a 1:1 ratio with the expected sample metabolite concentrations. Metabolites were then quantified using the ratio of the isotopic peak area to the sample peak area.

Sample Size Determination

To determine the minimum appropriate sample size, samples containing 25, 50, and 75 islets were analyzed at basal and stimulatory levels of glucose. All experiments were performed in triplicate. Samples were evaluated based on number of metabolites detected and relative standard error of the average peak areas for 42 known metabolites.

Protein Quantification

Proteins were quantified using a Pierce Bicinchoninic Acid (BCA) assay kit (Life Technologies, Carlsbad, CA) according to the manufacturer's protocol. Briefly, islet pellets were dissolved in 100 µL radio-immunoprecipitation assay (RIPA) lysis and extraction buffer. Samples and standards were then aliquoted in triplicate into a 96-well plate (25 µL per well) and 200 µL of working reagent was added to each well. After mixing briefly, the plates were incubated at room temperature overnight and then the absorbance at 562 nm was read using a plate reader.

Metabolite Measurement

Analyses for polar metabolites were performed using HPLC-TOF-MS. Chromatographic separations were carried out on a Phenomenex Luna NH_2 column (150 x 1 mm, 3 µm particle size). Mobile phase A consisted of acetonitrile and mobile phase B consisted of 5 mM ammonium acetate, adjusted to pH 9.9 with ammonium hydroxide. The gradient program was (time, %B, flow rate): 0 min, 20%, 70 µL min^{-1}; 25 min, 100%, 70 µL min^{-1}. Injection volume was 30 µL, column temperature was 25 ºC, and autosampler

temperature was 6 ºC. An Agilent Technologies LC/MSD TOF equipped with a dual electrospray ionization (ESI) source was used for detection in negative ion mode. Typical chromatograms obtained using this method are shown in Figure 3.1.

Analyses for nonpolar metabolites were performed using reverse-phase chromatography coupled to the aforementioned mass spectrometer in positive ion mode. Chromatographic separations were carried out on a Waters Acquity UPLC C18 column (2.1 x 50 mm, 1.7 µm particle size) equipped with a guard column (2.1 x 5 mm, 1.7 µm particle size). Mobile phase A consisted of 8:2 isopropanol/methanol and mobile phase B consisted of 4:4:2 water/acetonitrile/methanol. Injection volume was 15 µL, column temperature was 45 ºC, and autosampler temperature was 6 ºC.

Undirected data analysis was performed using XCMS online (27). Features with peak widths greater than 10 s and less than 120 s were aligned based on similar retention time (within 5 s deviation) and similar m/z (within 15 ppm deviation). Features that were likely induced by the same compound were grouped together to determine the total number of unique compounds detected in each sample group. Directed analysis was performed for a series of 87 metabolites previously identified in islets or in INS-1 cells. Of these, 62 were consistently detected to be present in our samples. We have chosen to focus here on those that exhibited changes due to glucose concentration. Metabolites were identified using retention time compared to standards and accurate mass. Combined peak areas were reported for unresolved isomers, like citrate/isocitrate and glucose-6-phosphate/fructose-6-phosphate (G6P/F6P). For most metabolites, peak areas were measured from extracted ion chromatograms of $[M-H]^-$ metabolite ions with ±70 ppm detection windows centered on the theoretical mass. $[M-2H]^{2-}$ ions were used for aCoA and other CoAs to improve sensitivity.

To account for instrumental drift, samples were randomized prior to injection onto the columns. To account for variations in MS sensitivity from run-to-run, metabolite peak area fold changes as compared to the average metabolite peak areas measured from

control samples maintained at basal levels of glucose were calculated and used to compare results from separate runs rather than absolute peak areas.

Statistical Analysis

Data are reported as means ± 1 standard error of the mean (SEM). Statistical significance (p value < 0.05) was determined using an independent sample, two-tailed Student's t-test, assuming equal variance.

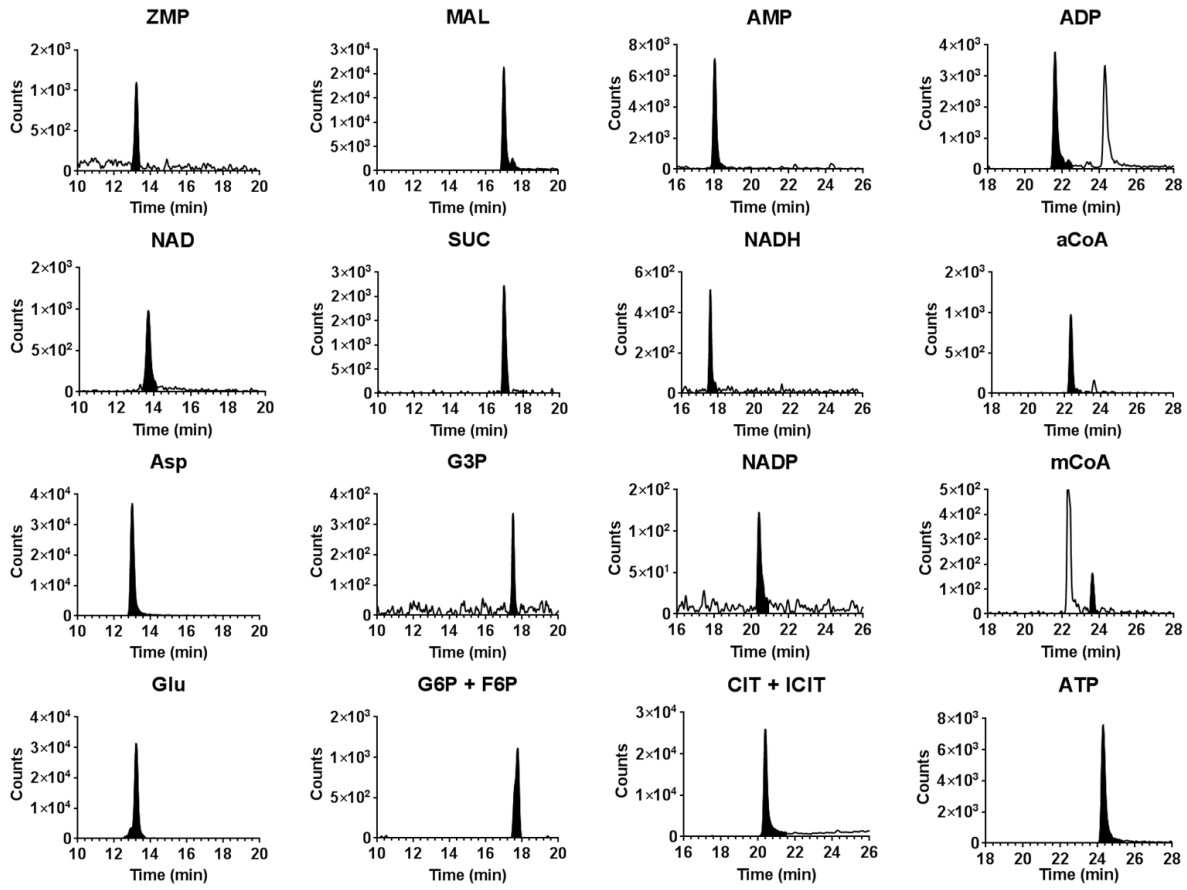

Figure 3.1. Typical metabolite chromatograms from islet extracts. Extracts were obtained from samples following 15 min stimulation with 16.7 mM glucose. Metabolites were extracted with m/z window ± 50 ppm. Peaks were smoothed using Gaussian smoothing with 15-pt function width and 5-pt Gaussian width.

Results and Discussion

We established a sample preparation method for the reproducible analysis of 62 metabolites from small groups of murine islets through optimization of metabolism quenching, extraction solvent, and sample size (Figure 3.2). Signal variability due to islet number was investigated as a facet of the optimization. We also examined the effect of an internal standard addition on sample-to-sample and run-to-run variability. Next, we performed glucose stimulation experiments and compared our results to known or expected outcomes to verify that our islet metabolomic method could accurately detect changes in metabolites. Finally, we compared the results obtained with our method to published results obtained using clonal INS-1 832/13 cells and identified some possible differences in metabolic regulation between primary and clonal cells.

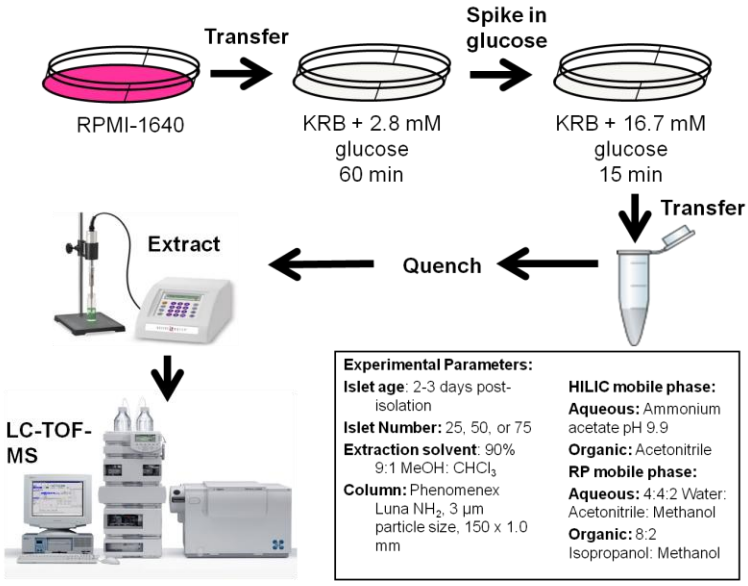

Figure 3.2. Metabolomic sample preparation method. Islets were cultured in RPMI-1640 media and transferred to minimal media supplemented with 2.8 mM glucose for 60 min, after which glucose was spiked in to a final concentration of 16.7 mM. After an incubation period of 5 or 15 min, the islets were transferred to an Eppendorf tube and the samples were quenched. After addition of extraction solvent, islet metabolites were extracted using a probe sonicator, and supernatant was injected onto an LC-TOF-MS.

Metabolism Quenching Method

Metabolism quenching serves to slow or ideally stop metabolism at a specific time point. Quenching is an important step in metabolomics because intracellular metabolite levels can change quickly, leading to possible misinterpretations of the metabolome if metabolism is not properly stopped at the desired point in time. Cold solvent addition (-75 ºC) is the most common quenching method, although some researchers have reported a loss of metabolites with cold (-40 ºC) methanol quenching due to metabolite leakage (8). Snap freezing with liquid nitrogen is another common quenching technique for tissue or adherent cell culture metabolomics (5, 28), and applying liquid nitrogen directly to plates of INS-1 cells was found to improve stability in storage compared to samples stored as extracts (9). We tested variations of both methods. For the liquid nitrogen method, we dropped the sample tube into a pool of liquid nitrogen, while for the cold solvent addition method, we added 100 µL of -75ºC extraction solvent directly to the islet pellet before placing the tube on dry ice.

To compare the two quenching methods, we used the ATP/ADP ratio and the energy charge ratio. ATP/ADP ratio is a good barometer for metabolome quenching because the molecules have rapid turnover (8) and the ratio has well-known changes in islets in response to glucose treatment (29, 30). Previous reports have found ratios of 1.9 ± 1.4 at 3 mM glucose (29), ~5.0 ± 0.5 at 5 mM glucose (31), and 4.1 ± 1.9 at 20 mM glucose (29). The energy charge ratio, calculated as ([ATP] + 1/2[ADP])/([ATP] + [ADP] + [AMP]) has an established physiological range in healthy cells of 0.80-0.95 (32).

When using the liquid nitrogen quenching method, the measured ATP/ADP ratio at 11 mM glucose was 1.6 ± 0.2 (n = 11), which is much lower than reported values for islets, and the energy charge ratio was 0.74 ± 0.02 (Figure 3.3a-b). In samples quenched via cold solvent addition, the ATP/ADP ratio was higher than with the liquid nitrogen method (6.5 ± 1.6, n = 4), and in line with the values expected. The energy charge ratio was also higher (0.89 ± 0.02) and in the expected range. Based on these results, we concluded that the liquid nitrogen quenching method was inefficiently quenching islet metabolism, probably due to the Leidenfrost effect (33). Cold solvent addition,

conversely, seemed to be a suitable metabolism quenching method, and was used in all subsequent experiments.

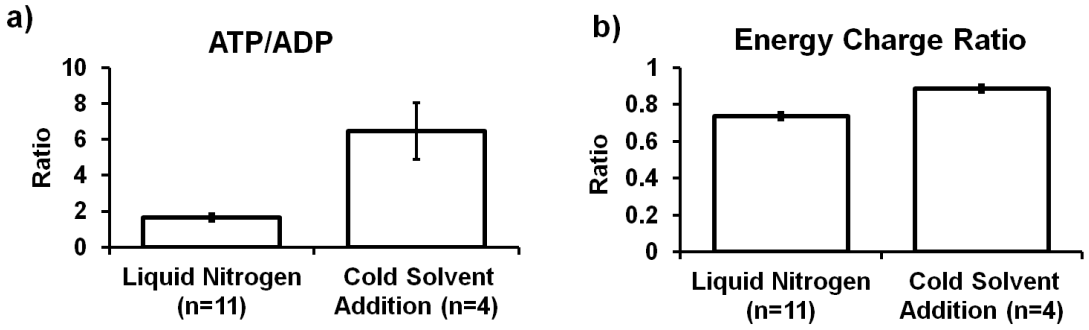

Figure 3.3. Metabolism quenching method comparison. Samples were cultured in KRB supplemented with 11 mM glucose for 1 h, then quenched using either liquid nitrogen or -75 ºC solvent addition. a) ATP/ADP ratio was 1.6 ± 0.2 using liquid nitrogen (n = 11) and 6.5 ± 1.6 using cold solvent addition (n = 4). b) Energy charge ratio was 0.74 ± 0.02 using liquid nitrogen and 0.89 ± 0.02 using cold solvent addition.

Extraction Solvent Screen

Choice of extraction solvent can have a significant effect on recovery, peak shape, metabolite coverage, and metabolite retention, with more polar solvents favoring improved recovery of more polar analytes, and vice versa. The best extraction solvent depends upon sample composition. We were interested in selecting an extraction solvent that was compatible with MS analysis and with analytes known to be important in stimulus-secretion coupling in β-cells, e.g. glycolysis, TCA, and pentose phosphate metabolites, nucleotides, fatty acids, and long chain CoAs.

Because of limited sample availability, we only tested 3 solvents. Methanol is the most commonly used extraction solvent for tissue metabolomics. A study comparing several different methanol/water ratios shows that the optimal ratio for endogenous metabolite extraction from E. coli samples (based on better yields of high-energy compounds than in higher organic content solvents and lower yield of decomposition products than in lower organic content solvents) is 80% (34). Previous work in our group using INS-1 cells demonstrates that a 70% 9:1 MeOH:$CHCl_3$ solvent tends to result in higher peaks with better sensitivity for glycolytic and TCA metabolites than 70% MeOH. The residual

water in the plate is estimated and included in the solvent ratios (9). Based on these reports, we selected 90% 9:1 MeOH:$CHCl_3$, 75% 9:1 MeOH:$CHCl_3$, and 80% MeOH as potential extraction solvents for our experiments in islets (results shown in Figure 3.4). We compared both peak shape and peak area. Peak shape is important for accurate quantification of peak area, while maximizing the peak area can improve metabolite coverage.

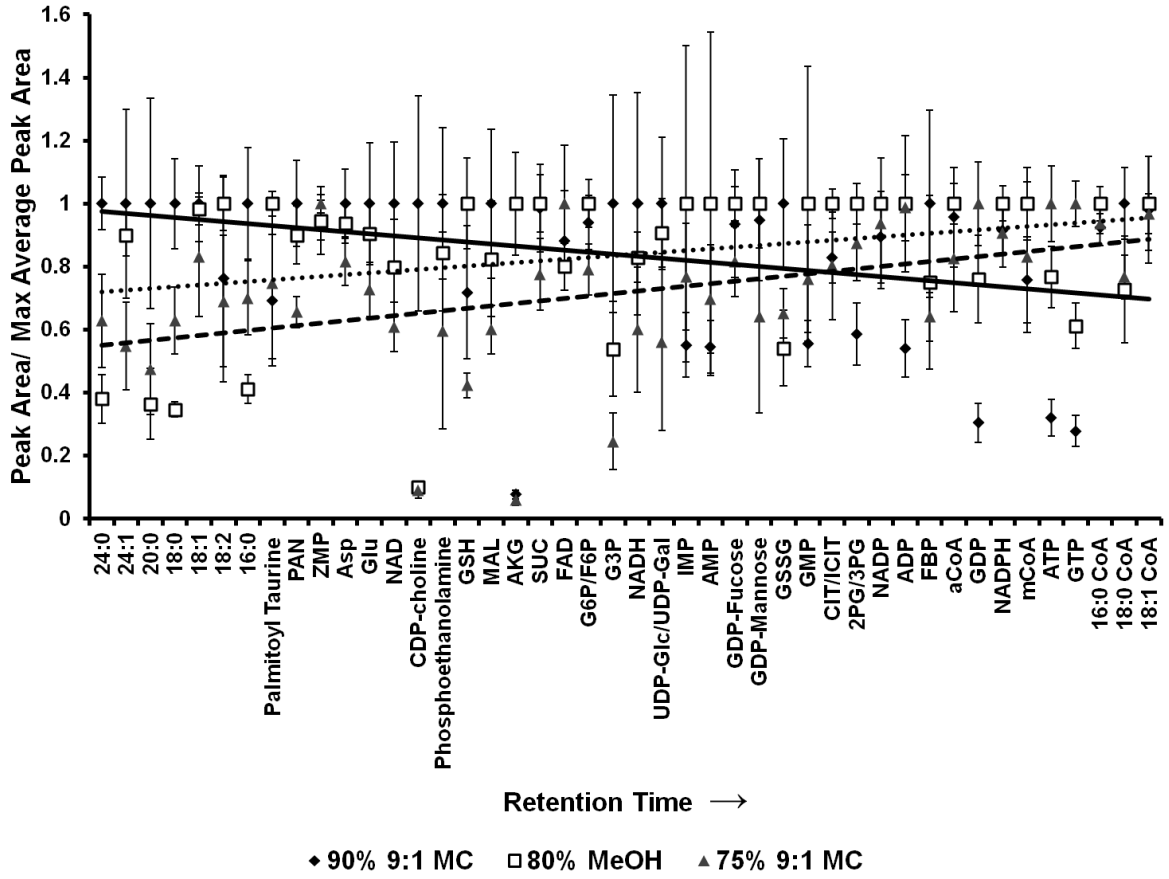

Figure 3.4. Extraction solvent effect on peak areas. Metabolites were extracted using either 90% 9:1 MC/10% H_2O, 80% MeOH/20% H_2O, or 75% 9:1 MC/25% H_2O (n = 3 for each solvent tested). Samples extracted using higher organic content solvents exhibited larger relative peak areas for early-eluting compounds, while samples extracted using lower organic content solvents showed larger relative peak areas for late-eluting compounds, especially nucleotides. Trend lines are displayed to show this trend. R^2 = 0.2068, 0.0942, and 0.1188 for 90% 9:1 MC (solid line), 80% MeOH (narrow dashed line), and 75% 9:1 MC (wide dashed line), respectively.

Qualitatively, the peak shapes using the 90% 9:1 MeOH:$CHCl_3$ were better than with either of the other two solvents for early-eluting peaks such as glutamate (Figure 3.5a-i).

The poor peak shapes could be caused by dissolving the sample in a solvent that is stronger than the mobile phase. Peak shapes could potentially be improved by changing the mobile phase gradient so the initial aqueous content is higher. Middle and late-eluting peaks did not exhibit solvent-specific differences in peak shape.

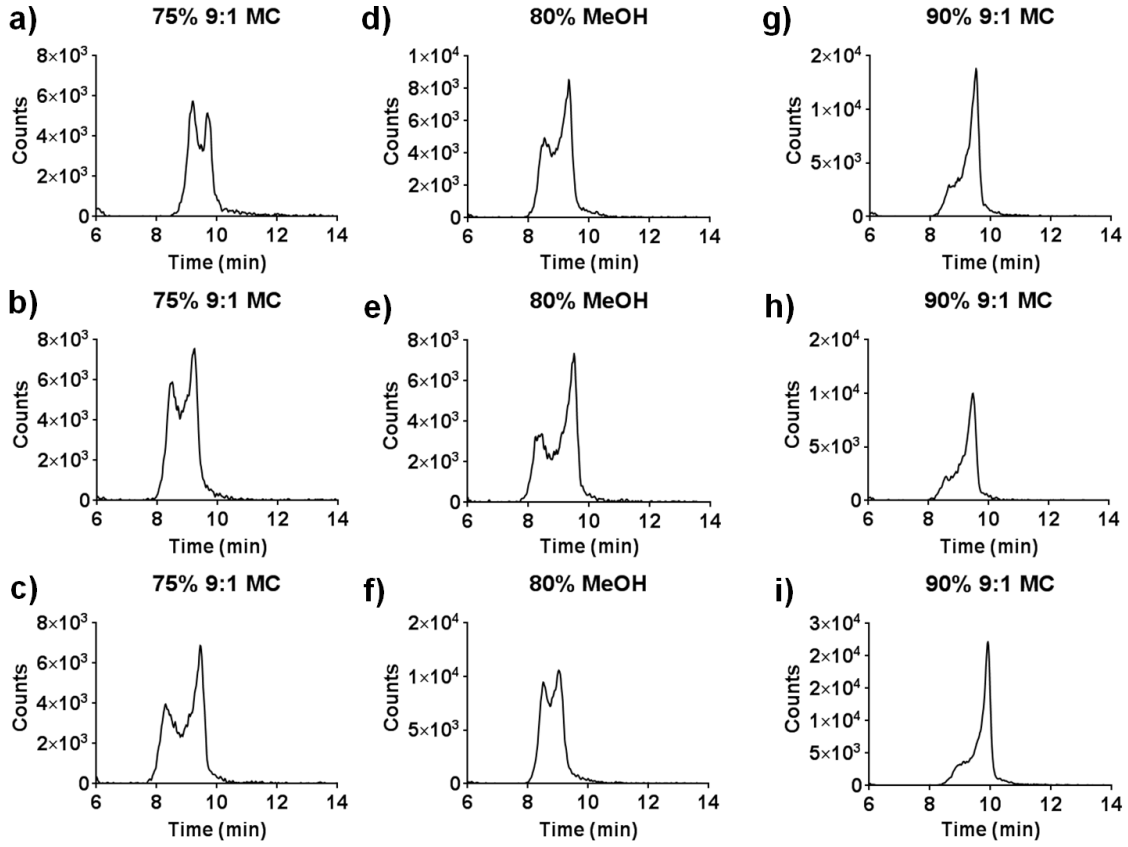

Figure 3.5. Glutamate chromatographic peak shapes by extraction solvent. Peak splitting is observed when samples are extracted using lower organic content extraction solvents, as in (a-f). The best peak shapes are observed with 90% 9:1 MC (g-i).

Quantitatively, peak areas tended to trend based on the polarity of the extraction solvent: early-eluting compounds, including fatty acids, amino acids, and some glycolytic metabolites, tended to have larger peaks in solvents with higher organic content. In the first 17 min of the chromatogram, the 90% 9:1 MeOH:$CHCl_3$ solvent corresponded to, on average, 17% larger peak areas than the 80% MeOH solvent ($p = 0.01$) and 29% larger peak areas than the 75% 9:1 MeOH:$CHCl_3$ solvent ($p < 0.00001$). Later-eluting compounds, namely nucleotides, tended to have much larger peaks in

solvents with lower organic content; the average peak areas of all nucleotides were 50% larger using the 75% 9:1 MeOH:$CHCl_3$ solvent than either of the other solvents ($p < 0.0001$). Middle-eluting compounds and long chain CoAs were comparable across all extraction solvents, with the exception of alpha-ketoglutarate (AKG), which was only detected with 80% MeOH, and CDP-choline, which was only detected with 90% 9:1 MeOH:$CHCl_3$. No significant difference in peak area RSE based on extraction solvent was observed (RSE was 16 ± 9%, 13 ± 11%, and 13 ± 7% for 90% 9:1 MeOH:$CHCl_3$, 80% MeOH, and 75% 9:1 MeOH:$CHCl_3$, respectively).

Based on these results, we decided to use 90% 9:1 MeOH:$CHCl_3$ for all subsequent experiments to preserve sensitivity and peak shape of early-eluting compounds; nucleotide sensitivity was not as important comparatively because these peaks are relatively abundant in islet samples regardless of the extraction solvent used.

Effect of Islet Number on Metabolome Coverage and Reproducibility

As discussed in the introduction, it is of interest to decrease islet numbers required for assay, but using too few islets could result in variability due to islet size and intra-islet nutrient concentration gradients. We therefore evaluated our sample preparation procedure on groups of 25, 50, and 75 islets to determine if these numbers could yield good metabolome coverage and reproducibility. These values represent numbers of islets that can be conveniently obtained from a single mouse; the smaller numbers would allow replicates or multiple experiments from a single subject.

For this study, we measured metabolites at basal (3 mM) and stimulatory (16.7 mM) glucose concentrations in islets that had been extracted into 200 µL extraction solvent. Each group contained 3 replicates. Using XCMS online for undirected analysis (27), we found that the LC-MS analysis of 25 islets yielded 3230 aligned features, of which 219 were determined to be likely to correspond to unique compounds; 50 islets yielded 4098 aligned features, of which 255 were unique compounds; and 75 islets generated 4275 aligned features, of which 273 were unique compounds. These values correlate to 86% metabolite coverage in 25 islet samples compared to 50 islet samples and 80%

metabolite coverage in 25 islet samples compared to 75 islet samples, demonstrating that, as expected, increasing the sample size increased the number of compounds that could be detected in islets. These results were obtained in a single MS run with randomized samples, so variability in MS sensitivity should not have contributed to any differences observed.

By comparison, recent islet metabolomic studies using 240 islets have measured comparable numbers of compounds. Using a GC-MS metabolomic method, 195 metabolite derivatives have been detected in INS-1 cells 15 min following glucose stimulation, of which 61 could be identified and measured via directed analysis in isolated rat islets (11). Other islet metabolomic studies do not report the total number of metabolites detected via undirected analysis (25, 35). The reason we were able to obtain similar metabolite numbers using 25-50 islets could be due to their use of GC-MS as opposed to LC-MS, as GC-MS is believed to measure fewer compounds. Other studies using INS-1 cells have found 325 unique peaks using GC-MS (13) and 345 unique peaks using LC-MS (El Azzouny, M. *et al*, unpublished data). Comparatively, we measured about 75% the number of metabolites using ~50-fold overall less material. We were able to achieve these results by using low volumes of extraction solvent to avoid sample dilution. Scaling the extraction solvent volume to the number of cells, our samples were only 5-10 times less concentrated than the INS-1 samples. Further reduction in extraction solvent volume was limited by injection volume requirements.

Next, we performed directed analysis on a series of 42 known metabolites in groups of 25, 50, and 75 islets at basal and stimulatory levels of glucose. Each condition was tested in triplicate. Of these 42 metabolites, we found that 37 were detected in 25 islet samples, with 31 detected in all six sample sets. All 42 metabolites were detected at least once in the 50 and 75 islet samples, although in the 50 islet samples, only 39 were detected in all 6 sample sets. To compare the reproducibility of the peak area measurements for the detected metabolites, we plotted the average RSE values obtained for all metabolites at basal and stimulatory glucose concentrations (Figure 3.6). We found that the 25 islet samples typically were the most variable, with an

average RSE of 26 ± 2%. This RSE was significantly higher than the average RSE values of the 50 and 75 islet samples, which were 20 ± 1% ($p = 0.02$) and 17 ± 1% ($p = 0.0001$), respectively. There was no significant difference in average RSE between 50 and 75 islet samples. These results were collected using a poor column, so only 42 metabolites were compared; 62 metabolites could be consistently detected in subsequent experiments using 50 islets.

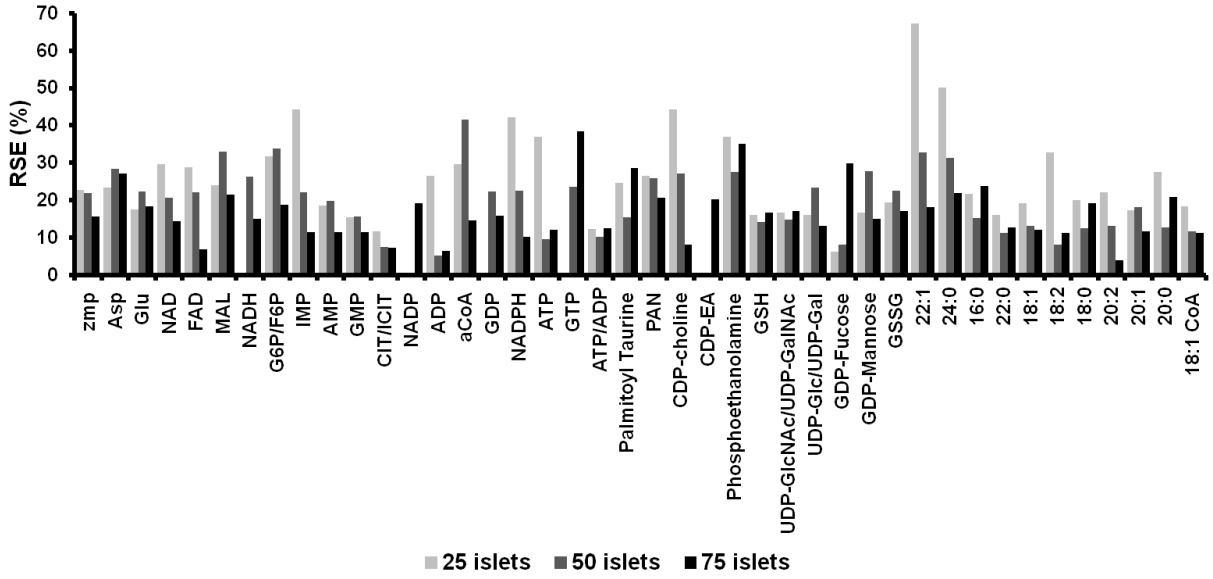

Figure 3.6. RSE dependence on sample size. RSE was measured for 42 metabolites extracted from sets of 25, 50, and 75 islets. Results were pooled from metabolites measured at basal and stimulatory levels of glucose (n = 6 for each bar). Average RSE was 26 ± 2%, 20 ± 1%, and 17 ± 1 % for 25, 50, and 75 islets, respectively.

Based on the results from both the directed and undirected analyses, we reasoned that 25 islets were too few to obtain adequate metabolite coverage and reproducibility using our current sample preparation and MS methods. Lower signal-to-noise ratios are a contributing factor for this higher variability, as the metabolites with the smallest peak areas tended to have high RSE (30-50%) for 25 islet samples. However, some large peaks, such as ADP and ATP, had similarly high RSE values that could not be attributed to signal-to-noise ratios, leading us to believe that this variability resulted from islet heterogeneity, which should have more of an impact at smaller sample sizes. Since 50 and 75 islet samples resulted in similar metabolite coverage in both directed and

undirected analysis and similar peak area variability, we decided to use samples containing 50 islets for all subsequent experiments.

Sample Tissue Variability

The above data suggests that 50 islets per sample provided a reasonable compromise between metabolite coverage and reproducibility and tissue requirements relative to 25 or 75 islets. We next sought to determine how variable total tissue would be for this islet number from sample-to-sample. For this study, we examined protein content in 18 groups of 50 islets. We found that the average protein content in all samples was 96.3 ± 19.9 µg mL^{-1} (standard deviation).

The variation in islet protein content (RSD = 21%) could account for some of the variability in islet metabolite measurements; thus, we corrected the measured peak areas by measured protein concentration of each sample. However, there was no difference in variability between corrected and uncorrected peak areas. Average RSE was 15 ± 2% and 17 ± 2% for uncorrected and protein-corrected samples incubated in 3 mM glucose, respectively (n = 9). Corresponding average RSE for samples incubated in 16.7 mM glucose was 9 ± 1% and 10 ± 1%, respectively (n = 9). The improved RSE with high glucose could have occurred because metabolite levels tend to be higher at high glucose, resulting in more signal. The ineffectiveness of protein content in improving metabolite variability could be related to differences in metabolic response from individual cells due to the intra-islet nutrient concentration gradient.

Internal Standard Metabolite Quantification

Stable isotope-labeled compounds can be added to samples and used as internal standards to correct for some variables in analysis including loss during sample preparation and signal variation from different injections. We had available stable isotopes for AMP, ADP, ATP, CIT, SUC, MAL, and aCoA. The isotopes were added to the samples during the quenching step. Absolute signal variation in a series of injections from 4 samples containing identical concentrations of stable isotopes is shown in Figure 3.7, demonstrating differences in peak area from sample-to-sample. As shown in Figure

3.8, the addition of the internal standards was able to correct for differences in peak areas based on extraction solvent composition. Although the raw peak area for ATP was significantly higher in samples extracted in lower organic content solvent, the quantified amount of ATP in all samples was the same (Figure 3.8a). Corrections for the other metabolites are shown in Figure 3.8b-g; there were no significant differences in metabolite levels based on extraction solvent in the stable-isotope corrected data.

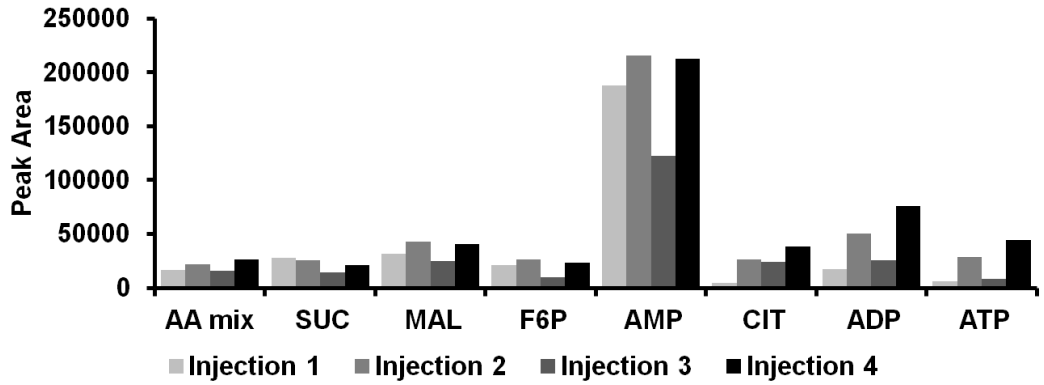

Figure 3.7. Sample-to-sample variability. Eight internal standards were spiked into four biological samples in equal concentrations. When injected sequentially onto the LC-TOF-MS, peak areas for each metabolite varied from injection-to-injection.

While stable isotopes were useful in correcting for large differences in metabolite concentrations, such as those introduced by varying the extraction solvent, they did not improve variability overall. The RSE for metabolite peak areas in replicate samples was, on average, 17% for both the raw data and the stable-isotope corrected data, indicating that most of the variation was due to the sample itself and not to variation in the MS.

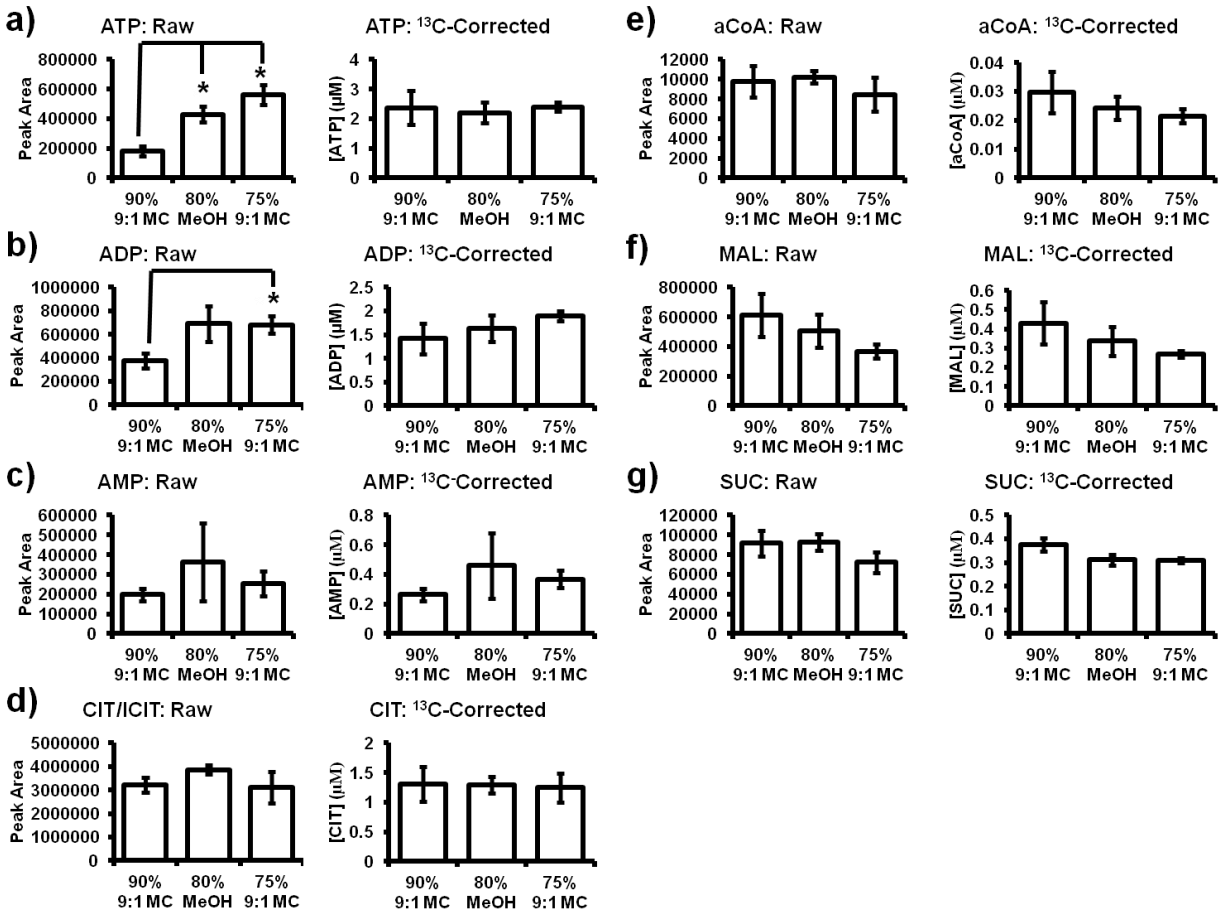

Figure 3.8. Internal standard correction of metabolomic data. Stable isotope-labeled metabolites were added to samples to quantify metabolite concentrations for a) ATP b) ADP c) AMP d) CIT/ICIT e) aCoA f) MAL g) SUC. Absolute quantification eliminated variations in measured metabolite peak areas due to extraction solvent effects (n = 3 for each bar). Error bars represent standard error.

Islet Metabolomic Method Verification

Using stable isotope-corrected data, we determined the absolute intracellular concentrations of 7 metabolites measured 15 min following stimulation with 16.7 mM glucose. Measured concentrations were on the same scale as previous reports, as shown in Table 3.1 (30, 36). We next wanted to verify that our method could accurately measure changes in metabolism. Therefore, we stimulated islets with 16.7 mM glucose and measured fold-change in peak areas with respect to islets maintained at basal glucose concentrations (2.8 mM). We compared our results with expected metabolic changes based on known glucose-stimulated insulin secretion (GSIS) pathways. In a normal β-cell, elevated levels of extracellular glucose result in glucose uptake across

glucose transporter-type 2 (GLUT-2). Inside the cell, glucose undergoes glycolysis. Glycolytic products enter the citric acid cycle and undergo oxidative phosphorylation, resulting in the production of ATP. The consequent increase in the ATP/ADP ratio causes ATP-regulated K^+ channels to close, leading to increased $[K^+]_i$ and ultimately membrane depolarization. Voltage-gated L-type Ca^{2+} channels then open to allow Ca^{2+} influx into the cell. Increased $[Ca^{2+}]_i$ induces vesicles containing insulin to fuse with the plasma membrane of the cell, releasing insulin into the extracellular space through exocytosis (2, 3). Anaplerotic pathways lead to a net increase in TCA cycle components (37).

Based on these pathways and reported results (11), we would expect to see increases in glycolytic and TCA cycle components following glucose stimulation. Our results, reported in Figure 3.9 as the average fold change of each metabolite as measured in relation to the average peak area at basal glucose concentration for a series of 62 metabolites, confirmed that our metabolomic method was able to reliably detect these expected changes in metabolites. We observed significant increases in G6P/F6P, MAL, ATP/ADP, NADH/NAD, and NADPH/NADP within 5 min of glucose stimulation, corresponding to 1st phase response. These metabolites remained elevated 15 min following stimulation, during the 2nd phase response. Additionally, other glycolytic and TCA cycle components 2-phosphoglycerate/3-phosphoglycerate (2PG/3PG), AKG, and malonyl CoA (mCoA) were also significantly elevated at this time, consistent with expected contribution of anaplerosis to 2nd phase glucose response (Figure 3.10a-b).

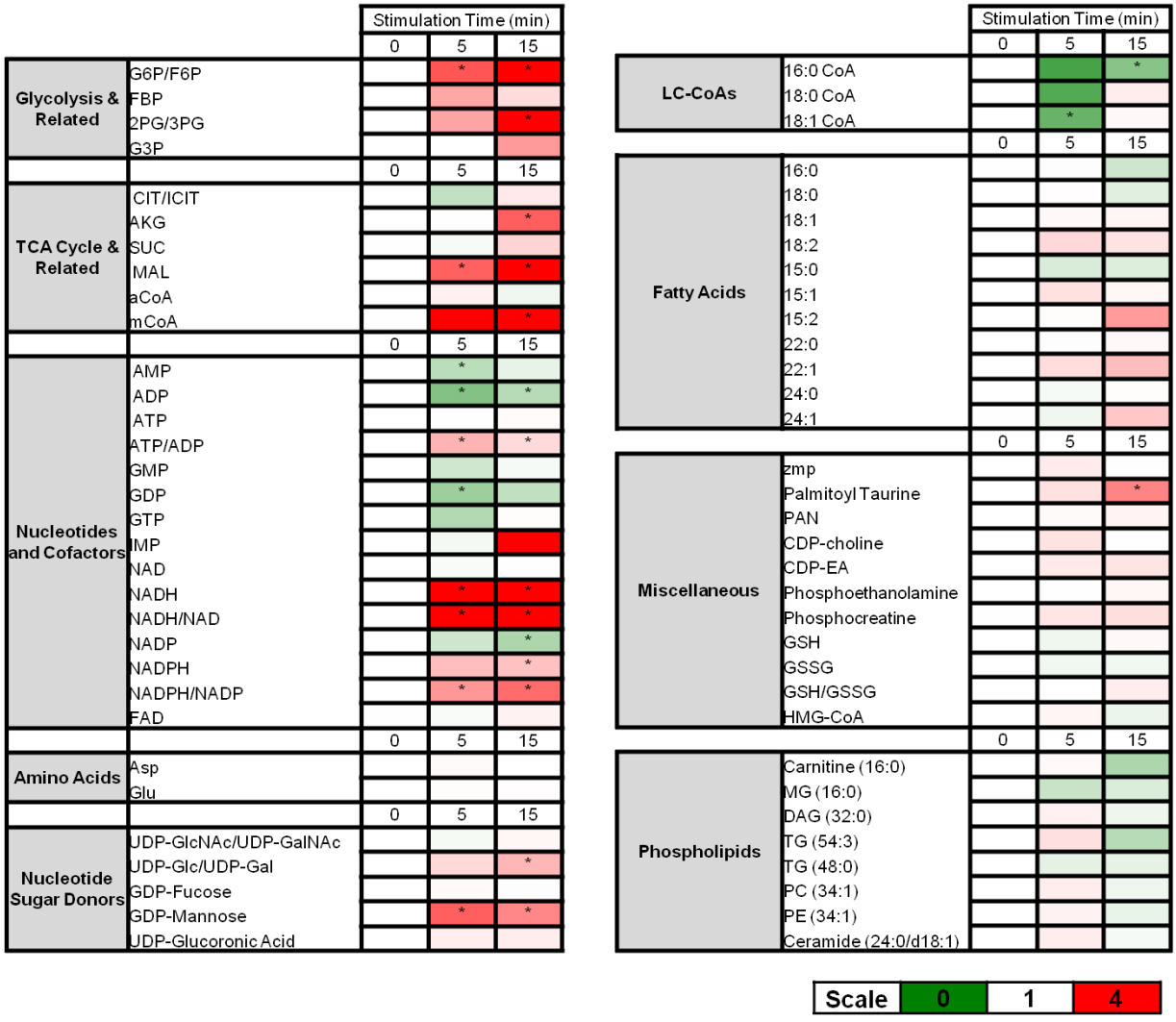

Figure 3.9. Metabolite heat maps. Concentrations of 62 metabolites and 4 metabolite ratios are expressed as fold changes versus time 0; n = 3 for each time point. Asterisks represent $p < 0.05$ vs. time 0 as determined by an independent sample, two-tailed student's t-test.

Glucose Stimulation: Islets vs. INS-1

Next, we sought to compare islet results to INS-1 data from our lab and other published results to determine if there were any inherent differences in metabolic responses to glucose. Comparing metabolic responses between islets and INS-1 cells is important for determining the applicability of data obtained using INS-1 cells to native islet metabolism. Due to different incubation conditions, the results are not directly comparable; however, by comparing data from a variety of sources and a variety of time points after glucose stimulation, some differences in metabolism between INS-1 cells

and islets can be established. Absolute concentrations of metabolites measured in islets and in INS-1 cells (10) are summarized in Table 1. Interestingly, concentrations of metabolites from INS-1 cells tend to be an order of magnitude higher than concentrations in our islet samples, possibly corresponding to higher metabolism rates in INS-1 cells. Because we only measured static metabolite levels, more experiments would need to be performed to explore this hypothesis. For a more in-depth analysis of metabolite levels, we compared fold changes in metabolite concentrations from basal to stimulatory levels of glucose in islets vs. INS-1 cells.

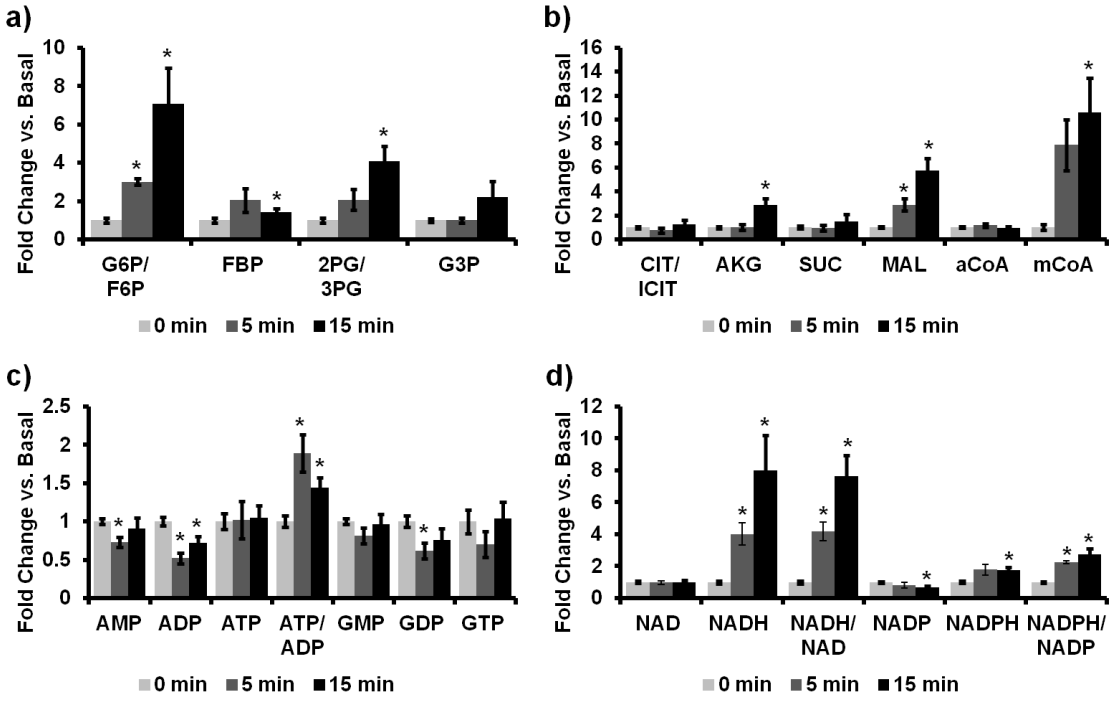

Figure 3.10. Metabolic changes in response to 16.7 mM glucose 5 and 15 min post-stimulation in a) glycolysis metabolites b) TCA cycle metabolites c) nucleotides d) cofactors. n = 3 for each bar. Error bars represent standard error. Asterisks indicate p <0.05 as determined by an independent sample, two-tailed student's t-test.

		Concentration (nmol mg^{-1} protein)			
	Source	Islet			INS-1
	Species	Mouse	Mouse	Rat	Rat
	[Glucose] (mM)	16.7	20	16.7	10
	Reference	Original data	30	36	10
Metabolites	MAL	4.3 ± 0.5	-	14	67
	SUC	1.0 ± 0.4	-	-	22
	CIT	13.8 ± 2.0	-	15	110
	aCoA	0.14 ± 0.03	-	-	1.6
	AMP	2.2 ± 0.1	-	-	11
	ADP	2.7 ± 0.3	8.5	-	18
	ATP	22.5 ± 1.7	90	-	850

Table 3.1. Absolute concentrations of metabolites measured in islets vs. INS-1 cells. Islets in our work were incubated at 2.8 mM glucose for 60 min prior to 16.7 mM glucose stimulation for 15 min. Islets in previously published work were incubated for 60 min at 15 mM glucose followed by 60 min at 20 mM glucose (30) or were incubated for 30 min at 5.5 mM glucose prior to 16.7 mM glucose stimulation for 60 min (36). INS-1 cells were incubated in 0.5 mM glucose for 30 min prior to 10 mM glucose stimulation for 30 min.

Islets vs. INS-1: Glycolysis

Glycerol-3-phosphate (G3P) was increased in response to glucose in both islets and INS-1 cells. The islet G3P fold increase (2.2 ± 0.8 fold after 15 min glucose stimulation) was comparable to INS-1 cells in one report (11), but the increase was significantly lower than in INS-1 cells in a second study (~30 fold in INS-1 cells) (10). This difference in metabolite levels between the INS-1 samples could be related to incubation conditions. In the second INS-1 study, INS-1 cells are pre-incubated in 0.5 mM glucose rather than 2.8 mM glucose as in the first study. G3P is formed from glycerol, which is released from triglycerides during β-oxidation. It is reasonable to believe that more glycerol may be available in cells that have been maintained at lower glucose concentrations. Thus, we concluded that G3P response is similar in islets and in INS-1 cells under similar incubation conditions.

Hexose phosphates have generally been reported to increase with a delayed response in glucose-stimulated INS-1 cells; increases reach 2-5 fold after 30-60 min of stimulation (10, 13, 38). In our islet samples, hexose phosphates increased 3.0 ± 0.2 fold within 5 min of stimulation and 7.1 ± 1.9 fold 20 min after stimulation. Because other glycolytic

metabolites were similar between INS-1 cells and islets (including 2PG/3PG), this is likely not due to any differences in glycolytic metabolism. It could be related to differences in flux through the pentose phosphate pathway, which also utilizes hexose phosphates. While a 2.4 fold sustained increase in the PPP metabolite sedoheptulose-7-phosphate (S7P) upon glucose stimulation was found in INS-1 cells (10), we observed a significant transient decrease (0.85 ± 0.05 fold) in S7P within 5 min of stimulation. Other pentose phosphate pathway metabolites were not detectable using our current metabolomic method; however, other studies have found 2.5 fold increases in ribose 5-phosphate in INS-1 cells and 1.6 fold increases in rat islets (11). This increase in hexose phosphates and slightly lower increase in ribose-5-phosphate in comparison to INS-1 cells could correlate with reduced flux through the pentose phosphate pathway in islets as compared to INS-1 cells. Additionally, our inability to detect other PPP metabolites, which in INS-1 cells are detected in concentrations similar to aCoA and NADPH (10), could be indicative of lower levels of these metabolites in islets as compared to INS-1 cells.

Islets vs. INS-1: TCA Cycle

We found similar glucose-stimulated increases in the TCA cycle components AKG, SUC, and MAL as has been reported in INS-1 cells (10, 11, 13). CIT/ICIT, however, has been found to increase about 4-fold in INS-1 cells, while in our islet data, there was not a significant increase (1.3 ± 0.3 fold). This is paralleled in published work, in which citrate has been found to increase 4-fold in INS-1 cells, but to have little-to-no effect on metabolic regulation in rat islets based on an OPLS loading plot (11). Because other TCA cycle components are similar between islets and INS-1 cells, this reduced response is not likely due to changes in flux through the TCA cycle. Instead, it could be caused by differences in citrate usage for cataplerotic reactions. Citrate exported from the mitochondria can be converted into aCoA-derived mCoA, which was found to be slightly upregulated in glucose-stimulated islets (10.6 ± 2.9 fold) as compared to glucose-stimulated INS-1 cells (~6-8 fold) (10). Alternatively, the reduced increase in citrate could be caused by decreased formation through anaplerosis. Evidence for an anaplerotic pathway in islets includes high levels of expression of pyruvate carboxylase

(PC) (4). Pyruvate/citrate cycling and/or pyruvate/isocitrate cycling have been suggested to be important for GSIS, and in particular, for the K_{ATP}-independent pathway (39). GSIS is reduced when the mitochondrial pyruvate carrier (MPC) is inhibited in both INS-1 cells and in rat islets (40), and this decrease in insulin secretion occurs mainly during the 2nd phase of insulin secretion (13).

Islets vs. INS-1: Nucleotides and Cofactors

Qualitatively, nucleotide and cofactor response were similar between INS-1 cells and islets. Decreased concentrations were observed in mono and di-nucleotides and NADP upon glucose stimulation, while tri-nucleotide levels remained constant and NADH concentration increased. NADPH/NADP, NADH/NAD, and ATP/ADP ratios correspondingly increased (Figure 3.9 and Figure 3.10c-d). Quantitatively, the changes were not as great in islets as in INS-1 cells. AMP decreased maximally 0.7 ± 0.1 fold and ADP 0.5 ± 0.1 fold following 5 min glucose stimulation in our data. Results in INS-1 cells show sustained 0.5-fold decreases in AMP and 0.3-fold decreases in ADP (10). Increases in NADH were likewise subdued; we reported 4-fold and 8-fold increases 5 and 15 min following glucose stimulation, respectively, whereas INS-1 data has shown increases of ~16-fold using similar glucose concentrations (10). These slightly smaller fold-changes in molecules involved in cellular energetics could indicate varying metabolic rates between the INS-1 cells and islets.

Islets vs. INS-1: Long Chain Acyl CoAs

Long chain acyl CoAs (LC-CoAs) have been suggested as a metabolic coupling factor for GSIS. Evidence has shown that LC-CoAs can open K_{ATP} channels, resulting in the closure of Ca^{2+} channels, which could be related to oscillations in $[Ca^{2+}]_i$ during the 2nd phase glucose response. LC-CoAs can also directly stimulate insulin exocytotic machinery (41). At stimulatory levels of glucose, mCoA levels increase, resulting in inhibition of CPT-1 and subsequent blockage of LC-CoA entry to the mitochondria for β-oxidation, leading to accumulation of LC-CoAs in the cytosol (42). Measuring compartmental LC-CoAs is difficult, and evidence for cytosolic LC-CoA accumulation is indirect (41). Total LC-CoA content (mitochondrial + cytosolic) has been reported to

rapidly decrease with glucose stimulation in INS-1 cells and remain lower than control for at least 45 min; these results are consistent with LC-CoA esterification with G3P for *de novo* synthesis of phosphatidic acid (PA) and diacylglycerol (DAG) (10). In our results, all LC-CoA levels decreased during 1st phase insulin secretion in accord with INS-1 data (significant only for 18:1 CoA; other LC-CoAs had $p < 0.09$), but except for 16:0 CoA, they all returned to basal levels within 15 min of glucose stimulation. This replenishment of LC-CoAs could indicate differences in glycerolipid/free fatty acid cycling in the 2nd phase of insulin secretion between islets and INS-1 cells.

Islets vs. INS-1: Other Metabolites

Differences were found between islets and INS-1 cells in several other metabolites, including ZMP, which is reported to increase 9-fold upon glucose stimulation in INS-1 cells (10), while we saw no effect of glucose on ZMP in islets. ZMP can act as an AMP analog to activate AMPK, which induces inhibition of mCoA formation and could act as a negative regulator of insulin release. It was hypothesized based on the observed increase in ZMP that ZMP could play a role in negative regulation of GSIS during the 2nd phase of insulin secretion (10). Reductions have also been reported in HMG-CoA, citicoline, and CDP-ethanolamine in INS-1 cells. HMG-CoA is involved in the mevalonate pathway, while citicoline and CDP-ethanolamine are involved in *de novo* synthesis of the phospholipids phosphatidylcholine (PC) and phospatidylethanolamine (PE) through the Kennedy pathway. In islets, we detected no significant change in HMG-CoA, citicoline, nor CDP-ethanolamine. Additionally, the sugar nucleotide donor GDP-Mannose was observed to increase 14-fold in INS-1 cells (10), while in islets, we observed a modest increase of 2.9 ± 0.4 fold.

A lot of these differences can be attributed to the proliferative nature of INS-1 cells as compared to non-proliferating primary islets, suggesting that there may be many differences in metabolism between INS-1 cells and primary islets that could affect data interpretation of metabolomic experiments if researchers only study metabolism in clonal cell lines. One such difference is in glucose-stimulated PPP metabolite levels, which increase significantly in INS-1 cells. In our data, the only detectable PPP

metabolite decreased upon glucose stimulation, and other studies have reported smaller increases in ribose 5-phosphate in islets than in INS-1 cells. This difference could be because the PPP is used in clonal cells for the synthesis of nucleotides used in cell division/growth. Likewise, differences in LC-CoA concentrations following extended (>15 min) stimulation could be related to increased biosynthesis of membrane phospholipids in the proliferating INS-1 cells. These ideas would require more testing. It is important to note that our islet measurements only measured static metabolite levels, so we cannot directly determine whether changes in metabolite concentrations were due to changes in flux through a pathway or to increased/decreased synthesis or usage of metabolites.

Conclusion

We have developed a sample preparation method for the analysis of 62 known metabolites from groups of 50 murine islets of Langerhans by HILIC-TOF-MS. This is comparable to the 87 metabolites that were previously measured by this method in samples of INS-1 cells containing ~200 times the number of cells used here, with loss of some less abundant metabolites like succinyl CoA, ribose phosphate, 6-phosphogluconic acid (6PG), phosphoribosyl pyrophosphate (PRPP), and phosphoenolpyruvate (PEP). Compared to other islet metabolomics papers using 240-500 islets, we measured comparable numbers of metabolites. Other papers focused more on amino acids, with up to 12 detected (we only measured glutamate and aspartate) (11). We could not quantify these other amino acids with our current method due to poor peak shapes. Additionally, those studies were able to measure aconitate, ribose 5-phosphate, and PEP. These differences were likely due to differences in analysis methods, as we used HILIC-MS as opposed to GC-MS. Based on the total number of metabolites detected by undirected and directed analysis in our work compared to others', and the inability of protein content or stable-isotope labeled standards to reduce variation between samples, we concluded that sample variation was a larger impediment to reducing islet number in islet metabolomics than was metabolite detection.

In comparing islets with INS-1 cells, we found that the absolute concentrations of 7 tested metabolites were an order of magnitude higher in INS-1 cells than in islets. We also discovered a number of differences in metabolic responses to glucose stimulation; namely, in islets, we observed larger increases in hexose phosphates, no significant increases in citrate or ZMP, and less reduction in many LC CoAs compared to previously reported INS-1 results. The differences between islets and INS-1 cells could indicate key differences in metabolism, particularly in the pentose phosphate pathway and/or in glycerolipid/free fatty acid cycling during 2nd phase insulin secretion. The cause of these disparities is unclear. They could be related to differences in β-cell metabolism, cell incubation conditions, or species from which the cells are derived. Future work in mouse-derived MIN-6 cells or in human islets could discern species-related differences in β-cell metabolism.

Additionally, the islet metabolic response could be confounded by the presence of other cell types. Islets consist of glucagon-secreting α-cells, insulin-secreting β-cells, somatostatin-secreting δ-cells, pancreatic polypeptide-secreting PP cells, and grehlin-secreting ε-cells, of which the β-cell is the most prevalent, constituting anywhere from 50-80% of an islet's mass (43). The varying ratios in cell type can also contribute to the sample-to-sample variability that is observed in islets. Regardless of the cause of the disparities in islet and INS-1 cell metabolic responses, this work both underscores the significance of sample preparation/cell culture methods in the interpretation of metabolomic results and highlights the importance of corroborating findings obtained using clonal cell lines with data derived from primary islets.

References

1. Henquin, J.-C. (2000) Triggering and amplifying pathways of regulation of insulin secretion by glucose. *Diabetes*. **49**, 1751–1760
2. Rutter, G. A. (2001) Nutrient-secretion coupling in the pancreatic islet beta-cell: Recent advances. *Mol. Aspects Med.* **22**, 247–284
3. Newsholme, P., Gaudel, C., and McClenaghan, N. H. (2010) Nutrient Regulation of Insulin Secretion and β-Cell Functional Integrity. in *The Islets of Langerhans* (Islam, M. S. ed), pp. 91–114, Springer Netherlands, Dordrecht, **654**, 91–114
4. Farfari, S., Schulz, V., Corkey, B., and Prentki, M. (2000) Glucose-regulated anaplerosis and cataplerosis in pancreatic beta-cells: possible implication of a pyruvate/citrate shuttle in insulin secretion. *Diabetes*. **49**, 718–726
5. Vuckovic, D. (2012) Current trends and challenges in sample preparation for global metabolomics using liquid chromatography–mass spectrometry. *Anal. Bioanal. Chem.* **403**, 1523–1548
6. Martineau, E., Tea, I., Loaëc, G., Giraudeau, P., and Akoka, S. (2011) Strategy for choosing extraction procedures for NMR-based metabolomic analysis of mammalian cells. *Anal. Bioanal. Chem.* **401**, 2133–2142
7. Tian, L., Kim, H. S., Kim, H., Jin, X., Jung, H. S., Park, K. S., Cho, K. W., Park, S., and Moon, W. K. (2013) Changes in Metabolic Markers in Insulin-Producing β-Cells during Hypoxia-Induced Cell Death As Studied by NMR Metabolomics. *J. Proteome Res.* **12**, 3738–3745
8. Dietmair, S., Timmins, N. E., Gray, P. P., Nielsen, L. K., and Krömer, J. O. (2010) Towards quantitative metabolomics of mammalian cells: Development of a metabolite extraction protocol. *Anal. Biochem.* **404**, 155–164
9. Lorenz, M. A., Burant, C. F., and Kennedy, R. T. (2011) Reducing Time and Increasing Sensitivity in Sample Preparation for Adherent Mammalian Cell Metabolomics. *Anal. Chem.* **83**, 3406–3414
10. Lorenz, M. A., El Azzouny, M. A., Kennedy, R. T., and Burant, C. F. (2013) Metabolome Response to Glucose in the β-Cell Line INS-1 832/13. *J. Biol. Chem.* **288**, 10923–10935
11. Spégel, P., Sharoyko, V. V., Goehring, I., Danielsson, A. P. H., Malmgren, S., Nagorny, C. L. F., Andersson, L. E., Koeck, T., Sharp, G. W. G., Straub, S. G., Wollheim, C. B., and Mulder, H. (2013) Time-resolved metabolomics analysis of β-cells implicates the pentose phosphate pathway in the control of insulin release. *Biochem. J.* **450**, 595–605
12. Huang, M., and Joseph, J. W. (2012) Metabolomic analysis of pancreatic β-cell insulin release in response to glucose. *Islets*. **4**, 210–222
13. Huang, M., and Joseph, J. W. (2014) Assessment of the Metabolic Pathways Associated With Glucose-Stimulated Biphasic Insulin Secretion. *Endocrinology*. **155**, 1653–1666
14. Wallace, M., Whelan, H., and Brennan, L. (2013) Metabolomic analysis of pancreatic beta cells following exposure to high glucose. *Biochim. Biophys. Acta BBA - Gen. Subj.* **1830**, 2583–2590
15. Dixon, G., Nolan, J., McClenaghan, N., Flatt, P. R., and Newsholme, P. (2003) A comparative study of amino acid consumption by rat islet cells and the clonal beta-cell line BRIN-BD11-the functional significance of L-alanine. *J. Endocrinol.* **179**, 447–454

16. Iwasaki, M., Minami, K., Shibasaki, T., Miki, T., Miyazaki, J., and Seino, S. (2010) Establishment of new clonal pancreatic β-cell lines (MIN6-K) useful for study of incretin/cyclic adenosine monophosphate signaling: Novel pancreatic β-cell lines. *J. Diabetes Investig.* 10.1111/j.2040-1124.2010.00026.x
17. Hohmeier, H. E., Mulder, H., Chen, G., Henkel-Rieger, R., Prentki, M., and Newgard, C. B. (2000) Isolation of INS-1-derived cell lines with robust ATP-sensitive K+ channel-dependent and-independent glucose-stimulated insulin secretion. *Diabetes*. **49**, 424–430
18. Liu, Z., Jeppesen, P. B., Gregersen, S., Chen, X., and Hermansen, K. (2008) Dose- and Glucose-Dependent Effects of Amino Acids on Insulin Secretion from Isolated Mouse Islets and Clonal INS-1E Beta-Cells. *Rev. Diabet. Stud.* **5**, 232–244
19. McClenaghan, N. H. (2007) Physiological regulation of the pancreatic β-cell: functional insights for understanding and therapy of diabetes: Insights into pancreatic β-cell regulation. *Exp. Physiol.* **92**, 481–496
20. Kelly, C., Guo, H., McCluskey, J. T., Flatt, P. R., and McClenaghan, N. H. (2010) Comparison of insulin release from MIN6 pseudoislets and pancreatic islets of Langerhans reveals importance of homotypic cell interactions. *Pancreas*. **39**, 1016–1023
21. Ronnebaum, S. M., Jensen, M. V., Hohmeier, H. E., Burgess, S. C., Zhou, Y.-P., Qian, S., MacNeil, D., Howard, A., Thornberry, N., Ilkayeva, O., Lu, D., Sherry, A. D., and Newgard, C. B. (2008) Silencing of Cytosolic or Mitochondrial Isoforms of Malic Enzyme Has No Effect on Glucose-stimulated Insulin Secretion from Rodent Islets. *J. Biol. Chem.* **283**, 28909–28917
22. Sargsyan, E., and Bergsten, P. (2011) Lipotoxicity is glucose-dependent in INS-1E cells but not in human islets and MIN6 cells. *Analysis*. **11**, 15
23. Alanentalo, T., Asayesh, A., Morrison, H., Lorén, C. E., Holmberg, D., Sharpe, J., and Ahlgren, U. (2007) Tomographic molecular imaging and 3D quantification within adult mouse organs. *Nat. Methods*. **4**, 31–33
24. Kauri, L. M., Jung, S.-K., and Kennedy, R. T. (2003) Direct measurement of glucose gradients and mass transport within islets of Langerhans. *Biochem. Biophys. Res. Commun.* **304**, 371–377
25. Li, C., Liu, C., Nissim, I., Chen, J., Chen, P., Doliba, N., Zhang, T., Nissim, I., Daikhin, Y., Stokes, D., Yudkoff, M., Bennett, M. J., Stanley, C. A., Matschinsky, F. M., and Naji, A. (2013) Regulation of Glucagon Secretion in Normal and Diabetic Human Islets by γ-Hydroxybutyrate and Glycine. *J. Biol. Chem.* **288**, 3938–3951
26. Pralong, W. F., Bartley, C., and Wollheim, C. B. (1990) Single islet beta-cell stimulation by nutrients: relationship between pyridine nucleotides, cytosolic Ca2+ and secretion. *EMBO J.* **9**, 53
27. Tautenhahn, R., Patti, G. J., Rinehart, D., and Siuzdak, G. (2012) XCMS Online: A Web-Based Platform to Process Untargeted Metabolomic Data. *Anal. Chem.* **84**, 5035–5039
28. Rammouz, R. E., Létisse, F., Durand, S., Portais, J.-C., Moussa, Z. W., and Fernandez, X. (2010) Analysis of skeletal muscle metabolome: Evaluation of extraction methods for targeted metabolite quantification using liquid chromatography tandem mass spectrometry. *Anal. Biochem.* **398**, 169–177

29. Edwards, J. L., and Kennedy, R. T. (2005) Metabolomic Analysis of Eukaryotic Tissue and Prokaryotes Using Negative Mode MALDI Time-of-Flight Mass Spectrometry. *Anal. Chem.* **77**, 2201–2209
30. Detimary, P., Van den Berghe, G., and Henquin, J.-C. (1996) Concentration dependence and time course of the effects of glucose on adenine and guanine nucleotides in mouse pancreatic islets. *J. Biol. Chem.* **271**, 20559–20565
31. Panten, U., Willenborg, M., Schumacher, K., Hamada, A., Ghaly, H., and Rustenbeck, I. (2013) Acute metabolic amplification of insulin secretion in mouse islets is mediated by mitochondrial export of metabolites, but not by mitochondrial energy generation. *Metabolism*. **62**, 1375–1386
32. Bolten, C. J., Kiefer, P., Letisse, F., Portais, J.-C., and Wittmann, C. (2007) Sampling for Metabolome Analysis of Microorganisms. *Anal. Chem.* **79**, 3843–3849
33. Chandra, S., and Avedisian, C. T. (1991) On the collision of a droplet with a solid surface. *Proceeding R. Soc. Math. Phys. Eng. Sci.* **432**, 13–41
34. Kimball, E., and Rabinowitz, J. D. (2006) Identifying decomposition products in extracts of cellular metabolites. *Anal. Biochem.* **358**, 273–280
35. Li, C., Nissim, I., Chen, P., Buettger, C., Najafi, H., Daikhin, Y., Nissim, I., Collins, H. W., Yudkoff, M., Stanley, C. A., and Matschinsky, F. M. (2008) Elimination of KATP Channels in Mouse Islets Results in Elevated [U-13C]Glucose Metabolism, Glutaminolysis, and Pyruvate Cycling but a Decreased -Aminobutyric Acid Shunt. *J. Biol. Chem.* **283**, 17238–17249
36. Liu, Y. Q., Moibi, J. A., and Leahy, J. L. (2004) Chronic High Glucose Lowers Pyruvate Dehydrogenase Activity in Islets through Enhanced Production of Long Chain Acyl-CoA: PREVENTION OF IMPAIRED GLUCOSE OXIDATION BY ENHANCED PYRUVATE RECYCLING THROUGH THE MALATE-PYRUVATE SHUTTLE. *J. Biol. Chem.* **279**, 7470–7475
37. MacDonald, M. J. (2004) Perspective: emerging evidence for signaling roles of mitochondrial anaplerotic products in insulin secretion. *AJP Endocrinol. Metab.* **288**, E1–E15
38. Spégel, P., Malmgren, S., Sharoyko, V. V., Newsholme, P., Koeck, T., and Mulder, H. (2011) Metabolomic analyses reveal profound differences in glycolytic and tricarboxylic acid cycle metabolism in glucose-responsive and -unresponsive clonal β-cell lines. *Biochem. J.* **435**, 277–284
39. Lu, D., Mulder, H., Zhao, P., Burgess, S. C., Jensen, M. V., Kamzolova, S., Newgard, C. B., and Sherry, A. D. (2002) 13C NMR isotopomer analysis reveals a connection between pyruvate cycling and glucose-stimulated insulin secretion (GSIS). *Proc. Natl. Acad. Sci.* **99**, 2708–2713
40. Patterson, J. N., Cousteils, K., Lou, J. W., Manning Fox, J. E., MacDonald, P. E., and Joseph, J. W. (2014) Mitochondrial Metabolism of Pyruvate Is Essential for Regulating Glucose-stimulated Insulin Secretion. *J. Biol. Chem.* **289**, 13335–13346
41. Deeney, J. T., Prentki, M., and Corkey, B. E. (2000) Metabolic control ofβ-cell function. *Semin. Cell Dev. Biol.* **11**, 267–275
42. Roduit, R., Nolan, C., Alarcon, C., Moore, P., Barbeau, A., Delghingaro-Augusto, V., Przybykowski, E., Morin, J., Massé, F., Massie, B., Ruderman, N., Rhodes, C., Poitout, V., and Prentki, M. (2004) A role for the malonyl-CoA/long-chain acyl-CoA

pathway of lipid signaling in the regulation of insulin secretion in response to both fuel and nonfuel stimuli. *Diabetes*. **53**, 1007–1019
43. In't Veld, P., and Marichal, M. (2010) Microscopic Anatomy of the Human Islet of Langerhans. in *The Islets of Langerhans* (Islam, M. S. ed), pp. 1–19, Springer Netherlands, Dordrecht, **654**, 1–19

CHAPTER 4

Application of Metabolomic Method to the Study of Oxidative Stress in Islets

Cynthia M. Cipolla, Mahmoud El Azzouny, Shusheng Lu, Robert T. Kennedy

Introduction

Islets are susceptible to oxidative damage due to their low levels of the antioxidants catalase, selenium-dependent glutathione peroxidase 1 (GPX1), and Cu,Zn-superoxide dismutase 1 (SOD1) (1). Oxidative stress temporarily blocks glycolysis, after which cells can either be repaired or undergo apoptosis (2, 3). Previous studies have shown that oxidative stress (induced via transient hyperglycemia (4), lipid peroxidation (5), or transient hydrogen peroxide administration (6, 7)) results in DNA strand breaks, mitochondrial dysfunction, alterations in calcium homeostasis, and inhibition of glucose-stimulated insulin secretion (GSIS) in islets.

Oxidative stress-induced damage can occur to islets as a result of reactive oxygen species (ROS) formed during autoimmune reactions in type 1 diabetes (8) or as a result of increased mitochondrial respiration due to high insulin demand in type 2 diabetes (9). Therefore, better understanding of the mechanisms of oxidative damage may be useful in understanding β-cell dysfunction that accompanies diabetes.

Oxidative damage to islets is also a known impediment to islet transplantation, a promising treatment for type 1 diabetes. Current isolation and culture methods induce stresses on islets that can result in oxidative damage in culture, while after the islets are transplanted, poor vascularization can also result in oxidative damage to the cells (10). In turn, this damage leads to impaired islet function, cell death and poor outcome to the

transplant. One study found that treating human pancreata with the antioxidant glutamine intra-ductally prior to islet isolation leads to higher occurrences of diabetes reversal when islets are transplanted into mice than conventional isolation procedures (10). Better understanding of oxidative damage may therefore be useful in understanding how to more effectively preserve islets for transplant.

Understanding oxidative damage more completely may also be useful in evaluating islets for their potency and viability prior to transplant. Such a method is necessary for regulatory reasons and to improve the success rate of clinical islet transplants. At present, standard islet viability and potency testing prior to transplantation involve inclusive and exclusive dyes (11) and static GSIS measurements. However, results from these tests do not correlate well with clinical results; i.e., islets with strong GSIS *in vitro* do not always result in a successful transplantation and vice versa. Many times, islet transplant patients need several islet infusions to obtain insulin-independence, and the rates of long-term insulin-independence (~55%, sustained over 5 years) have been relatively poor compared to other treatments (12). These results suggest that the currently used measures do not sufficiently capture the status of cells and their potential for longer term function. More in depth measures may be needed to for adequate markers of islet viability and potency.

To address these needs, we used a metabolomic approach to assess islets before and after oxidative stress. As illustrated in previous work using NMR to study the metabolome of β-cells during hypoxia, measuring many metabolites provides a powerful tool for investigating stress-induced alterations in cellular pathways (13). We felt that it may be possible to identify potential markers of oxidative stress that could be useful in an islet potency test prior to transplant.

A desirable metabolomic method should be able to quantify many classes of metabolites with good reproducibility, sensitivity, and dynamic range. Accordingly, we used high performance liquid chromatography-time-of-flight mass spectrometry (HPLC-TOF-MS) here because of its high sensitivity, selectivity, and applicability to many types

of metabolites. Previous metabolomic studies have typically been conducted with clonal beta-cells due to their ease of access and specificity for beta-cell metabolism (14–22). However, clonal cells are derived from a cancer line and as such may favor pathways involved in cell growth, which could result in different metabolic regulation than would be seen in a native cell population. For this reason, it is important to corroborate data obtained from clonal cells with data derived from native islets.

In this work, islets treated with hydrogen peroxide were used as a model of oxidative stress, based on the biological role of hydrogen peroxide as an intermediate in free radical cytotoxicity and on its capability to diffuse across plasma membranes (23). We measured islets' insulin, calcium, and metabolic responses to basal and stimulatory levels of glucose at multiple time points following acute hydrogen peroxide administration. Our goal was to examine the immediate and long term responses to acute oxidative stress on the metabolic pathways involved in GSIS. Such study should help reveal short term and longer lasting alterations in metabolite levels and the ability of islets to recover normal metabolic response after an oxidative challenge. We also aimed to determine if the metabolic profile could indicate whether islets had previously undergone oxidative stress, which would be valuable for use as a biomarker. This work has possible implications on type 1 and type 2 diabetes pathogenesis and on islet viability assays.

Experimental Procedures

Materials

Electrophoresis buffers were: balanced salt solution (BSS), consisting of 125 mM NaCl, 5.9 mM KCl, 1.2 mM $MgCl_2$, 2.4 mM $CaCl_2$, 25 mM tricine, and 0.7 mg mL^{-1} BSA; immunoassay buffer, consisting of 60 mM NaCl, 1 mM EDTA, 20 mM tricine, 0.1% (w/v) Tween-20, and 0.7 mg mL^{-1} BSA; and electrophoresis buffer, consisting of 20 mM NaCl and 150 mM tricine. Kreb's Ringer Buffer (KRB) consisted of 20 mM HEPES, 118 mM NaCl, 5.4 mM KCl, 1.2 mM $MgSO_4 \bullet 7H_2O$, 1.2 mM KH_2PO_4, and 2.4 mM $CaCl_2$. All buffers were adjusted to pH 7.4.

Roswell Park Memorial Institute (RPMI) culture medium, fetal bovine serum, penicillin-streptomycin, collagenase, fura-2 dye, and anti-insulin antibody were purchased from Life Technologies (Carlsbad, CA). FITC-insulin, acetonitrile, ammonium acetate, methanol, and chloroform were purchased from Sigma-Aldrich (St. Louis, MO). All other chemicals were purchased from Thermo Fisher Scientific (Waltham, MA).

Glass Microfluidic Chip Fabrication

Glass microfluidic chips were fabricated as previously described (24). Briefly, blank 2.5 cm x 7.6 cm x 1.1 mm glass slides coated with a 530 nm thick layer of AZ1518 positive photoresist over a 120 nm chrome layer (Telic Co., Santa Monica, CA) were exposed to collimated UV light through patterned photomasks for 5 s. The exposed slides were developed in AZ726 MIF Developer (Microchemicals) for 30 s, and the underlying chrome was removed using CEP-200 Chrome Etchant (Microchrome Technologies, Inc., San Jose, CA). The exposed glass was etched in a solution of 14:20:66 (v/v/v) HNO_3/HF/H_2O for variable times depending on desired channel depth. Carbide drill bits (Kyocera Precision Tools, Inc., Hendersonville, NC) were used to drill 360 µm diameter access holes. The remaining photoresist and chrome were then removed using acetone and CEP-200 chrome etchant, respectively, and the etched glass plates were cleaned in piranha solution (3:1 v/v H_2SO_4/H_2O_2) for 20 min followed by heated RCA solution (5:1:1 v/v/v H_2O/NH_4/H_2O_2) for 40 min. Chips were aligned under water, dried, and annealed at 640 ºC for 8 h. Microfluidic reservoirs (Upchurch Scientific, Oak Harbor, WA) were applied over access holes after bonding.

Cell Culture and H_2O_2 Treatment

Pancreatic islets were isolated from 20-30 g male CD-1 mice as previously described (25). Islets were cultured in RPMI-1640 media supplemented with 11 mM glucose, 10% fetal bovine serum, and 1% penicillin/streptomycin at 37 ºC and 5% CO_2 for 2-3 days prior to experimentation. Islets were then incubated in culture media with 100 µM H_2O_2 for 30-40 min, after which they were rinsed with fresh media and incubated in RPMI for an additional 0, 1, 2, or 4 hours. Following incubation, islets were used immediately for calcium and insulin experiments, while for metabolomic experiments, they were then

incubated for 1 h in KRB supplemented with 2.8 mM glucose. This hour was accounted for in the reported culture time, so immediate response experiments were performed with H_2O_2 added to the KRB.

Dynamic Insulin Secretion

Dynamic insulin secretion was measured by microchip-based electrophoretic competitive immunoassay as previously reported (26). Briefly, islets were rinsed with balanced salt solution (BSS) and loaded into a microfluidic perfusion chamber. Secreted insulin was sampled by electroosmotic flow (EOF), mixed with fluorescein isothiocyanate (FITC)-labeled insulin and anti-insulin antibody, and injected onto a separation channel in 8 s intervals. Laser-induced fluorescence at the end of the separation channel was detected using a photomultiplier tube (PMT). The ratio of FITC-insulin bound to antibody to FITC-insulin free in solution (B/F) was calculated and converted to insulin concentrations using calibration standards. This approach allowed insulin secretion from islets to be continuously measured at 8 s intervals in real-time.

Calcium Flux Measurement

$[Ca^{2+}]_i$ was measured using fura-2 dye as previously described (27). Briefly, islets were loaded with 2 µM fura-2-AM via a 45 min incubation. They were then rinsed with KRB and loaded into a microfluidic chamber, where they were perfused with KRB containing basal (2.8 mM) and stimulatory (16.7 mM) levels of glucose. The dye was excited alternately with 340 nm (Ca^+-complexed dye) and 380 nm (free dye) light and emission was collected at 510 nm. The ratio of complexed to free dye was calculated and converted to Ca^+ concentrations using calibration standards.

Metabolite Measurement

Groups of 50 islets were incubated in KRB supplemented with 2.8 mM glucose for 1 h, after which glucose was spiked into the high glucose samples to a final concentration of 16.7 mM. Following an additional 15 min incubation, islets were collected into Eppendorf tubes, samples were centrifuged for 30 s, supernatant was removed, and metabolism was quenched via addition of 100 µL of 90% 9:1 methanol:chloroform/10%

water at -75 ºC (stored on dry ice). Samples were stored at -80 ºC for up to 2 weeks prior to use. Over this time, there should be no significant loss or alteration of the metabolite profile (14). Immediately before analysis, islets were lysed using a probe sonicator. Samples were then centrifuged at 4 ºC for 5 min and the supernatant was transferred to LC vials.

Analyses were performed using HPLC-TOF-MS. Chromatographic separations of polar compounds were carried out on a Phenomenex Luna NH_2 column (150 x 1 mm, 3 µm particle size). Mobile phase A consisted of acetonitrile and mobile phase B consisted of 5 mM ammonium acetate, adjusted to pH 9.9 with ammonium hydroxide. The gradient program was (time, %B, flow rate): 0 min, 20%, 70 µL min^{-1}; 25 min, 100%, 70 µL min^{-1}. Injection volume was 30 µL, column temperature was 25 ºC, and autosampler temperature was 6 ºC. Separations of nonpolar compounds were performed on a Waters Acquity UPLC C18 column (2.1 x 50 mm, 1.7 µm particle size) equipped with a guard column (2.1 x 5 mm, 1.7 µm particle size). Mobile phase A consisted of 8:2 isopropanol/methanol and mobile phase B consisted of 4:4:2 water/acetonitrile/methanol. Injection volume was 15 µL, column temperature was 45 ºC, and autosampler temperature was 6 ºC. An Agilent Technologies LC/MSD TOF equipped with a dual electrospray ionization (ESI) source was used for detection in negative ion mode for HILIC analysis and in positive ion mode for reverse phase separations.

Directed analysis was performed for a series of 87 metabolites previously identified in islets or in INS-1 cells. Of these, 62 were consistently measured in our samples. We have chosen to focus here on those that exhibited changes due to glucose concentration or H_2O_2 treatment. Metabolites were identified using retention time compared to standards and accurate mass. Combined peak areas were reported for unresolved isomers, like citrate/isocitrate (CIT/ICIT) and glucose-6-phosphate/fructose-6-phosphate (G6P/F6P). For most metabolites, peak areas were measured from extracted ion chromatograms of $[M-H]^-$ metabolite ions with ±70 ppm detection windows

centered on the theoretical mass. $[M-2H]^{2-}$ ions were used for acetyl-CoA (aCoA) and other CoAs to improve sensitivity.

To account for instrumental drift, samples were randomized prior to injection onto the columns. To account for variations in MS sensitivity from run-to-run, metabolite peak area fold changes as compared to the average metabolite peak areas measured from control samples maintained at basal levels of glucose were calculated and used to compare results from separate runs rather than absolute peak areas.

Apoptosis Assay

Apoptosis was measured using the Apo-ONE Homogenous Caspase 3/7 Assay kit (Promega, Corporation, Madison, WI) according to the manufacturer's protocol as previously described (28). Briefly, islets were treated with H_2O_2 for 40 min, then rinsed with culture media and aliquoted into an opaque 96-well plate in triplicate (25 islets/well), where they were incubated for 0-4 h. Apo-One Caspase 3/7 reagent, containing active substrate Z-DEVD-R110, was then added to each well. Caspase 3/7 activity cleaved the DEVD peptide groups to create the fluorescent product Rhodamine 110. After 1.5 h incubation, the fluorescence was read using a plate reader equipped with 485 nm excitation and 535 nm emission filters.

Protein Quantification

Proteins were quantified using a Pierce Bicinchoninic Acid (BCA) assay kit (Life Technologies, Carlsbad, CA) according to the manufacturer's protocol. Briefly, islet pellets were dissolved in 100 µL radio-immunoprecipitation assay (RIPA) lysis and extraction buffer. Samples and standards were then aliquoted in triplicate into a 96-well plate (25 µL per well) and 200 µL of working reagent was added to each well. After mixing briefly, the plates were incubated at room temperature overnight and then the absorbance at 562 nm was read using a plate reader.

PI Staining

Islets were treated with 100 μM H_2O_2 for 40 min, then transferred to a microfluidic chip, where they were perfused with culture media for 0-4 h. Islets were then perfused with 100 ng/mL propidium iodide (PI) solution in culture media for 30 min prior to rinsing and imaging. PI stained late apoptotic and necrotic cells. The fluorescence was imaged using a xenon arc lamp, green filter, and CCD camera.

Immunohistochemical Staining

Islets were treated with 100 μM H_2O_2 for 30 min in RPMI, then were rinsed and incubated for 4 h in fresh RPMI. Immunohistochemical staining was used to quantify insulin and glucagon-containing cells as previously described (29). Briefly, islets were fixed for 1 h with Bouin's solution and then with formalin until they were embedded in paraffin blocks. The embedded islets were sectioned and then stained with anti-insulin and anti-glucagon antibodies. Fluorescent secondary antibodies were used for detection of β-cells and α-cells via fluorescence microscopy. ImageJ software was used for cell counting.

Statistical Analysis

Data are reported as means ± 1 standard error of the mean (SEM). Statistical significance ($p < 0.05$) was determined using either 2-way ANOVA or an independent sample, two-tailed Student's t-test, assuming equal variance.

Results

Dynamic Insulin Secretion and Calcium Flux

We measured $[Ca^{2+}]_i$ and insulin secretion in response to an increase in extracellular glucose concentration from 3 to 16.7 mM in control islets and islets that had been treated with H_2O_2 for 30 min. The treated islets were removed from H_2O_2 either 0, 1, 2, or 4 h prior to testing. Basal $[Ca^{2+}]_i$ and insulin secretion were elevated as compared to control immediately following H_2O_2 treatment, reaching maximal levels 1 h following exposure, as shown in Figure 4.1a-b. Basal $[Ca^{2+}]_i$ returned to control concentrations within 4 h following H_2O_2 treatment.

Control islets showed an immediate rise in $[Ca^{2+}]_i$ and insulin secretion in response to glucose stimulation (Figure 4.2a). The $[Ca^{2+}]_i$ response tended to stay level, but the insulin plot showed a biphasic response with a distinct first phase peak that lasted ~4 min followed by a second phase of elevated insulin secretion. Immediately after treatment with H_2O_2, $[Ca^{2+}]_i$ increased slowly in response to glucose stimulation, while insulin secretion increased abruptly but plateaued with no distinct 1st phase peak, as shown in Figure 4.2b. One hour following treatment, $[Ca^{2+}]_i$ response to glucose stimulation showed a slow rise qualitatively similar to that immediately after H_2O_2. The insulin response showed first phase and second phase dynamics that began to resemble controls (Figure 4.2c). Two hours after H_2O_2 exposure, immediate influx of Ca^{2+} in response to glucose stimulation was observed while insulin response to glucose exhibited exaggerated 1st and 2nd phase responses as compared to control (Figure 4.2d).

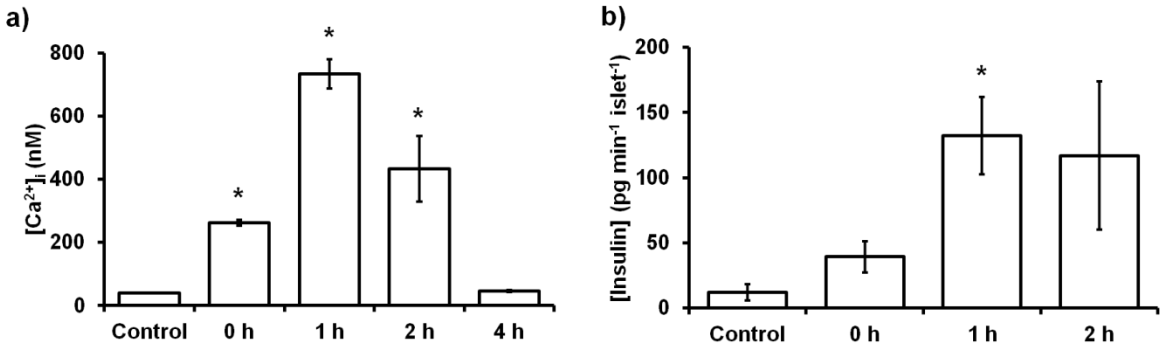

Figure 4.1. Basal $[Ca^{2+}]_i$ and insulin secretion following 30-40 min H_2O_2 treatment. At the indicated time points following treatment, islets were placed in a microfluidic device and were perfused with 3 mM glucose while a) $[Ca^{2+}]_i$ or (b) insulin secretion was measured. n = 4-9 islets per bar. Error bars represent SEM. Asterisks indicate significant difference ($p < 0.05$) compared to control as determined by an independent samples, two-tailed student's t-test.

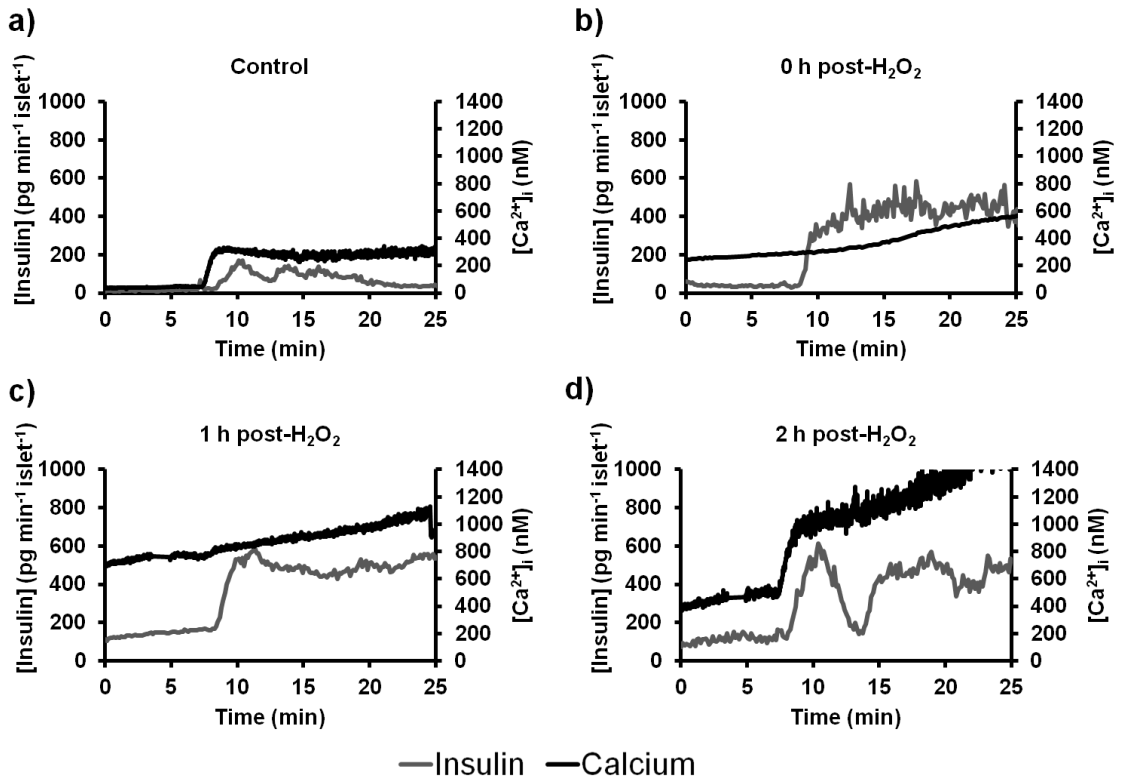

Figure 4.2. Average $[Ca^{2+}]_i$ and insulin secretion timescale responses to 16.7 mM glucose stimulation at various times following acute H_2O_2 treatment. Time points were a) control b) 0 h c) 1 h d) 2 h (n = 4-9 islets per trace). Basal was 2.8 mM glucose.

Islet Morphology

Murine islets are typically oblong to spherical in shape with smooth membranes and a diameter of ~100-300 µm, as shown in Figure 4.3a. Immediately following exposure to H_2O_2, the islet morphology remained largely unchanged (Figure 4.3b). However, after 1 h perfusion with fresh culture media, significant membrane blebbing started to occur (Figure 4.3c), and was even more pronounced 2 h post-H_2O_2 (Figure 4.3d). After 4 h, blebbed cells (Figure 4.3e) were easily shed by mechanical disturbance (i.e. by pipetting), resulting in islets consisting of reduced mass and lowered total protein content (Figure 4.4), but that had regained their membrane boundaries (Figure 4.3f).

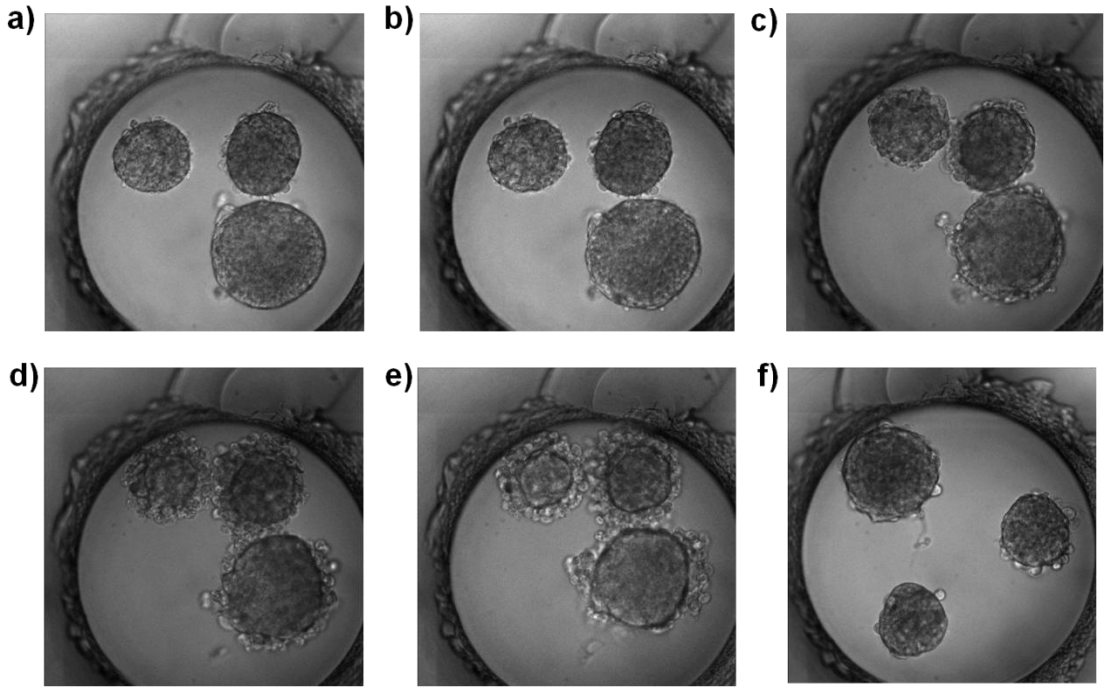

Figure 4.3. Islet morphology at various time points following H_2O_2 treatment. a) Control islets were placed on a microfluidic chip and imaged. b) Islets were then perfused with 100 µM H_2O_2 in RPMI for 40 min, after which they were imaged. Perfusion solution was switched to RPMI (no H_2O_2), and islets were imaged c) 1 h d) 2 h and e) 4 h later. f) A separate 3 islets were treated with H_2O_2 off-chip using the same conditions and transferred to the chip for imaging 4 h following removal of H_2O_2. Mechanical disturbance via pipette caused shedding of blebbed cells, resulting in redefined plasma membranes.

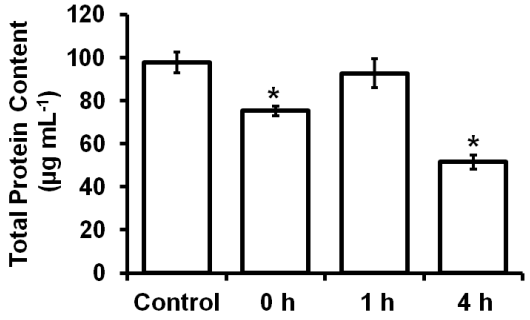

Figure 4.4. Protein content in islets at various time points following exposure to 100 µM H_2O_2 (n = 6-18 sets of 50 islets per bar). Error bars represent SEM. Asterisks indicate significant difference ($p < 0.05$) compared to control, as determined by an independent samples, two-tailed student's t-test.

Sample Group Equivalency

All metabolomic experiments were performed on groups of 50 islets with 1 h exposure to KRB supplemented with 3 mM glucose. However, after H_2O_2 treatment, a portion of

cells underwent apoptosis and/or necrosis, reducing islet mass in those sample groups, as substantiated by a 2-fold decrease in total sample protein content 4 h post-H_2O_2 stress ($p < 0.0001$), as shown in Figure 4.4. This leads to the possibility that the 4 h post-H_2O_2 sample group did not contain a comparable number of cells as the other groups, thus obfuscating the results. To overcome this issue, we normalized the raw peak areas to protein content for all islet samples.

A second concern was that the ratio of β-cells to α-cells in the islet would be altered by H_2O_2 treatment. Because α-cells are located on the periphery of the islet in rodents (30), they could be more susceptible to damage. We used immunohistochemical staining to image insulin and glucagon-containing cells in control and H_2O_2-treated islets subjected to a 4 h culture period post-stress, as shown in Figure 4.5a-b. Of total cells counted, control islets contained 10 ± 2% α-cells. As suspected, H_2O_2-treated islets exhibited very few α-cells overall, with several islets not containing any α-cells. Because the amount of α-cells in the control islets was low, we assumed they did not contribute significantly to the metabolite levels measured.

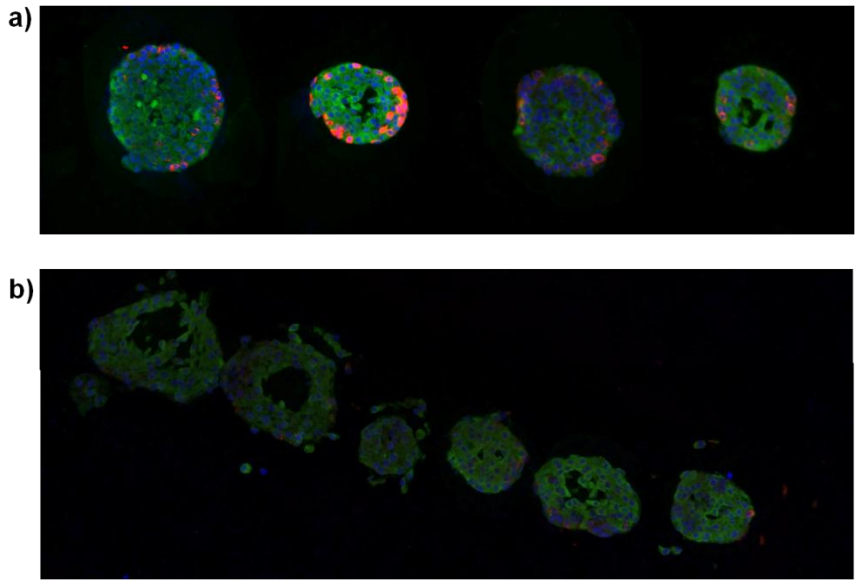

Figure 4.5. Immunohistochemical staining of islets. Islets were stained for insulin (blue) and glucagon (red). a) Control islets contained 10 ± 2% α-cells (n = 6). b) Islets treated for 30 min with H_2O_2 followed by 4 h incubation in fresh RPMI exhibited poor islet architecture and very few α-cells (n = 8). Images courtesy of Lynda Elghazi-Cras.

Metabolomic Profile

We examined the immediate effect of H_2O_2 administered in KRB on the metabolic profile in islets, shown in Figures 4.6a and 4.7a-c. Metabolite amounts are reported as fold changes compared to control islets at basal glucose concentration. Control islets exhibited increased amounts of glycolysis and tricarboxylic acid (TCA) cycle components and increased cellular energetics following stimulation with high glucose, which correlated with previously reported responses in islets and in INS-1 cells (15–17), indicating that the metabolomic method was able to reliably detect changes in intracellular metabolites.

In the H_2O_2-treated islets, we found evidence of oxidative stress immediately following the treatment, as shown by a 2-fold decrease in reduced to oxidized glutathione ratio (GSH/GSSG). We also observed changes consistent with a blockage in glycolytic flux at this time point, as demonstrated by significant increases in upstream metabolites G6P/F6P and fructose 1,6-bisphosphate (FBP) at both basal and stimulatory glucose concentrations. These results were consistent with a block of the enzyme glyceraldehyde 3-phosphate dehydrogenase (GAPDH) (4). Adenosine monophosphate (AMP), adenosine diphosphate (ADP), guanosine monophosphate (GMP), and guanosine diphosphate (GDP) were all elevated as well, which resulted in decreased ATP/ADP and GTP/GDP ratios. Nucleotide cofactors nicotinamide adenine dinucleotide (NAD^+) and reduced nicotinamide adenine dinucleotide phosphate (NADPH) were decreased, although nicotinamide adenine dinucleotide phosphate ($NADP^+$) was elevated, resulting in reduced NADPH/$NADP^+$ ratios. Most TCA cycle components were unaffected, with the exception of malonyl CoA (mCoA), which was reduced 3-fold. Several long chain CoA (16:0 and 18:0 CoA) concentrations also trended down immediately following H_2O_2 treatment, although the decrease was not significant ($p = 0.09$).

Next, we investigated how metabolome response to glucose stimulation was affected in islets that had been treated with H_2O_2 and then cultured in fresh media for either 1 or 4 h (Figures 4.6b and 4.7). We observed that all nucleotides that had been affected in the

immediate response returned to or near control levels within 4 h. Glycolysis apparently resumed normal function shortly after H_2O_2 treatment ended, with most metabolites returning to or approaching control levels after 4 h culture. FBP remained elevated at both basal and stimulatory levels of glucose 4 h post-H_2O_2; however, the levels were only 3-fold above control, whereas they had reached 7-fold above control with high glucose immediately following H_2O_2 administration. TCA cycle components remained unaffected, except for continued reduced levels of mCoA until at least 4 h post-stress and 1.5-fold lower acetyl CoA (aCoA) levels 1 h post-stress. Several other compounds were significantly affected during culture following H_2O_2 stress, including increases in levels of many fatty acids following 1 h culture and increases in many phospholipid levels following 4 h culture.

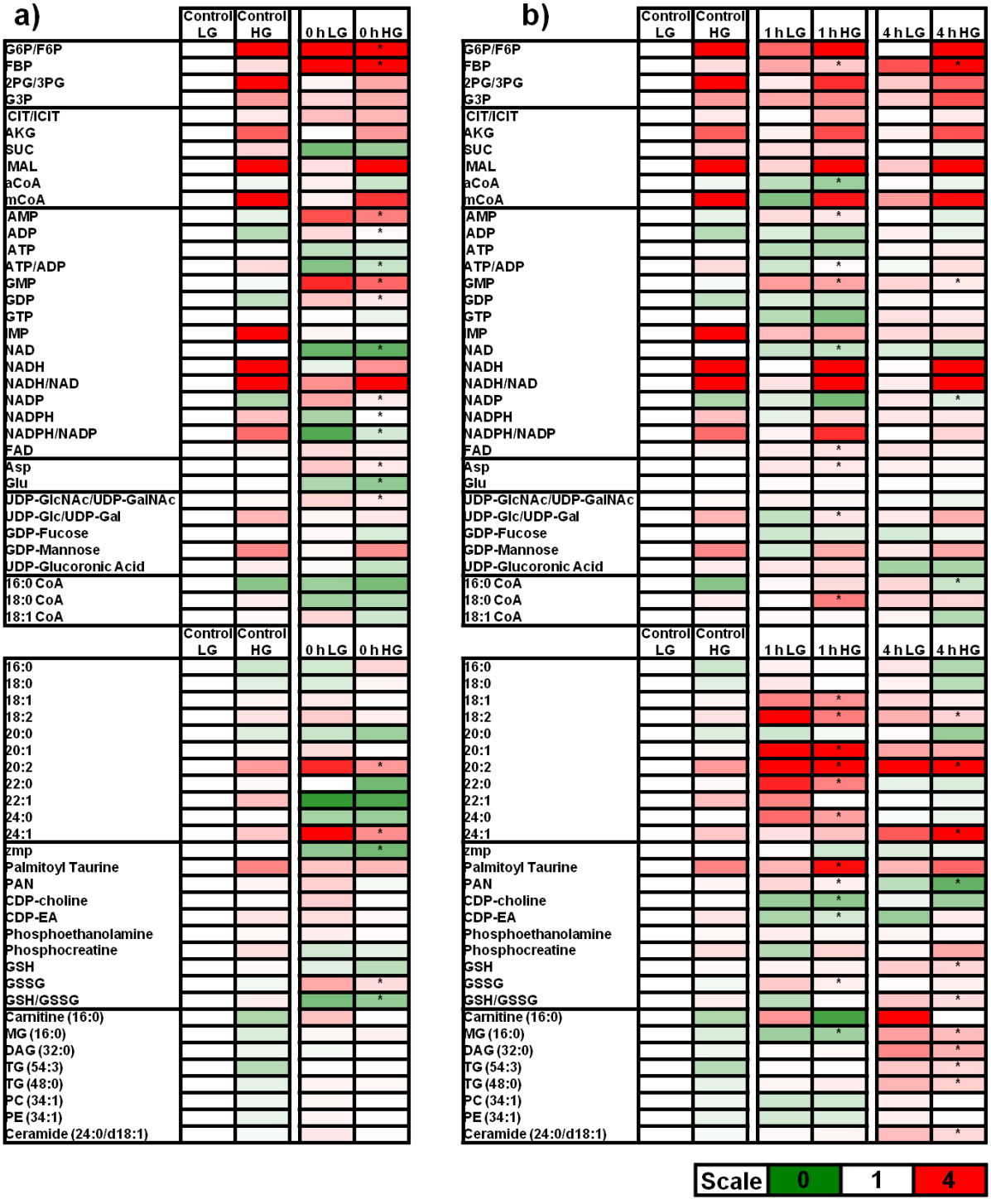

Figure 4.6. Metabolite heat maps for islets exposed to 100 μM H_2O_2. a) Islets were incubated in KRB supplemented with 3 mM glucose for 1 h prior to 16.7 mM glucose stimulation for 15 min. H_2O_2 was added 40 min prior to metabolism quenching. b) Islets were treated with H_2O_2 in RPMI (11 mM glucose) for 40 min. Islets were then cultured in fresh media for 1 or 4 h (the final hour of which was in KRB supplemented with 3 mM glucose) prior to stimulation with 16.7 mM glucose for 15 min. LG = low glucose, HG = high glucose, n = 3-9 sets of 50 islets per condition. Asterisks represent significance ($p < 0.05$) between control and treated conditions as determined by 2-way ANOVA.

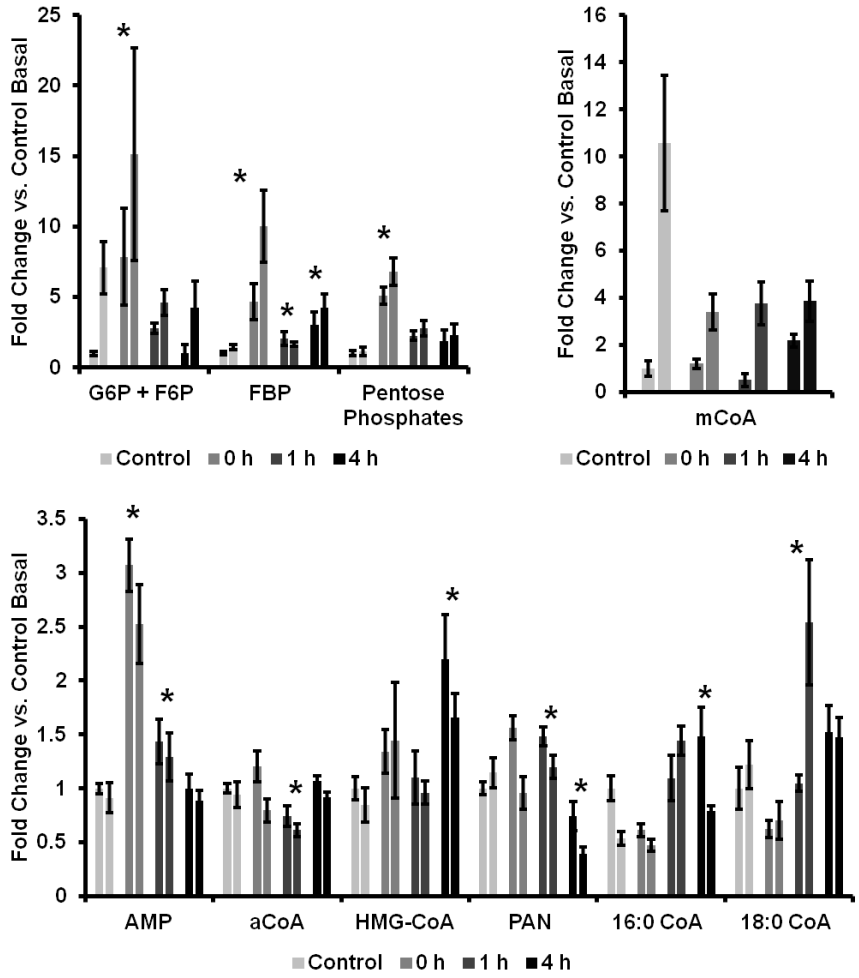

Figure 4.7. Metabolite fold changes following H_2O_2 exposure in a) PPP metabolites b) mCoA c) mevalonate pathway metabolites. Bars represent measurements at low (2.8 mM) and high (16.7 mM) glucose for each time point (n = 3-9 samples per condition). Error bars represent SEM and asterisks indicate significance ($p < 0.05$) as determined by 2-way ANOVA.

Apoptosis Assay and PI Staining

Caspase 3/7 activity was elevated compared to control immediately following H_2O_2 treatment, and reached maximum levels after 1 h culture in RPMI, as demonstrated in Figure 4.8. Presumably, after this point, many of the cells were already dead. Caspase 3/7 activity remained elevated above control levels 2-4 h post-H_2O_2. As a complementary method of cell death detection, islets were stained with PI, which detected late-stage necrotic and apoptotic cells. PI staining showed an increasing amount of dead cells per islet over time (Figure 4.9a-e), although mechanical

disturbance of islets led to removal of dead cells and reduced islet mass, with minimal staining (Figure 4.9f).

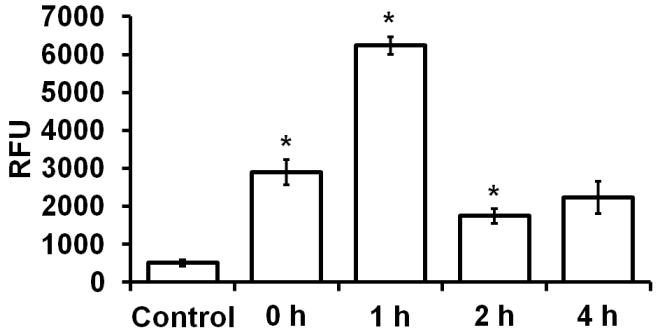

Figure 4.8. Caspase 3/7 activity assay. Islets were treated with 100 μM H_2O_2 for 40 min and then cultured in fresh media for the indicated amounts of time. n = 3 sets of 25 islets per condition. Error bars represent SEM. Asterisks indicate significance ($p < 0.05$) compared to control as determined by an independent samples, 2-tailed student's t-test.

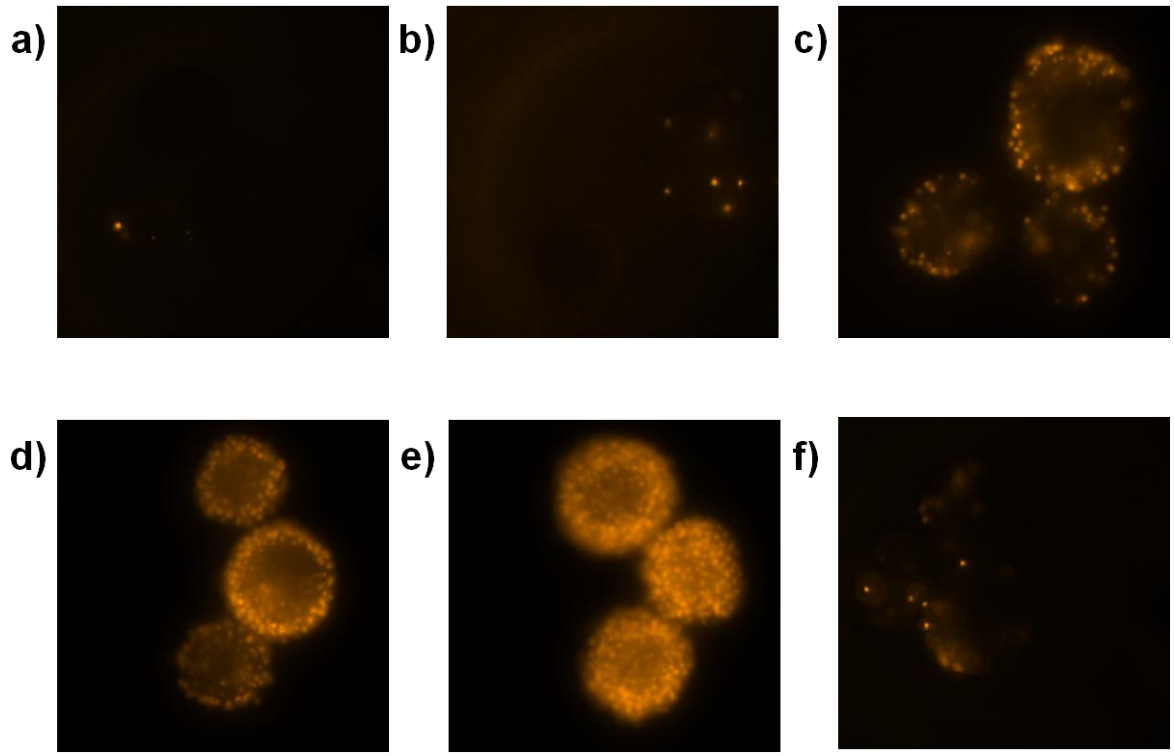

Figure 4.9. PI staining of H_2O_2-treated islets. Control islets (a) were compared to islets that had been treated with 100 μM H_2O_2 for 30 min and then transferred to a microfluidic chip, where they were perfused with RPMI for b) 0 h c) 1 h d) 2 h e) 4 h. Following perfusion, islets were stained for late apoptotic/necrotic cells with propidium iodide (PI). f) H_2O_2-treated islets were cultured for 4 h in an incubator prior to transfer to the microfluidic chip. Mechanical disturbance with a pipette caused shedding of the apoptotic/necrotic cells, resulting in minimal staining.

Discussion

We stressed islets with hydrogen peroxide as a model of oxidative stress and measured their insulin, calcium, and metabolic responses to basal and stimulatory levels of glucose. These responses were correlated to measures of apoptotic and necrotic cell death. Insulin release and $[Ca^{2+}]_i$ responses to glucose were immediately distorted. Soon thereafter, cell blebbing was visually observed and increased rates of apoptosis were measured. Following a culture period of 2-4 h in fresh media, insulin secretion and $[Ca^{2+}]$ responses returned to normal and gross islet morphology looked healthy. We identified metabolites and pathways that were immediately affected by H_2O_2 stress and investigated whether these perturbations were reversible 1-4 h following removal of the stress. In doing so, we gained insight into metabolic pathways potentially involved in diabetes pathogenesis and also established possible markers of islet viability for the purpose of islet evaluation prior to islet transplantation.

Suppression of Glucose-Stimulated Insulin Secretion (GSIS) Pathway

Insulin secretion and Ca^{2+} flux are often considered to be hallmarks of islet function, because insulin secretion is specific to β-cells and Ca^{2+} is an important part of the GSIS pathway. In a functioning β-cell, elevated levels of extracellular glucose result in uptake of glucose across glucose transporter-type 1 (GLUT-1) in humans or type 2 (GLUT-2) in rodents. Inside the cell, glucose undergoes glycolysis, and glycolytic products enter the citric acid cycle and undergo oxidative phosporylation, resulting in the production of ATP. The consequent increase in the ATP/ADP ratio causes ATP-regulated K^+ channels to close, thus preventing K^+ efflux from the cell. The increased positive charge inside the cell due to increased intracellular K^+ levels leads to membrane depolarization, resulting in the opening of voltage-gated L-type Ca^{2+} channels. Increased $[Ca^{2+}]_i$ induces vesicles containing insulin to fuse with the plasma membrane of the cell, releasing insulin into the extracellular space through exocytosis (31, 32).

In H_2O_2-treated INS-1 cells, it has been shown that insulin secretion is suppressed, $[Ca^{2+}]_i$ is elevated, and $[Ca^{2+}]_i$ and mitochondrial membrane potentials are unresponsive to glucose stimulation in experiments performed immediately following 10 min treatment

with 200 µM H_2O_2 (6). We observed similar immediate insulin release and $[Ca^{2+}]_i$ responses to H_2O_2 treatment. It has been suggested that the initial elevation in basal $[Ca^{2+}]_i$ could be related to inhibition of the mitochondrial Na^{2+}/Ca^{2+} antiporter, preventing efflux of Ca^{2+} from the mitochondria (6). Ca^{2+} influx into the cytosol has also been reported in H_2O_2-treated islets (33). This increase is thought to be due to release of Ca^{2+} from intracellular stores as well as increased influx from the extracellular space due to membrane permeabilization through lipid peroxidation (34). The increase in basal $[Ca^{2+}]_i$ likely results in the increase in basal insulin secretion we observed, because Ca^{2+} promotes exocytosis from insulin vesicles. However, membrane hyperpolarization in response to H_2O_2 interferes with normal K_{ATP}-dependent stimulus-secretion coupling, resulting in loss of response of $[Ca^{2+}]_i$ to glucose.

By using LC-MS analysis, we found that the observed H_2O_2-induced changes in $[Ca^{2+}]_i$ and insulin secretion correlated with lowered ATP/ADP ratio and increases in G6P/F6P, FBP, and, to a lesser extent, CIT/ICIT. It has been shown that H_2O_2 induces a glycolytic block in cells that is restored within approximately 2 h post-stress, at which point cells can either be repaired or undergo apoptosis (3). Our results were consistent with this observation, as we have shown here immediate increases in metabolites upstream of the glycolytic enzyme GAPDH, likely due to its inactivation (Figure 4.7). GAPDH activity could be measured via spectroscopic assay to confirm this observation. As glycolysis and subsequent ATP/ADP increase is necessary for the K_{ATP}-dependent GSIS pathway, insulin secretion and $[Ca^{2+}]_i$ were not responsive to glucose stimulation. Apoptosis assays and PI staining showed that cells tended to die about 1-2 h after removal of the H_2O_2 stress. Glycolytic flux appeared to resume normal function after this time, as ATP/ADP and glycolytic metabolites returned to normal levels. Upon restoration of glycolysis, both insulin secretion and $[Ca^{2+}]_i$ were capable of recovering from transient oxidative stress, with both returning to normal amounts within 4 h post-treatment.

Taken together, this data seems to show that once the damaged cells were removed, the remaining islet cluster was able to function normally. Interestingly though, not all of the affected metabolites returned to control levels, indicating that there were potentially

other pathways affected that were not repaired within 4 h of removal of the stress, even though insulin release and $[Ca^{2+}]_i$ function appeared normal at this time.

Although K_{ATP}-dependent GSIS has been well-characterized, investigations have determined that it cannot be responsible for all GSIS. When diazoxide is used to hold K_{ATP} channels open, glucose is still able to stimulate insulin release when cell membranes are depolarized using high $[K^+]$ (35). Additionally, when sulfonylureas are used to hold K_{ATP} channels closed, a glucose stimulus again increases insulin secretion (36). Taken together, these experiments provide evidence for K_{ATP}-independent pathways of GSIS. As such, we investigated the possibility that H_2O_2 stress influenced function in these pathways.

PARP-Activated Pathways

Oxidative stress has been reported to increase poly (ADP-ribose) polymerase (PARP) activity in islets, with PARP immunoreactivity increasing significantly within 30 min of H_2O_2 treatment, though the increase is transient and not seen 60 min or 90 min post-stress (37). Inhibiting PARP reduces H_2O_2-induced $[Ca^{2+}]_i$ elevations in clonal β-cells (38). PARP is an inhibitor of GAPDH, which catalyzes the oxidative phosphorylation of glyceraldehyde-3-phosphate (G3P) in the presence of NAD^+. GAPDH inactivation in islets results in the observed accumulation of upstream metabolite G6P (4). We observed immediate significant increases in G6P/F6P as well as another upstream metabolite, FBP, in islets following H_2O_2 treatment, as shown in Figures 4.7a and 4.10. Thus, our results were consistent with early-stage PARP activation.

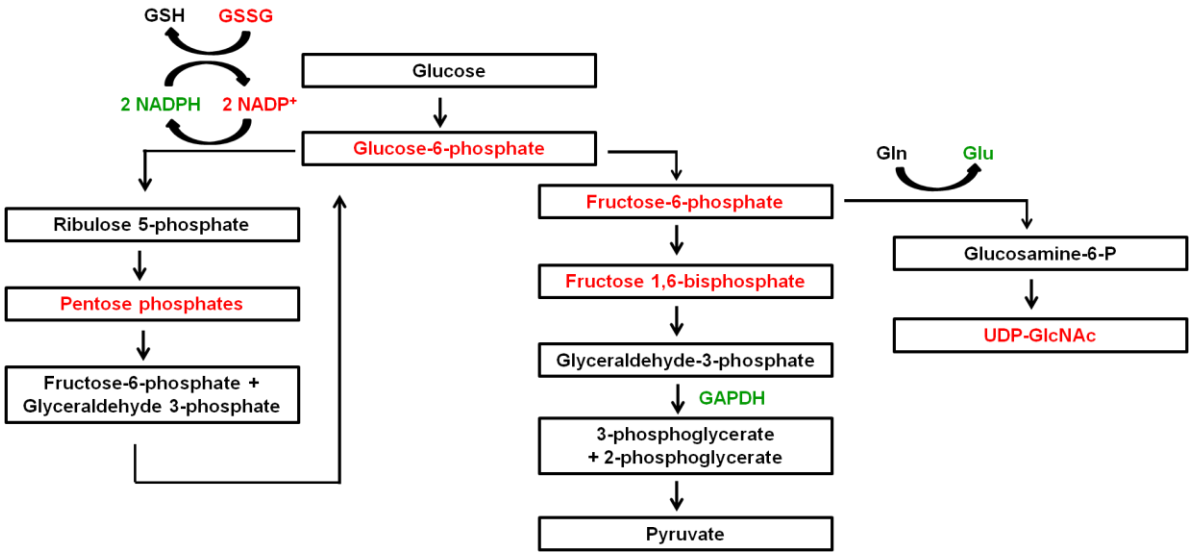

Figure 4.10. Metabolite changes in PPP (left), glycolytic (middle) and hexosamine (right) pathways in immediate response to H_2O_2 treatment. Red = upregulated metabolites and green = downregulated metabolites.

One reported consequence of hyperglycemia-induced PARP activation/GAPDH inactivation induced during hyperglycemia in mesangial cells by overproduction of superoxide is increased flux through the hexosamine pathway (39). The hexosamine pathway synthesizes the substrates for N- and O-glycosylation of proteins such as UDP N-acetylglucosamine (40), as shown in Figure 4.10. We observed a transient increase in UDP N-acetylglucosamine (1.5 fold) immediately following H_2O_2 treatment, supporting increased flux through the hexosamine pathway during early-stage H_2O_2 injury.

We observed several changes in the pentose phosphate shunt pathway (PPP) that could explain the loss and then recovery of distinct first phase insulin release following H_2O_2 exposure. Although the PPP is not highly active in β-cells, recent studies using clonal INS-1 cells and rat islets have found increases in PPP metabolites in response to glucose stimulation (15, 16). Furthermore, H_2O_2 induces several enzymes involved in the PPP in Saccharomyces cerevisiae (41). In the PPP, glucose-6-phosphate is oxidized and decarboxylated, generating ribulose-5-phosphate and reducing $NADP^+$ in the process (Figure 4.10). $NADP^+$ is a positive regulator of the PPP. In the immediate response to H_2O_2 stress, we observed increased amounts of $NADP^+$ and G6P/F6P, which would suggest that the PPP should be more active. Our observations support this

idea, as pentose phosphates were only detectable in islets quenched immediately following H_2O_2 stress.

Increased flux through the PPP could help the cells to replenish NADPH that is oxidized in the process of reducing glutathione, as demonstrated in Figure 4.10. GSH is an important antioxidant that helps limit ROS-induced cellular damage, and GSH/GSSG levels were significantly reduced immediately following H_2O_2 stress (0.5 fold). NADPH-mediated glutathione reduction is thought to play a role in the potentiation of insulin release (42), which could help explain the loss of phase dynamics in insulin release immediately following H_2O_2 treatment. At later time points, after the stress had been removed, $NADP^+$, NADPH, GSH/GSSG, and G6P concentrations were normal and pentose phosphates were not detectable, indicating that the H_2O_2 had likely been neutralized by this point and increased flux through the PPP was no longer necessary.

Anaplerotic Pathways

Anaplerosis has been hypothesized to be involved in the K_{ATP}-independent pathways of glucose-stimulated insulin secretion through either malonyl CoA formation and lipid esterification processes or through a pyruvate/malate or pyruvate/citrate shuttle (43). Evidence for an anaplerotic pathway includes high levels of expression of pyruvate carboxylase (PC) and malic enzyme (ME) in islets (43).

Culturing islets with high glucose and high fatty acids has been reported to increase glucose oxidation despite 30% lower pyruvate dehydrogenase activity. This observation could indicate enhanced metabolic flux through PC and the malate-pyruvate shuttle (44). PC produces oxaloacetate, which reacts with aCoA to produce CIT. We found no change in these metabolites and therefore did not obtain any evidence of changes in PC activity; however, we cannot rule out a change in flux through the pathway. Both malate dehydrogenase and citrate synthase have been found to be insensitive to H_2O_2-induced oxidative stress in isolated nerve terminals, which is consistent with our observation that malate and citrate concentrations were not affected by H_2O_2 exposure (45).

Lipid/Fatty Acid Biosynthetic Pathways

Several molecules have been implicated as possible amplifiers of insulin secretion, including glutamate (21), long chain acvl CoAs (LC-CoAs) (46), mitochondrial GTP (47), and AKG (48). Malonyl CoA has been suggested to be involved in the regulation of insulin secretion (49, 50) and has been shown to correlate with GSIS in a dose-dependent manner (51). The initial increase in mCoA levels following glucose stimulation is Ca^{2+}-independent (43).

We observed an immediate impairment in glucose-induced mCoA following H_2O_2-induced oxidative stress (Figure 4.7b). This impairment was seen concomitantly with a rise in AMP, so it could result from AMPK-induced inhibition of mCoA formation via ACC phosphorylation. AMPK activation by pioglitazone has been shown to slow glucose metabolism and insulin secretion in INS 832/13 cells at glucose concentrations below 10 mM, but to have no such effect at concentrations above 16 mM (52). AMPK expression was not found to be altered by transient exposure of H_2O_2 to islets in a recent study (53), but AMPK was shown to be activated by H_2O_2 in a different study (37). In our experiments, the mCoA inhibition persisted until at least 4 h post-stress, whereas AMP levels returned to normal. This maintained reduction in mCoA makes it plausible as a potential marker of previously induced oxidative stress, as might occur in the islet isolation process. The question then becomes: how is mCoA production/utilization affected by H_2O_2, and why do lowered levels not seem to negatively affect insulin secretion following acute oxidative stress?

Malonyl CoA abundance rose 10-fold in response to glucose in control islets (Figure 4.7b). This metabolite can inhibit CPT-1, resulting in accumulation of long chain fatty acids in the cytosol and blockage of β-oxidation. However, it has recently been suggested that the reduction of β-oxidation that occurs at high glucose could result primarily from a redirection of acyl CoA toward esterification instead of CPT-1 inhibition (54). We observed increased levels of many fatty acyl CoAs, fatty acids, and phospholipids (monoacylglycerol (MG), diacylglycerol (DAG), and triacylglycerol (TG)) 4 h post-H_2O_2, indicating that β-oxidation inhibition was probably not affected by the

reduced mCoA levels. Instead, mCoA could have been consumed for lipogenesis. Fatty acid pathways possibly affected by H_2O_2 treatment are shown in Figure 4.11.

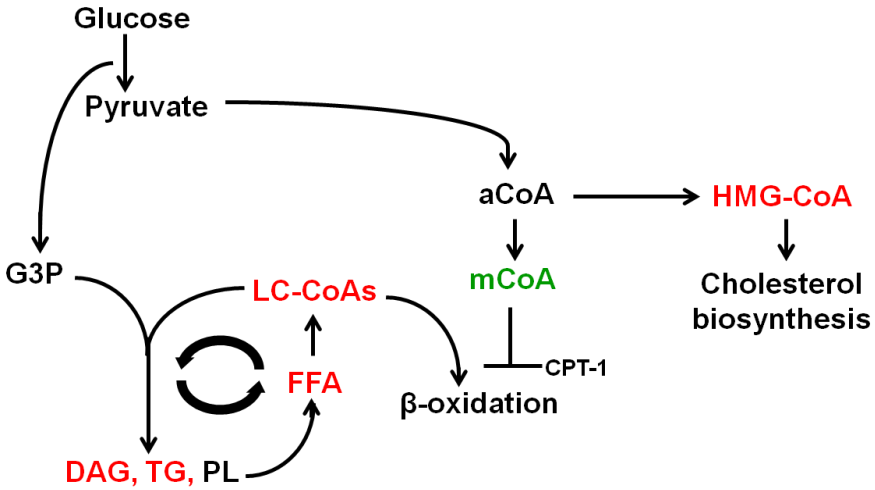

Figure 4.11. Regulation of fatty acid and mevalonate pathways 4 h post-H_2O_2 stress. Red = upregulated metabolites and green = downregulated metabolites.

Another possibility is that mCoA production was compromised by diversion of precursors to formation of other molecules, like HMG-CoA. In addition to the previously discussed metabolites, pantothenic acid (PAN) amounts were decreased, HMG-CoA, NADP, GSH, and GSH/GSSG concentrations were increased, and aCoA abundance remained unchanged 4 h post-H_2O_2 (Figure 4.7c). Increased export of NADPH from the mitochondria could account for many of these changes in metabolite levels (48). Although overall NADPH levels did not change in comparison to control, NADPH increased in response to glucose stimulation in control islets, whereas no such increase was observed in islets 4 h post-H_2O_2. PAN is involved in CoA synthesis, so the decreased levels could indicate that it was consumed for CoA production. HMG-CoA is involved in the mevalonate pathway, which leads to isoprenylation of proteins and cholesterol biosynthesis as shown in Figure 4.11. Isoprenylation of proteins is important for GSIS, as shown by a recent study in which inhibition of the mevalonate pathway prior to HMG-CoA synthesis negatively regulates GSIS in murine islets, while downstream inhibition of cholesterol synthesis without interruption of isoprenyl molecule synthesis has no effect on GSIS (55). It is thus possible that cholesterol synthesis and

thus secretory granule membrane properties were affected in formerly stressed cells, even though normal insulin secretion resumed at this point. Flux through the mevalonate/isoprenylation pathway could explain the reduction in mCoA observed with H_2O_2, and could also explain how it was possible for insulin secretion to be normal or even slightly more active than normal even though mCoA levels were blunted.

Potential Markers of Damaged Cells

Many of the early responses to H_2O_2 were reversed following stress removal; however, several metabolites were significantly different compared to control islets 4 h post-H_2O_2. FBP, GMP, NADP, fatty acids, and LC-CoA amounts were all elevated and mCoA downregulated after 4 h. These metabolites could comprise a metabolic signature for islets that have been previously damaged by oxidative stress. Such a signature could be valuable for detecting islet damage during islet isolation for transplantation. A metabolic signature is important because islets need to be evaluated for viability; this evaluation would happen after the initial damage has occurred and prior to transplantation. Most evidence of initial damage, including alterations in $[Ca^{2+}]_i$ and insulin secretion (especially if measured only statically and not as a temporal profile), was not present only 1-4 h post-stress, even though the islets had sustained previous damage. By screening islets for levels of these metabolites, we could potentially create a more accurate measure of islet health than current islet viability tests and thus improve the outcomes of islet transplantation.

Conclusion

We have identified several key components in islets' response to oxidative stress, including an initial blockage of glycolysis coupled with probable increased flux through the pentose phosphate and hexosamine pathways followed by recovery. Although glycolysis resumed and insulin secretion and $[Ca^{2+}]_i$ dynamics returned to normal, several metabolites remained affected, most notably decreased mCoA concentrations and increased amounts of FBP, fatty acids, and LC-CoAs. These altered metabolite levels could indicate a shift in some of the K_{ATP}-independent pathways of glucose-

stimulated insulin secretion. Possible targets include fatty acid/lipid biosynthetic pathways like the mevalonate pathway following H_2O_2-induced stress.

One disadvantage of these experiments is that static metabolite levels were measured, which makes it difficult to discern information about flux through a pathway; increased levels of a metabolite could indicate increased flux or decreased usage, for example. Future improvements to the sample preparation and/or MS method will allow less abundant metabolites to be measured, and could improve metabolite signal for future metabolic flux experiments. The work presented here identified some important metabolites and pathways that could be involved in diabetes pathogenesis and/or that could be targeted as markers of oxidative stress for the purpose of islet functionality screening prior to islet transplantation.

References

1. Lenzen, S., Drinkgern, J., and Tiedge, M. (1996) Low antioxidant enzyme gene expression in pancreatic islets compared with various other mouse tissues. *Free Radic. Biol. Med.* **20**, 463–466
2. Spragg, R. G., Hinshaw, D. B., Hyslop, P. A., Schraufstätter, I. U., and Cochrane, C. G. (1985) Alterations in adenosine triphosphate and energy charge in cultured endothelial and P388D1 cells after oxidant injury. *J. Clin. Invest.* **76**, 1471–1476
3. Colussi, C., Albertini, M. C., Coppola, S., Rovidati, S., Galli, F., and Ghibelli, L. (2000) H2O2-induced block of glycolysis as an active ADP-ribosylation reaction protecting cells from apoptosis. *FASEB J.* **14**, 2266–2276
4. Sakai, K., Matsumoto, K., Nishikawa, T., Suefuji, M., Nakamaru, K., Hirashima, Y., Kawashima, J., Shirotani, T., Ichinose, K., Brownlee, M., and Araki, E. (2003) Mitochondrial reactive oxygen species reduce insulin secretion by pancreatic β-cells. *Biochem. Biophys. Res. Commun.* **300**, 216–222
5. Miwa, I., Ichimura, N., Sugiura, M., Hamada, Y., and Taniguchi, S. (2000) Inhibition of Glucose-Induced Insulin Secretion by 4-Hydroxy-2-Nonenal and Other Lipid Peroxidation Products. *Endocrinology*. **141**, 2767–2772
6. Maechler, P., Jornot, L., and Wollheim, C. B. (1999) Hydrogen Peroxide Alters Mitochondrial Activation and Insulin Secretion in Pancreatic Beta Cells. *J. Biol. Chem.* **274**, 27905–27913
7. Li, N., Brun, T., Cnop, M., Cunha, D. A., Eizirik, D. L., and Maechler, P. (2009) Transient Oxidative Stress Damages Mitochondrial Machinery Inducing Persistent β-Cell Dysfunction. *J. Biol. Chem.* **284**, 23602–23612
8. Lei, X. G., and Vatamaniuk, M. Z. (2011) Two tales of antioxidant enzymes on β cells and diabetes. *Antioxid. Redox Signal.* **14**, 489–503
9. Novials, A., Montane, J., and Cadavez-Trigo, L. (2014) Stress and the inflammatory process: a major cause of pancreatic cell death in type 2 diabetes. *Diabetes Metab. Syndr. Obes. Targets Ther.* 10.2147/DMSO.S37649
10. Avila, J., Barbaro, B., Gangemi, A., Romagnoli, T., Kuechle, J., Hansen, M., Shapiro, J., Testa, G., Sankary, H., Benedetti, E., Lakey, J., and Oberholzer, J. (2005) Intra-Ductal Glutamine Administration Reduces Oxidative Injury During Human Pancreatic Islet Isolation: Islet Transplantation and Glutamine Treatment. *Am. J. Transplant.* **5**, 2830–2837
11. Yamamoto, T., Horiguchi, A., Ito, M., Nagata, H., Ichii, H., Ricordi, C., and Miyakawa, S. (2009) Quality control for clinical islet transplantation: organ procurement and preservation, the islet processing facility, isolation, and potency tests. *J. Hepatobiliary. Pancreat. Surg.* **16**, 131–136
12. CITR Coordinating Center Scientific Summary of the Collaborative Islet Transplant Registry (CITR) 2012 (Eighth) Annual Report. [online] https://web.emmes.com/study/isl/reports/20150218_CITR_2012EighthAnnualReportScientificSummary.pdf (Accessed February 18, 2015)
13. Tian, L., Kim, H. S., Kim, H., Jin, X., Jung, H. S., Park, K. S., Cho, K. W., Park, S., and Moon, W. K. (2013) Changes in Metabolic Markers in Insulin-Producing β-Cells during Hypoxia-Induced Cell Death As Studied by NMR Metabolomics. *J. Proteome Res.* **12**, 3738–3745

14. Lorenz, M. A., Burant, C. F., and Kennedy, R. T. (2011) Reducing Time and Increasing Sensitivity in Sample Preparation for Adherent Mammalian Cell Metabolomics. *Anal. Chem.* **83**, 3406–3414
15. Lorenz, M. A., El Azzouny, M. A., Kennedy, R. T., and Burant, C. F. (2013) Metabolome Response to Glucose in the β-Cell Line INS-1 832/13. *J. Biol. Chem.* **288**, 10923–10935
16. Spégel, P., Sharoyko, V. V., Goehring, I., Danielsson, A. P. H., Malmgren, S., Nagorny, C. L. F., Andersson, L. E., Koeck, T., Sharp, G. W. G., Straub, S. G., Wollheim, C. B., and Mulder, H. (2013) Time-resolved metabolomics analysis of β-cells implicates the pentose phosphate pathway in the control of insulin release. *Biochem. J.* **450**, 595–605
17. Huang, M., and Joseph, J. W. (2014) Assessment of the Metabolic Pathways Associated With Glucose-Stimulated Biphasic Insulin Secretion. *Endocrinology*. **155**, 1653–1666
18. Spégel, P., Malmgren, S., Sharoyko, V. V., Newsholme, P., Koeck, T., and Mulder, H. (2011) Metabolomic analyses reveal profound differences in glycolytic and tricarboxylic acid cycle metabolism in glucose-responsive and -unresponsive clonal β-cell lines. *Biochem. J.* **435**, 277–284
19. Fernandez, C., Fransson, U., Hallgard, E., Spégel, P., Holm, C., Krogh, M., Wårell, K., James, P., and Mulder, H. (2008) Metabolomic and Proteomic Analysis of a Clonal Insulin-Producing β-Cell Line (INS-1 832/13). *J. Proteome Res.* **7**, 400–411
20. Wallace, M., Whelan, H., and Brennan, L. (2013) Metabolomic analysis of pancreatic beta cells following exposure to high glucose. *Biochim. Biophys. Acta BBA - Gen. Subj.* **1830**, 2583–2590
21. Gheni, G., Ogura, M., Iwasaki, M., Yokoi, N., Minami, K., Nakayama, Y., Harada, K., Hastoy, B., Wu, X., Takahashi, H., Kimura, K., Matsubara, T., Hoshikawa, R., Hatano, N., Sugawara, K., Shibasaki, T., Inagaki, N., Bamba, T., Mizoguchi, A., Fukusaki, E., Rorsman, P., and Seino, S. (2014) Glutamate Acts as a Key Signal Linking Glucose Metabolism to Incretin/cAMP Action to Amplify Insulin Secretion. *Cell Rep.* **9**, 661–673
22. Collier, J. J., Burke, S. J., Eisenhauer, M. E., Lu, D., Sapp, R. C., Frydman, C. J., and Campagna, S. R. (2011) Pancreatic β-Cell Death in Response to Pro-Inflammatory Cytokines Is Distinct from Genuine Apoptosis. *PLoS ONE*. **6**, e22485
23. Yu, B. P. (1994) Cellular defenses against damage from reactive oxygen species. *Physiol. Rev.* **74**, 139–162
24. Roper, M. G., Shackman, J. G., Dahlgren, G. M., and Kennedy, R. T. (2003) Microfluidic Chip for Continuous Monitoring of Hormone Secretion from Live Cells Using an Electrophoresis-Based Immunoassay. *Anal. Chem.* **75**, 4711–4717
25. Pralong, W. F., Bartley, C., and Wollheim, C. B. (1990) Single islet beta-cell stimulation by nutrients: relationship between pyridine nucleotides, cytosolic Ca2+ and secretion. *EMBO J.* **9**, 53
26. Shackman, J. G., Dahlgren, G. M., Peters, J. L., and Kennedy, R. T. (2005) Perfusion and chemical monitoring of living cells on a microfluidic chip. *Lab. Chip*. **5**, 56
27. Grynkiewicz, G., Poenie, M., and Tsien, R. Y. (1985) A New Generation of Ca2+ Indicators with Greatly Improved Fluorescence Properties. *J. Biol. Chem.* **260**, 3440–3450

28. Scholz, H., Lund, T., Dahle, M. K., Collins, J. L., Korsgren, O., Wang, J. E., and Foss, A. (2009) The synthetic liver X receptor agonist GW3965 reduces tissue factor production and inflammatory responses in human islets in vitro. *Diabetologia*. **52**, 1352–1362
29. Jiménez-Palomares, M., López-Acosta, J. F., Villa-Pérez, P., Moreno-Amador, J. L., Muñoz-Barrera, J., Fernández-Luis, S., Heras-Pozas, B., Perdomo, G., Bernal-Mizrachi, E., and Cózar-Castellano, I. (2015) Cyclin C stimulates β-cell proliferation in rat and human pancreatic β-cells. *Am. J. Physiol. - Endocrinol. Metab.* **308**, E450–E459
30. Heller, R. S. (2010) The Comparative Anatomy of Islets. in *The Islets of Langerhans* (Islam, M. S. ed), pp. 21–37, Springer Netherlands, Dordrecht, **654**, 21–37
31. Rutter, G. A. (2001) Nutrient-secretion coupling in the pancreatic islet beta-cell: Recent advances. *Mol. Aspects Med.* **22**, 247–284
32. Newsholme, P., Gaudel, C., and McClenaghan, N. H. (2010) Nutrient Regulation of Insulin Secretion and β-Cell Functional Integrity. in *The Islets of Langerhans* (Islam, M. S. ed), pp. 91–114, Springer Netherlands, Dordrecht, **654**, 91–114
33. Krippeit-Drews, P., Krämer, C., Welker, S., Lang, F., Ammon, H. P., and Drews, G. (1999) Interference of H2O2 with stimulus-secretion coupling in mouse pancreatic β-cells. *J. Physiol.* **514**, 471–481
34. Nakazaki, M., Kakei, M., Yaekura, K., Koriyama, N., Morimitsu, S., Ichinari, K., Yada, T., and Tei, C. (2000) Diverse Effects of Hydrogen Peroxide on Cytosolic Ca2+ Homeostasis in Rat Pancreatic b-cells. *Cell Struct. Funct.* **25**, 187–193
35. Gembal, M., Gilon, P., and Henquin, J. C. (1992) Evidence that glucose can control insulin release independently from its action on ATP-sensitive K+ channels in mouse B cells. *J. Clin. Invest.* **89**, 1288–1295
36. Panten, U., Schwanstecher, M., Wallasch, A., and Lenzen, S. (1988) Glucose both inhibits and stimulates insulin secretion from isolated pancreatic islets exposed to maximally effective concentrations of sulfonylureas. *Naunyn. Schmiedebergs Arch. Pharmacol.* **338**, 459–462
37. Meares, G. P., Fontanilla, D., Broniowska, K. A., Andreone, T., Lancaster, J. R., and Corbett, J. A. (2013) Differential responses of pancreatic β-cells to ROS and RNS. *AJP Endocrinol. Metab.* **304**, E614–E622
38. Ishii, M., Hagiwara, T., Mori, Y., and Shimizu, S. (2014) Involvement of TRPM2 and L-type Ca2+ channels in Ca2+ entry and cell death induced by hydrogen peroxide in rat B-cell line RIN-5F. *J. Toxicol. Sci.* **39**, 199–209
39. Du, X., Matsumura, T., Edelstein, D., Rossetti, L., Zsengellér, Z., Szabó, C., and Brownlee, M. (2003) Inhibition of GAPDH activity by poly(ADP-ribose) polymerase activates three major pathways of hyperglycemic damage in endothelial cells. *J. Clin. Invest.* **112**, 1049–1057
40. Leighton R. James, Tang, D., Ingram, A., Ly, H., Thai, K., Cai, L., and Scholey, J. W. (2002) Flux Through the Hexosamine Pathway Is a Determinant of Nuclear Factor KB-Dependent Promoter Activation. *Diabetes*. **51**, 1146–1156
41. Godon, C., Lagniel, G., Lee, J., Buhler, J.-M., Kieffer, S., Perrot, M., Boucherie, H., Toledano, M. B., and Labarre, J. (1998) The H2O2 stimulon in Saccharomyces cerevisiae. *J. Biol. Chem.* **273**, 22480–22489

42. Ivarsson, R., Quintens, R., Dejonghe, S., Tsukamoto, K., Renström, E., Schuit, F. C., and others (2005) Redox control of exocytosis regulatory role of NADPH, thioredoxin, and glutaredoxin. *Diabetes*. **54**, 2132–2142
43. Farfari, S., Schulz, V., Corkey, B., and Prentki, M. (2000) Glucose-regulated anaplerosis and cataplerosis in pancreatic beta-cells: possible implication of a pyruvate/citrate shuttle in insulin secretion. *Diabetes*. **49**, 718–726
44. Liu, Y. Q., Moibi, J. A., and Leahy, J. L. (2004) Chronic High Glucose Lowers Pyruvate Dehydrogenase Activity in Islets through Enhanced Production of Long Chain Acyl-CoA: PREVENTION OF IMPAIRED GLUCOSE OXIDATION BY ENHANCED PYRUVATE RECYCLING THROUGH THE MALATE-PYRUVATE SHUTTLE. *J. Biol. Chem.* **279**, 7470–7475
45. Tretter, L., and Adam-Vizi, V. (2000) Inhibition of Krebs cycle enzymes by hydrogen peroxide: A key role of α-ketoglutarate dehydrogenase in limiting NADH production under oxidative stress. *J. Neurosci.* **20**, 8972–8979
46. Henquin, J.-C. (2000) Triggering and amplifying pathways of regulation of insulin secretion by glucose. *Diabetes*. **49**, 1751–1760
47. Kibbey, R. G., Pongratz, R. L., Romanelli, A. J., Wollheim, C. B., Cline, G. W., and Shulman, G. I. (2007) Mitochondrial GTP Regulates Glucose-Stimulated Insulin Secretion. *Cell Metab.* **5**, 253–264
48. MacDonald, M. J. (2004) Perspective: emerging evidence for signaling roles of mitochondrial anaplerotic products in insulin secretion. *AJP Endocrinol. Metab.* **288**, E1–E15
49. Prentki, M., Vischer, S., Glennon, M. C., Regazzi, R., Deeney, J. T., and Corkey, B. E. (1992) Malonyl-CoA and long chain acyl-CoA esters as metabolic coupling factors in nutrient-induced insulin secretion. *J. Biol. Chem.* **267**, 5802–5810
50. Roduit, R., Nolan, C., Alarcon, C., Moore, P., Barbeau, A., Delghingaro-Augusto, V., Przybykowski, E., Morin, J., Massé, F., Massie, B., Ruderman, N., Rhodes, C., Poitout, V., and Prentki, M. (2004) A role for the malonyl-CoA/long-chain acyl-CoA pathway of lipid signaling in the regulation of insulin secretion in response to both fuel and nonfuel stimuli. *Diabetes*. **53**, 1007–1019
51. Prentki, M., Matschinsky, F. M., and Madiraju, S. R. M. (2013) Metabolic Signaling in Fuel-Induced Insulin Secretion. *Cell Metab.* **18**, 162–185
52. Lamontagne, J., Pepin, É., Peyot, M.-L., Joly, É., Ruderman, N. B., Poitout, V., Madiraju, S. R. M., Nolan, C. J., and Prentki, M. (2009) Pioglitazone Acutely Reduces Insulin Secretion and Causes Metabolic Deceleration of the Pancreatic β-Cell at Submaximal Glucose Concentrations. *Endocrinology*. **150**, 3465–3474
53. Brun, T., Scarcia, P., Li, N., Gaudet, P., Duhamel, D., Palmieri, F., and Maechler, P. (2013) Changes in Mitochondrial Carriers Exhibit Stress-Specific Signatures in INS-1Eβ-Cells Exposed to Glucose Versus Fatty Acids. *PLoS ONE*. **8**, e82364
54. El-Azzouny, M., Evans, C. R., Treutelaar, M. K., Kennedy, R. T., and Burant, C. F. (2014) Increased Glucose Metabolism and Glycerolipid Formation by Fatty Acids and GPR40 Receptor Signaling Underlies the Fatty Acid Potentiation of Insulin Secretion. *J. Biol. Chem.* **289**, 13575–13588
55. Zuniga-Hertz, J. P., Rebelato, E., Kassan, A., Khalifa, A. M., Ali, S. S., Patel, H. H., and Abdulkader, F. (2014) Distinct pathways of cholesterol biosynthesis impact on insulin secretion. *J. Endocrinol.* **224**, 75–84

CHAPTER 5
Summary and Future Directions

Summary

The overall goal of this work was to develop analytical techniques for evaluating function in pancreatic islets of Langerhans, with the ultimate purpose of screening islet viability prior to clinical islet transplantation in type 1 diabetes patients. A secondary objective of islet evaluation was to study islet physiology and effects of stressors on islet function as they relate to mechanisms of diabetes pathogenesis. Although this work focused specifically on islets, the methods developed could potentially be used to study other cell systems as well.

Dual Detection of GSIS Pathway Components

Dual detection of $[Ca^{2+}]_i$ and insulin secretion from groups of islets was realized using a two-chip system. Islets were perfused on the first chip with basal and stimulatory levels of glucose, and $[Ca^{2+}]_i$ was measured via fluorescence microscopy while perfusate was collected for later analysis on a second chip by microchip electrophoresis coupled with laser-induced fluorescence detection (MCE-LIF). Two methods of perfusate collection were explored. In the first method, perfusate was collected continuously in a narrow bore capillary, while in the second method, perfusate was collected in fractions in a multi-well plate. These fractions were than segmented with oil in tubing to prevent diffusion between the fractions. Immediately prior to analysis by MCE-LIF, the aqueous droplets were de-segmented from the oil phase by flowing the solutions through a hydrophobic device coupled to a hydrophilic extraction capillary.

Both of these methods provided rapid measurement of $[Ca^{2+}]_i$ and GSIS from a single batch of islets, with total analysis times <90 min. Temporal resolution of GSIS was 80-150 s, which was adequate for measuring first phase and second phase dynamics. Basal and peak 1st phase insulin secretion were measured to be 10-25 pg min^{-1} $islet^{-1}$ and 100-200 pg min^{-1} $islet^{-1}$, respectively. These concentrations were comparable to those measured previously in single islets. This work demonstrated the first on-chip multimodal detection of GSIS pathway components that is compatible with the time-sensitive requirements of islet transplantation.

Islet Metabolomics Sample Preparation Method Optimization

As an alternative method for islet analysis, we explored a metabolomics approach. Our hypothesis was that intracellular metabolites might provide an indicator of cell stressors and health that could be used to evaluate islets. In considering our method, we sought to decrease the number of islets required because of the difficulty in obtaining them. We developed a sample preparation method for the reproducible analysis of 62 metabolites from 50 islets of Langerhans. Through optimization of quenching method, extraction solvent, and sample size, we established a method in which islets were quenched via cold solvent addition (90% 9:1 MeOH:$CHCl_3$/10% H_2O, -75ºC), extracted with probe sonication, and analyzed via HPLC-TOF-MS (HILIC and reverse phase columns, sequentially). Using this method, we obtained an average RSE of 20% and similar metabolite coverage to previous methods using larger numbers of islets.

We applied the method to measure metabolite levels in islets incubated in basal concentrations of glucose (2.8 mM) and islets incubated in stimulatory levels of glucose (16.7 mM) for 5 or 15 min, roughly corresponding to first phase and second phase responses. We observed similar absolute concentrations of quantified metabolites as have previously been reported in islets under similar conditions. Furthermore, we observed increased levels of glycolysis and TCA cycle components and increased cellular energetics in response to glucose stimulation, consistent with reported responses in beta-cells and/or islets. This suggested that our method was able to reliably detect changes in intracellular metabolites.

We then compared the results obtained using our method to published results obtained in either islets or clonal cell lines to investigate whether any metabolic differences exist between native islets and clonal β-cells. We identified a number of differences, including larger increases in hexose phosphates, no significant increase in citrate or ZMP, less reduction in many long chain CoAs, and ~10-fold lower total absolute concentration of 7 tested metabolites (AMP, ADP, ATP, aCoA, MAL, SUC, and CIT) in islets as compared to INS-1 cells. These differences could indicate key differences in metabolism between islets and INS-1 cells, particularly in the pentose phosphate pathway and/or in glycerolipid/free fatty acid cycling during 2nd phase insulin secretion. This work demonstrated the importance of corroborating metabolomic data derived from clonal cells with data obtained from native islets.

Application of Islet Metabolomic Method to Studies of Oxidative Stress

Towards our goal of evaluating islets and to better understand how stressors can affect the metabolome, we treated islets with H_2O_2 as a model of oxidative stress. We measured their secreted insulin, $[Ca^{2+}]_i$, and metabolic responses to basal and stimulatory levels of glucose immediately following the stress or after a subsequent culture period in fresh media. Immediately following exposure to H_2O_2, basal $[Ca^{2+}]_i$ and secreted insulin concentrations were elevated, and their responses to glucose were distorted. We observed several differences in metabolite levels, including decreased GSH/GSSG, ATP/ADP, GTP/GDP and NADPH/$NADP^+$ ratios, and decreased mCoA concentration. We also observed increased G6P/F6P, FBP, and AMP concentrations. These differences were consistent with increased PARP/decreased GAPDH activity and associated glycolysis blockage, coupled with probable increased flux through the pentose phosphate and hexosamine pathways. This data showed evidence for an antioxidant role in the pentose phosphate pathway in islets.

One hour following acute H_2O_2 exposure, damaged cells blebbed and underwent apoptosis. $[Ca^{2+}]_i$ and insulin secretion returned to control levels within 4 h following stress. While many of the early metabolic responses to H_2O_2 also were reversed in this timeframe, interestingly, several metabolites were significantly different compared to

control islets after 4 h recovery, including increased amounts of FBP, GMP, $NADP^+$, fatty acids, and long chain acyl CoAs and decreased concentration of mCoA. These altered metabolite levels could indicate a shift in some of the K_{ATP}-independent pathways of GSIS following H_2O_2-induced stress; one potential target identified was the mevalonate pathway. Additionally, these metabolites could create a metabolic signature for islets that have been previously damaged by oxidative stress, like could occur during islet isolation for transplantation or in diabetes pathogenesis.

Islet Potency Evaluation

This dissertation presented two general approaches for islet evaluation. The first, involving multimodal detection on-chip of $[Ca^{2+}]_i$ and insulin, achieved rapid islet analysis (<90 min), as is necessary in order to make effective decisions about islet viability prior to transplantation. However, for use in a clinical setting, these devices would need to be less manually intensive and more high-throughput (devices described here evaluated 7-20 islets, while 200-300 islets are currently evaluated prior to transplantation at UIC). It also is vital to verify that these measures correlate to islet function post-transplant prior to developing this method for this purpose further.

For the second approach to islet evaluation, we developed a metabolomic method to identify potential biomarkers of islet health for transplant. After exposing islets to oxidative stress to mimic damage that can occur during islet isolation, we identified several metabolites and pathways that were altered immediately following treatment and up to 4 hours later. The ability of this method to distinguish between healthy and previously stressed cells makes it promising as a tool for islet evaluation. However, now that some differences have been identified, it is important to determine what effect they have on islet viability. Previous stress could result in islets being more likely to fail or could help condition islets so that they are better suited to deal with future stress- a study has shown, for example, that although hypoxia diminishes $[Ca^{2+}]_i$ and insulin responses to glucose, this effect could be mitigated by preconditioning islets with intermittent hypoxia (1). Once the relationship between the identified metabolic signature and islet function is determined, the method can be optimized for the

detection of significant metabolites. The current system is ideal for global metabolite identification during the hypothesis-forming stage; however, the methods are slow (37 and 45 min per HILIC and reverse phase, respectively). Specific assays for metabolites of interest could be developed with faster analysis times that are more compatible with the requirements of islet transplant.

Future Directions

Several advancements to the developed methodology can be made to move closer towards our goal of islet evaluation. Microfluidic devices need to be further automated, possibly by reducing manual handling steps in sequential detection methods or by moving to a one-chip system using miniaturized detectors. Metabolomic methods can benefit from improved detection limits to provide better metabolite coverage and pathway analysis. Likewise, flux analyses can provide greater insights into the metabolites and pathways affected during and following stress. Following these technical improvements, we can measure more complete responses to oxidative stress and other common islet stressors, and corroborate rodent islet data with human islets. Once probable markers have been identified, we can test their correlation with transplant outcome.

On-Chip Segmentation of Islet Perfusate

While segmentation of aqueous samples with oil preserves temporal information, we are currently limited in the temporal resolution achieved in insulin secretion experiments by the amount of time necessary to collect the required fraction volume. Furthermore, the current method is labor-intensive, requiring an analyst to collect samples, transfer the well plate to an xyz stage for droplet formation, and then connect the droplet tube to an extraction device and electrophoresis chip. We could eliminate the droplet formation step from the process by forming droplets directly on-chip rather than collecting fractions of perfusate.

A chip has been developed by our collaborators at the University of Illinois at Chicago to create droplets containing perfusate, FITC-insulin, and anti-insulin antibody, as shown

in Figure 5.1a. With an islet perfusate flow rate of 2.5 µL min^{-1}, FITC-insulin and antibody flow rates of 1 µL min^{-1} each, and an oil flow rate of 5 µL min^{-1}, 20 nL droplets were formed on-chip at a frequency of ~8 Hz (Figure 5.1b). However, several problems were encountered. First, the ratio of mixing from the 3 aqueous channels was not stable throughout the experiment. This could be attributed to oil entering the aqueous channels during connection of the oil tubing to the chip. Redesign of the chip to incorporate a longer oil channel and an aqueous mixing channel prior to segmentation could improve the stability of the device.

A second concern with on-chip segmentation is the length of tubing required to store all of the samples from a 25 min experiment. While droplets formed well, we observed coalescence of droplets as they moved through the 5 ft tube, likely due to increased back pressure. When droplet size varies, then the droplets will move at different rates, thus impeding the ability to relate the droplets' measurements back to the time that they were collected. One possible solution is to reduce the size of the microfluidic system so that lower flow rates could be achieved. Additionally, samples could be collected in a series of smaller tubes rather than one long tube, or a flow split could be introduced to further reduce the volume of fluid being collected in the tubing.

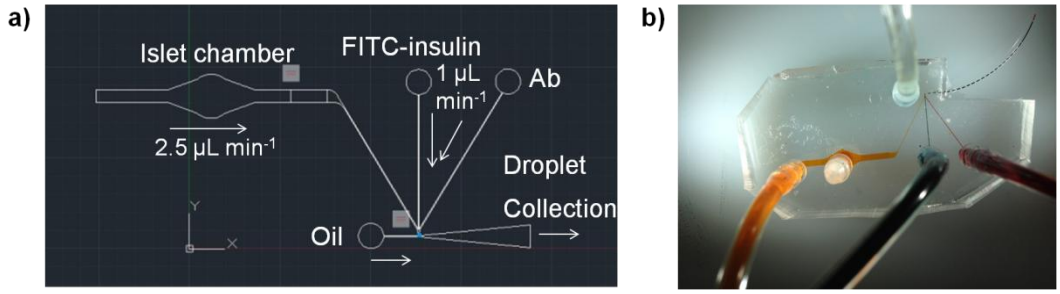

Figure 5.1. Microfluidic device for on-chip droplet generation. a) Schematic of chip design. Secreted insulin, FITC-insulin, and anti-insulin antibody were combined in a 2.5:1:1 ratio. Perfluorinated oil was used to segment the flow, creating 20 nL droplets at a frequency of 8 Hz that were collected in tubing. Fluid flow is controlled using syringe pumps. b) Image of PDMS-based device. Channels were filled with food dye for visualization. Droplets formed showed good mixing of reagents and uniformity in size.

One-Chip System for Simultaneous Detection of $[Ca^{2+}]_i$ and Insulin Secretion

The methods presented for detecting $[Ca^{2+}]_i$ and insulin secretion from a single group of islets consisted of collecting perfusate from one chip used for $[Ca^{2+}]_i$ detection that could later be perfused into a second chip used for insulin detection. The rationale was that we could use the same microscope system to measure both analytes via LIF. However, an alternative method would be to use a compact detector for one or both of the measurements. The advantage of such a system is that it allows simultaneous detection of both analytes, thus reducing the time required for analysis and eliminating extra manual handling steps.

We developed a microfabricated fiber optic probe detection system with integrated optics that could be coupled to microfluidic devices by aligning the probe to a detection channel. The dimensions of the probe (1.1 mm wide x 500-600 μm deep) allow it access to detection in confined spaces, such as those encountered on a microfluidic chip containing several fluidic reservoirs. This microprobe could potentially be used to measure insulin secreted from islets at the end of a separation channel while $[Ca^{2+}]_i$ is measured using a traditional microscope in an islet chamber located on the same chip (schematic shown in Figure 5.2). However, the current detection limits of the microprobe are not sensitive enough to measure levels of FITC that would be relevant for an electrophoretic immunoassay.

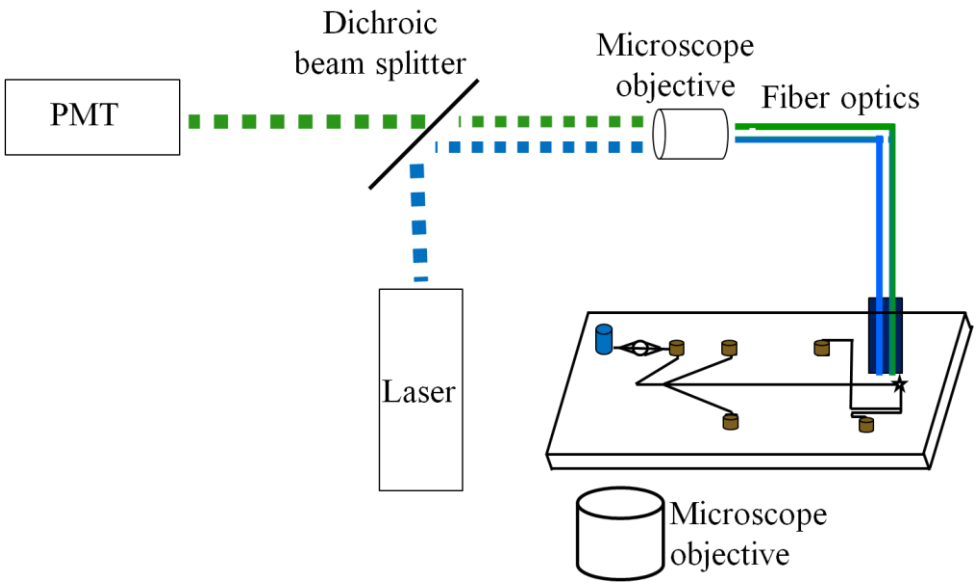

Figure 5.2. Schematic of one-chip microfluidic system for dual detection of $[Ca^{2+}]_i$ and insulin secretion. $[Ca^{2+}]_i$ is measured via traditional confocal microscopy, while insulin secretion is measured via MCE-LIF. A PDMS microprobe is aligned to the detection region of the chip. Excitation laser light is guided into the channel using a fiber optic coupled with microfabricated optical elements, while fluorescence is collected from the channel in a similar manner. Signal is detected using a PMT.

Further improvements to the microprobe can improve the sensitivity to the level required for our assay. One simple improvement is to use glass-based photomasks rather than film. The microfabricated optical faces were measured to have a feature edge surface roughness of ~2 µm, which resulted in backscattering from the optical faces. By using higher quality masks, this background light scattering can be diminished.

A second method for improving the detection limits is to integrate filters directly onto the tips of the fibers. By integrating filters directly into the probe, we can reduce the effect of light scattering that occurs along the length of the fiber and thus reduce the fluorescent background. We have successfully been able to mill dielectric filters down to 200 µm x 500 µm while leaving the optical layer intact. To incorporate them into the probe, the filters can be thinned and back polished to a smoothness tolerance of 1 µm. Filters can be handled using vacuum suction and inserted into designed holders on the mask.

UHPLC

The sensitivity of the metabolomic method can be greatly improved by using an ultra high pressure liquid chromatography (UHPLC) system that is currently being developed in our lab. UHPLC utilizes 25-100 cm long capillary columns packed with sub-2 µm particles that are operated at pressures greater than 1000 bar (2). One effect of using a UHPLC column is that the peak capacity is increased, thus resulting in less co-elution and ion suppression and consequently improved sensitivity (3). Because of this improvement in ion suppression, UHPLC has become an important method for proteomics (4) and has become increasingly used for metabolomics and lipidomics (5). While most experiments have been conducted using reverse phase columns, HILIC columns have been used more frequently recently due to an increase in the number of commercially available HILIC columns with sub-2 µm particles (6). Intensity RSD for a reverse phase column was found to be less than 30% for most features, and retention time RSD less than 5%, demonstrating good peak stability for undirected data analysis (5).

One advantage of UHPLC is that flow rates can be slowed down, making this system compatible with nano-ESI. Recent work showed similar reproducibility in nano-UHPLC compared to conventional UHPLC, with detection limits 2-2000 times lower for all (xeno)metabolites analyzed (7). By using a nano-UHPLC system, we can potentially improve detection of low abundance or poorly ionized metabolites. As a secondary advantage, the injection volumes will be much lower, thus allowing us to use smaller extraction volumes and thus improve the sensitivity even more.

Metabolic Flux Analysis

One disadvantage of the work shown in Chapters 3 and 4 is that we were measuring static levels of metabolites at specified time points. Although we could determine whether metabolite levels had changed over a certain time span, we could not specify whether these variations were due to changes in formation of a metabolite or changes in the utilization of that metabolite. Additionally, since many metabolites are involved in multiple pathways, it can be challenging to determine which pathways are affected by a

specific metabolic change. For example, we would be interested in determining the relative flux through pathways involving malonyl CoA, since we observed sustained decreases in levels of this metabolite following oxidative stress. There can also be experimentally important changes in flux through a pathway even though the metabolite levels remain constant. For these reasons, it is beneficial to study metabolic flux.

Metabolic flux analysis, or "fluxomics", involves adding a ^{13}C-labeled precursor to cells and measuring its propagation through various known pathways (8). By knowing the location of the ^{13}C label on the precursor and the reactions involved in the pathways, it is possible to determine the relative flux through each of the pathways involved. One of the challenges in metabolic flux analysis is that instead of generating one peak per compound, each compound will be split into several peaks based on the number of ^{13}C atoms that are incorporated. When using small sample sizes, this can mean that many low abundance metabolites are no longer detectable, thus limiting the utility of this method. In order to run metabolic flux analysis on islet samples, we would first want to improve the sensitivity of the metabolomic method.

Other Cell Stressors

While we have been able to obtain information on the effects of oxidative stress on islet function, other types of stress can also occur during islet isolation and diabetes pathogenesis. Because multiple stressors likely act on islets simultaneously, it is important to understand the effects of multiple types of stress on islet viability. Other potential stressors include hypoxia and cytokines. Studies have previously been conducted in β-cells under both of these conditions.

One study used ^{1}H NMR to study changes in metabolic markers in INS-1 cells during hypoxia-induced cell death. A decrease in creatine-containing compounds was observed during early-stage hypoxia (2-6 h), while increased levels of taurine-containing compounds were observed in late-stage hypoxia (12-24 h) (9). Since our LC-MS method measures many different compounds than the published NMR method, we can potentially obtain complementary data that gives more insight into the particular

pathways affected. In preliminary studies, for example, following 1 h of hypoxia, we observed increased levels of FBP and decreased levels of mCoA, NAD, CDP-ethanolamine, and citicoline. Measuring responses to hypoxia is also interesting from the standpoint that islets preconditioned with intermittent hypoxia have been found to have improved insulin secretion under hypoxic conditions as compared to control islets (1). Further exploration into the effects of hypoxia on islets can provide insights into the effects of islet preconditioning on islet function.

Cytokines are another potential stressor of islets. Cytokines are released as part of the immune response to oxidative and ER stress and can cause cell death (10). Cytokine release occurs at several points in the islet isolation process, beginning with increased cytokine production in the pancreas from the moment of brain death in the islet donor. Islets have also been shown to express several proinflammatory cytokines during culture. After transplantation, immune responses in the recipient can stimulate additional cytokine release (11). Previous work has suggested that cytokines induce cell death through a necrotic, rather than apoptotic, pathway (12). However, this work does not include any glucose stimulation studies and does not give any indication of possible lasting effects of cytokine treatment on the surviving cells, which is important from the viewpoint of islet evaluation and is an area for potential future investigation.

Human Islets

All of the work presented here was completed using rodent islets; however, as human islets become more readily available for research, it would be beneficial to replicate experiments in human islets to ensure transferability of the method. Human islets are morphologically different from rodent islets. While rodent islets contain a core of β-cells surrounded by a shell of α-cells, human islets show no such organization. Additionally, the ratio of β-cells can vary significantly in human islets, reportedly from 28-75%, so sample variability may be a greater issue (13). Metabolic differences have been reported between rodent and human islets as well. While pathways incorporating the enzymes pyruvate carboxylase (PC) and ATP citrate lyase are important in rodent islets, research has suggested that pathways involving the enzymes succinyl-CoA:3-

ketoacid-CoA transferase (SCOT) and acetacetyl-CoA synthetase may be preferred in human islets (14). Since our main goal is to develop a method to evaluate islets for human islet transplantation, identification of robust biomarkers relevant to human islet metabolic processes is imperative.

Development of Islet Scoring System

The primary goal of this work was to develop analytical methods to evaluate islet viability for the purpose of islet transplantation. In order to use the methods that we developed to evaluate viability, we would need to transplant islets that have been evaluated via our methods into mice and determine the outcome of the transplantation. This could be done in collaboration with islet surgeons at the University of Illinois at Chicago. We would then use statistical methods to develop a scoring system that would correlate the measurements taken with the expected outcome of the transplantation, and create a cut-off value for "healthy" vs. "unhealthy" islets. Finally, we would use our scoring system to evaluate islets prior to transplantation in mice and determine the efficacy of our system in predicting future islet viability and potency.

References

1. Lo, J. F., Wang, Y., Blake, A., Yu, G., Harvat, T. A., Jeon, H., Oberholzer, J., and Eddington, D. T. (2012) Islet Preconditioning via Multimodal Microfluidic Modulation of Intermittent Hypoxia. *Anal. Chem.* **84**, 1987–1993
2. Jorgenson, J. W. (2010) Capillary Liquid Chromatography at Ultrahigh Pressures. *Annu. Rev. Anal. Chem.* **3**, 129–150
3. Schappler, J., RudaZ, S., and Veuthey, J.-L. (2013) Coupling UHPLC With MS: The Needs, Challenges, and. *Ultra-High Perform. Liq. Chromatogr. Its Appl.*
4. Zhao, Y.-Y., and Lin, R.-C. (2014) UPLC–MSE application in disease biomarker discovery: The discoveries in proteomics to metabolomics. *Chem. Biol. Interact.* **215**, 7–16
5. Witting, M., Maier, T. V., Garvis, S., and Schmitt-Kopplin, P. (2014) Optimizing a ultrahigh pressure liquid chromatography-time of flight-mass spectrometry approach using a novel sub-2μm core–shell particle for in depth lipidomic profiling of Caenorhabditis elegans. *J. Chromatogr. A*. **1359**, 91–99
6. Nováková, L., Havlíková, L., and Vlčková, H. (2014) Hydrophilic interaction chromatography of polar and ionizable compounds by UHPLC. *TrAC Trends Anal. Chem.* **63**, 55–64
7. Chetwynd, A. J., David, A., Hill, E. M., and Abdul-Sada, A. (2014) Evaluation of analytical performance and reliability of direct nanoLC-nanoESI-high resolution mass spectrometry for profiling the (xeno)metabolome: nanoUHPLC-nanoESI-TOFMS for (xeno)metabolomics. *J. Mass Spectrom.* **49**, 1063–1069
8. Nöh, K., and Wiechert, W. (2011) The benefits of being transient: isotope-based metabolic flux analysis at the short time scale. *Appl. Microbiol. Biotechnol.* **91**, 1247–1265
9. Tian, L., Kim, H. S., Kim, H., Jin, X., Jung, H. S., Park, K. S., Cho, K. W., Park, S., and Moon, W. K. (2013) Changes in Metabolic Markers in Insulin-Producing β-Cells during Hypoxia-Induced Cell Death As Studied by NMR Metabolomics. *J. Proteome Res.* **12**, 3738–3745
10. Wang, M., Crager, M., and Pugazhenthi, S. (2012) Modulation of Apoptosis Pathways by Oxidative Stress and Autophagy in β Cells. *Exp. Diabetes Res.* **2012**, 1–14
11. Kanak, M. A., Takita, M., Kunnathodi, F., Lawrence, M. C., Levy, M. F., and Naziruddin, B. (2014) Inflammatory Response in Islet Transplantation. *Int. J. Endocrinol.* **2014**, 1–13
12. Collier, J. J., Burke, S. J., Eisenhauer, M. E., Lu, D., Sapp, R. C., Frydman, C. J., and Campagna, S. R. (2011) Pancreatic β-Cell Death in Response to Pro-Inflammatory Cytokines Is Distinct from Genuine Apoptosis. *PLoS ONE*. **6**, e22485
13. In't Veld, P., and Marichal, M. (2010) Microscopic Anatomy of the Human Islet of Langerhans. in *The Islets of Langerhans* (Islam, M. S. ed), pp. 1–19, Springer Netherlands, Dordrecht, **654**, 1–19
14. MacDonald, M. J., Longacre, M. J., Stoker, S. W., Kendrick, M., Thonpho, A., Brown, L. J., Hasan, N. M., Jitrapakdee, S., Fukao, T., Hanson, M. S., Fernandez, L. A., and Odorico, J. (2011) Differences between Human and Rodent Pancreatic Islets: LOW PYRUVATE CARBOXYLASE, ATP CITRATE LYASE, AND PYRUVATE

CARBOXYLATION AND HIGH GLUCOSE-STIMULATED ACETOACETATE IN HUMAN PANCREATIC ISLETS. *J. Biol. Chem.* **286**, 18383–18396

APPENDIX A

Monolithic Integrated Microscale Spectroscopic Probes (MiMS Probes)

Thitaphat Ngernsutivorakul, Cynthia M. Cipolla, Colleen E. Dugan, Michael D. Morris, Robert T. Kennedy, Francis W. L. Esmonde-White

Introduction

Fluorescence spectroscopy is a powerful technique due to its high sensitivity, fast response, and ease of use. Most conventional optical systems are formed through an assembly of individual components, such as microscope objectives, mirrors, and lenses. This approach requires fixtures and an assembly process which incurs an inherent base cost, and limits the ability to develop highly integrated analytical devices. Chemical measurements in tight spaces are also restricted due to size, particularly for multi-position detection and parallel analysis on microfluidic chips. Miniaturization of optical detection systems is currently a hot topic.

Many recent spectroscopic applications have been investigated which necessitate miniaturized optical probes. These probes are generally made by assembling compact optics and by integrating fiber optics into the analytical devices (1, 2). For instance, optical fibers have been integrated with micro-lenses in order to develop miniature portable Raman probes. While these probes are commercially available, they are typically expensive because of costs associated with material handling and precise optical alignment. Furthermore, they are limited to sizes larger than 1 mm to accommodate the required alignment hardware and optical elements. For biomedical applications, additional bulk is also added to the probes in order to allow autoclaving. Nonetheless, fiber optic probes with lenses have been reported with 2 mm diameter, and fiber optic probes without lenses have been made as small as 1 mm diameter (3–5). Optical detection systems have alternatively been miniaturized using

microfabrication techniques (6–11). By microfabrication, the optics can be integrated into a microfluidic chip with precise alignment and can be mass produced. The integrated devices can be used for a variety of applications such as protein separation, DNA analysis, and flow cytometry (12–14). Most designs have utilized the common photoresist and PDMS (poly(dimethylsiloxane)) rapid prototyping method due to several advantages of the materials, for example, low-cost and ease of fabrication (15, 16). Typical designs use fiber optics to deliver the light from the light source and to collect the light from microfluidic channels (17–22). Additionally, optical elements such as built-in lenses and other waveguides can be incorporated into the devices using air-PDMS (23–28) or liquid-liquid interfaces (11, 29–34). These systems are typically developed with extensive integration in mind, and their sophisticated designs allow specific performance to be achieved. However, they also require fixed optics and therefore low flexibility. In addition, the optics and the microfluidic systems must be manufactured simultaneously, leading to more potential points of failure and complication in fabrication processes, especially for chips requiring multiplexing (35).

In this work, we have used microfabrication (22, 23, 36) to develop miniaturized optical probes. The probes are smaller than traditional fluorescence probes made using fiber optics by other techniques. The miniaturized probes allow measurements in small spaces. The system also allows easy integration with microfluidic devices via a “plug-and-play” configuration. Finally, the potentially low cost of fabrication suggests the possibility of disposable probes that would facilitate diagnostics and other applications.

Experimental Section

Refractive Index (RI) Characterization and Optical Design

The RI of PDMS (Sylgard 184, Dow Corning, Midland, MI) from 200 to 830 nm was measured on the flat surface of the polymer using an ellipsometer (Sopra GESP-5 system). The PDMS was prepared as a 1/4" thick slab cast against a glass plate and cured between 90°C and 100°C for 45 min according to the manufacturer directions (standard 1:10 ratio of parts A:B). ZEMAX was used in non-sequential mode to model multimode glass optical fibers and air-gap optical elements in a PDMS device. The

measured RI values of the PDMS were used to design a series of lensed probes for collecting light from a liquid sample outside the PDMS probe through 0.22 NA low-OH multimode optical fibers. Mirror elements were created using total internal reflection by designing the angle of incidence on the mirror elements to be greater than the critical angle. Mold elements forming the optics were designed to avoid high aspect ratio elements of the mold that would resist demolding of the final device. Lens and mirror properties (position, angle, height, thickness and curvature) were optimized to maximize the fluence arriving at the focal region of the probe. For simplicity, both the excitation and collection fibers were treated as fiber optic light sources in the model. An example of ZEMAX simulation is shown in Figure A.1a.

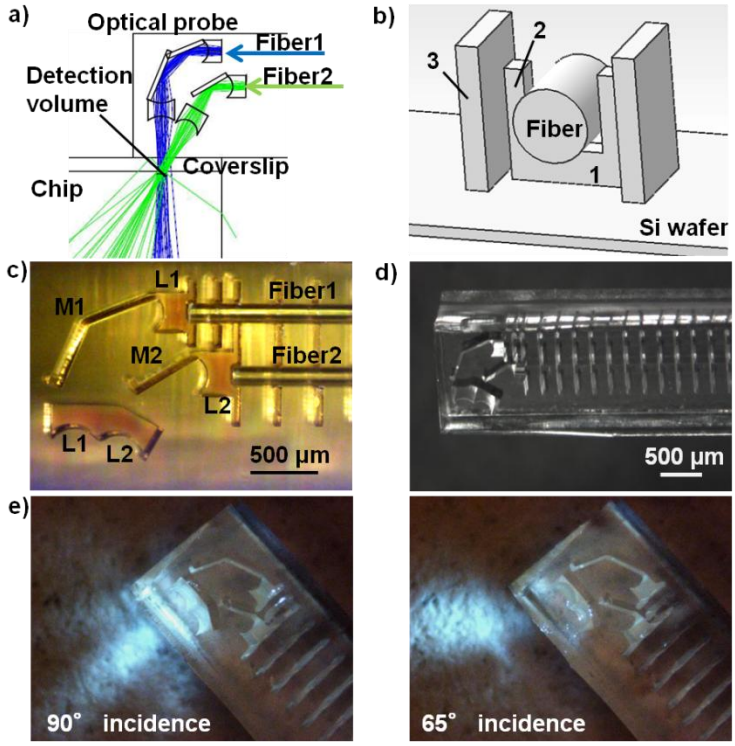

Figure A.1. Design of a microfabricated probe. a) Zemax simulation of the optical pathway of the probe coupled to a microfluidic system. The lenses were designed to focus 100 µm below the coverslip. b) Schematic of probe cross-section. Layer 1 elevated the fibers, layer 2 created the optics and held the fiber in place, and layer 3 formed the boundary. c) Optical fibers inserted into specially-designed SU-8 mold. L = lens, M = mirror. d) Microscale image of microfabricated probe with dimensions of 1.1 mm wide x 0.6 mm thick. e) Line-shaped focus of white light through each fiber, corresponding to the design in (c).

Mask Design

AutoCAD was used to design lithographic masks based on the optimized ZEMAX models. Additional features were incorporated such as skid-and-post structures for holding the fiber optics, a bounding box to act as the outer edge of the probe mold, and registration patterns for allowing spatial alignment of the multiple feature layers. An illustration of the fiber encapsulation features is shown in Figure A.1b, which shows the skids made in the first lithographic layer, the posts in the second lithographic layer, and the bounding box formed in the third lithographic layer, along with a fiber snapped into place after development of the unexposed SU8. For the exposure times used, each subsequent exposure during the UV lithography process crosslinked all polymer in the lower layers, creating solid structures down to the silicon wafer substrate. Three separate layers were designed and printed onto emulsion film masks with a 7 μm minimum feature size (Fineline Imaging, Colorado Spring, Colorado). These masks were used to sequentially expose each physical layer in the lithography process.

SU-8 master mold fabrication

The master mold was microfabricated using SU-8 2075 photoresist (MicroChem, Newton, MA) on a 4-inch Si wafer (ID: 1116, University Wafer , Boston, MA). This mold consisted of 3 layers. The first layer was created by spin-coating a 110 μm thick layer of photoresist onto the wafer, followed by a soft-bake process heating the level wafer. The wafer was aligned to the photomask and UV exposed for 18 seconds at 17 mW/cm^2. The photoresist layer was then post-exposure baked to polymerize the exposed pattern. The second and third layers of the device were created via a similar process. The second layer was 300 μm thick using an exposure time of 28 seconds, while the third layer was 110 μm thick with 34 second exposure time. All times and temperatures used for soft-bake and post-exposure bake were according to the MicroChem SU-8 2000 processing guidelines for the cumulative thickness. After the final post-exposure bake, SU-8 developer solution (MicroChem, Newton, MA) with sonication was used to dissolve unexposed photoresist. The SU-8 mold surfaces were exposed to trichloro(methyl)silane (Sigma-Aldrich, St. Louis, MO) vapor to later aid the release of PDMS from the molds.

Probe Fabrication

Two 2 meter segments of 105 μm core/125 μm clad/250 μm polyamide buffer coated low-OH optical fiber (FG105LCA, Thorlabs, Newton, NJ) were cut. A 4 cm segment at the end of each fiber was stripped to remove the polyamide buffer, and then flat-cleaved using a wide-blade fiber scribe (F-CL1, Newport, Irvine, CA). The flat-cleaved optical fiber segments were manually positioned in the SU-8 skid-and-post mold structures so that the cleaved end of the fiber was in contact with a physical stop designed at the entrance of the optical system, as shown in Figure A.1c. A small volume of PDMS prepolymer (approx. 1 mL Sylgard 184, Dow Corning, Midland, MI) was prepared gravimetrically in a 1:10 ratio, mixed, and poured into the SU-8 molds after insertion of the optical fibers. The wafer assembly was placed in a vacuum chamber to degas the PDMS. A glass microscope slide was pressed firmly into contact with the upper surface of the SU-8 mold to control the probe thickness. The silicon wafer/SU-8 mold/PDMS/glass assembly was placed in an oven at 95°C and allowed to cure for 45 min. The lensed fiber optic probes were de-molded by carefully separating the glass slide and SU-8 mold. An image of the final probe is shown in Figure A.1d. The free ends of the optical fibers were then terminated with standard FC-PC connectors using low-fluorescence epoxy (EPO-TEK 301, Epoxy Technology, Billerica, MA).

Probe Optical Characterization

The transmission efficiency and spectral throughput characteristics of the microprobe were measured and compared against a probe consisting of two bare cleaved fibers. Light transmission through both probes was measured using an optical power meter (PM100, Thorlabs, Newton, NJ) and a 543 nm 1.5 mW He-Ne laser (Melles Griot, Carlsbad, CA). The transmittance of a NIST calibrated white light source (HCA, Kaiser Optical Systems, Ann Arbor, MI) was measured using a spectrometer (USB2000, Ocean Optics, Dunedin, FL) to determine the spectral throughput characteristics of each probe from 200 to 800 nm with an integration time of 1 s. Reflectance spectra using one fiber as a source and the other as a collector were conducted using a fiber optic illuminator (Fiber-Lite 3100, Dolan-Jenner Industries, Woburn, MA) as a source and the

same spectrometer, using Teflon as a high reflectance standard. These provided data on the collection efficiency and the background of the probes.

Characterization of the fluorescence performance of the probes was conducted using integration times of 0.1 s to 0.5 s using the USB2000 spectrometer and 543 nm He-Ne laser source described earlier. The probe was placed into contact with a droplet of 10 μM resorufin on a silver-coated glass coverslip (EMF, Ithaca, NY) to determine the response of a bulk solution. To evaluate the probe performance on a microfluidic chip, the probes were aligned to a PDMS microfluidic chip consisting of 100 μm wide x 60 μm deep channels, with a 100 μm thick cover layer of PDMS.

Microfluidic Experimental Protocol

The utility of the fabricated probe was initially characterized with dye filled capillary and subsequently with a microfluidic fluorescence based enzyme assay of glycerol. For fluorescence detection, a 543 nm He-Ne laser source and a photomultiplier tube (PMT) detector (Model R1547, Hamamatsu, Japan) were used with a 580 nm band pass filter (XF3022, Omega Optical, Brattleboro, VT) as an emission filter. The voltage and amplifier gain of the PMT were set at 0.75kV and 10^7 V/A, respectively. Initial data was collected with resorufin standards flowed through a fused silica capillary with 150 μm inner diameter and 360 μm outer diameter (Polymicro Technologies, Phoenix, AZ). This initial data was used to determine the detection limit using a 251 point (~1 s) boxcar smoothing. The performance of the microprobe on a microfluidic chip was also characterized for a glycerol assay. Figure A.2 illustrates the arrangement of the probe for on chip fluorescence detection. A PDMS microfluidic chip was fabricated by soft lithography with a channel network design similar to a previously published device (37). Glycerol standard solutions (Sigma-Aldrich, St. Louis, MO) were diluted to concentrations of 14, 28, 56, and 112 μM with Hank's Balanced Salt Solution (Life Technologies, Carlsbad, CA) before on-chip mixing with free glycerol reagent (Sigma-Aldrich, St. Louis, MO) and 1 mM Amplex UltraRed (Life Technologies, Carlsbad, CA) in 20% DMSO. The solutions were pumped at 1 μL min^{-1} using a syringe pump (Chemyx, Stafford, TX). The channel was designed to mix and then incubate the flowing mixture

using serpentine channels. The fluorescent product (analogous to resorufin) was detected at the outlet by a microfabricated probe. The probe was aligned to the detection zone of the microfluidic chip using a stereotaxic alignment frame (Model 900, KOPF, Tujunga, CA). An analog-to-digital converter (NI USB-6008, National Instruments, Austin, TX) was used for data acquisition and collection at 250 samples/s with LabVIEW (Version 10.0.1, National Instruments, Austin, TX). Data was processed in MATLAB (R2012b, MathWorks, Natick, MA).

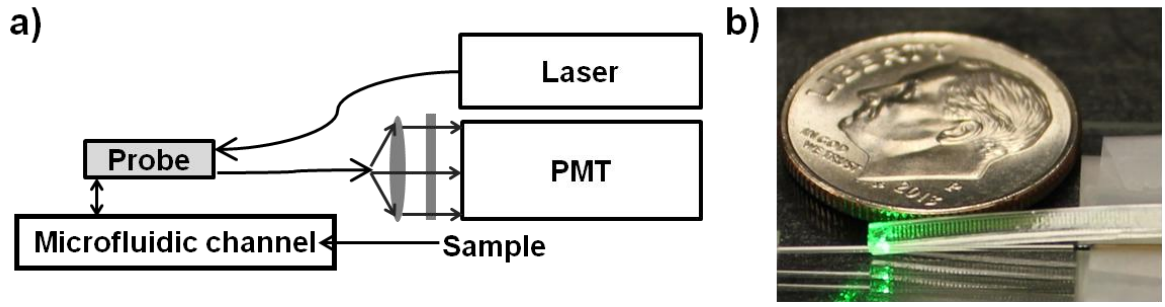

Figure A.2. Probe performance in a microfluidic channel. a) Schematic of probe set-up with 150 µm i.d. x 360 µm o.d. capillary. b) Microscopic image of the probe on the capillary.

Results and Discussion

Design and Fabrication of Probes

RI of PDMS can vary significantly depending on selected wavelengths, curing times, and temperatures, necessitating its measurement to allow for precise design of optical PDMS elements. Measured RI values were used to design optical elements using ZEMAX. The cylindrical optics in the fabricated probe generated a line-shaped focus, perpendicular to the plane of the optical system, as demonstrated in Figure A.1e. The probe design shown in this work used a side-firing configuration, to unambiguously demonstrate the functionality of the integrated lenses and mirrors. This design had the added benefit of maintaining the source and collection optical fibers along a common axis on a single side of the sample, which was comparable to a microscopy epi-configuration. The configuration facilitated having a small but robust probe because the fibers were together along their length. Folding mirrors are necessary in any design where the optical fibers are parallel in order to have the excitation and collection regions

overlap. Furthermore, a side-firing design is well suited to microfluidic applications, and avoids probe deformation during alignment to the sample. Additional designs were tested, including forward facing probes with more than two fibers, 45^0 side firing, and non-lensed probes, but results have not been included for clarity.

In order to accommodate two 125 μm optical fibers, the width of these probes had to be at least 400 μm. In practice, a 90^0 side firing probe incorporating two 30^0 incidence total-internal-reflectance based mirrors requires a minimum width of approximately 1.1 mm. These probes had structures based on three layers, giving a total thickness of approximately 500-600 μm, including an externally bonded 100 μm PDMS cover layer. By microfabrication, the probes have the potential to match the surface quality that has been previously demonstrated in SU-8 and PDMS systems. Examples include features replicated on a micrometer scale with optical quality surfaces (23). In the present work, we fabricated devices using inexpensive emulsion masks with a surface roughness of approximately 2 μm. The aspect ratio was not well optimized; instead, feature sizes were deliberately kept large to avoid issues with mold fabrication and demolding of the PDMS structures. Using manufacturer defined processing steps, the layer thicknesses were within 2% of the design values, and the optical features were within 2% of the target size. Optimization of mask material and the SU-8 processing steps will enable the optical performance of the microprobes to be enhanced.

Probe Optical Performance

To evaluate the optical performance of the microprobe, a series of comparisons were made to a probe consisting of two cleaved bare fibers assembled side by side with identical FC connectorization. The optical throughput of the microfabricated probe was determined by injecting laser light at the rear FC fiber interface and measuring the optical power transmitted through the probe face. The bare fiber probe had 84% throughput while the probe with fabricated optics had 70% throughput. We assumed that the majority of the 16% loss in the bare fiber was due to losses in injecting light through the FC connector, and in the microprobe an additional 14% loss was due to the probe optical elements.

To verify if any spectral artifacts were caused by the microfabricated optics, we compared white light (HCA) throughput of the microfabricated probes to the throughput of a bare fiber using a spectrometer (Ocean Optics). The spectra were identical for both probe types, as illustrated in Figure A.3a, indicating that no spectral artifacts were generated by the microoptical system.

A series of reflectance tests were conducted to evaluate the relative performance of the microprobe to the bare fiber probe. To compare the background scattering arising from the probe optics, a white light reflectance spectrum was collected with the probes pointing into free space in a dark room, as shown in Figure A.3b. The scattered white light background generated from the microfabricated probe was significant, while the bare fiber probe had no discernible background because the bare fiber probe has no interfaces which can scatter light from the excitation channel back into the collection channel. The microprobe optical faces were fabricated with a lithographic mask having approximately 2 μm feature edge roughness, causing backscattering from the optical faces. Through the use of higher quality lithographic masks, the background light scattering can be diminished. Next, the collection efficiency from a highly scattering (teflon) surface was measured. Both probe types had approximately the same collection efficiency, with a slightly different spectral collection efficiency due to wavelength-dependent light scattering effects. However, when collection efficiency was tested against a transparent PDMS slab, the bare fiber probe collected 3.3 times more signal than the microprobe. This was because the surface reflections from the PDMS slab were collected very efficiently by the two parallel fibers. The spatial offset between the excitation and collection paths in the microprobe allowed very little reflectance to be collected, with half of this reflectance arising within the microprobe as shown by the reflectance in air.

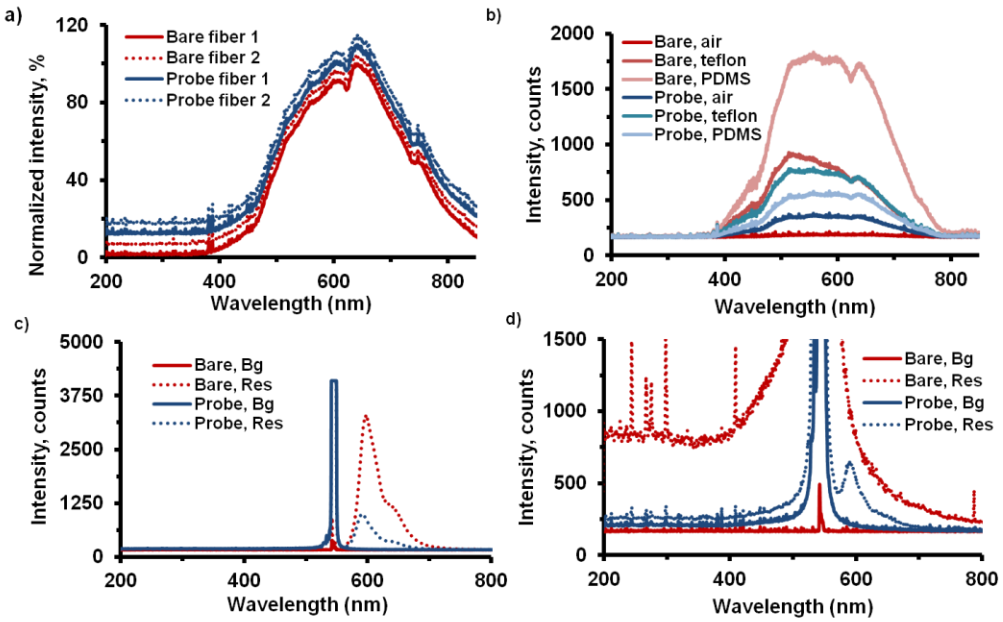

Figure A.3. Spectroscopic performance of probe in comparison to bare fibers. a) Detection of white light through bare fibers (red) and through each lensed fiber (blue), showing identical spectral shapes. Data were offset for comparison. b) White light reflectance spectrum from varied materials. c) Laser excitation of 10 µM resorufin with lensed and unlensed fibers immersed in the bulk solution and d) in microfluidic channels through a 100 µm PDMS coverslip. The microfabricated optics' focusing capability offset the reduced light transmission and resulted in stronger fluorescence on chip.

When measuring resorufin in bulk solution, the bare fiber probe outperformed the microfabricated probe because of a higher overall collection solid angle. Based on the integrated area of fluorescence emission from 575-595 nm, the bare fibers outperformed the microfabricated probe 2.2 fold when in contact with the bulk fluorescence solution (Figure A.3c). However, when measuring resorufin in a channel buried 100 µm below the surface of the PDMS microfluidic device, the microfabricated probe detected fluorescence efficiently, whereas fluorescence was not detectable using the bare fiber probe. The lensed microprobe focused the light into the sample channel. The bare fiber probe collected the excitation laser light reflected from the PDMS microchip, with the laser signal swamping any fluorescence (Figure A.3d). The high collected intensity of laser light caused the wings of the 543 nm laser line to become apparent. The much higher reflectance from the PDMS surface when using the bare probe was in agreement with the results shown in Figure A.3b, where the surface

reflectance of the bare fiber probe was several fold greater than for the microprobe. This demonstrated the utility of using microfabricated optics on a microprobe.

Fluorescence Detection

Preliminary experiments were performed measuring resorufin standards in a 150 µm i.d./360 µm o.d. fused-silica capillary. Results are shown in Figure A.4a. The calibration curve was linear with R^2 of 0.997 and RMSE of 0.69. The limit of detection (LOD), determined as the concentration to give a signal 3 times the standard deviation of the blank, was 6 nM. Figure A.4b presents a trace of 52 nM resorufin flowing through the capillary alternating with a blank. Our results demonstrated that the probe was adequately stable for analytical microfluidic experiments.

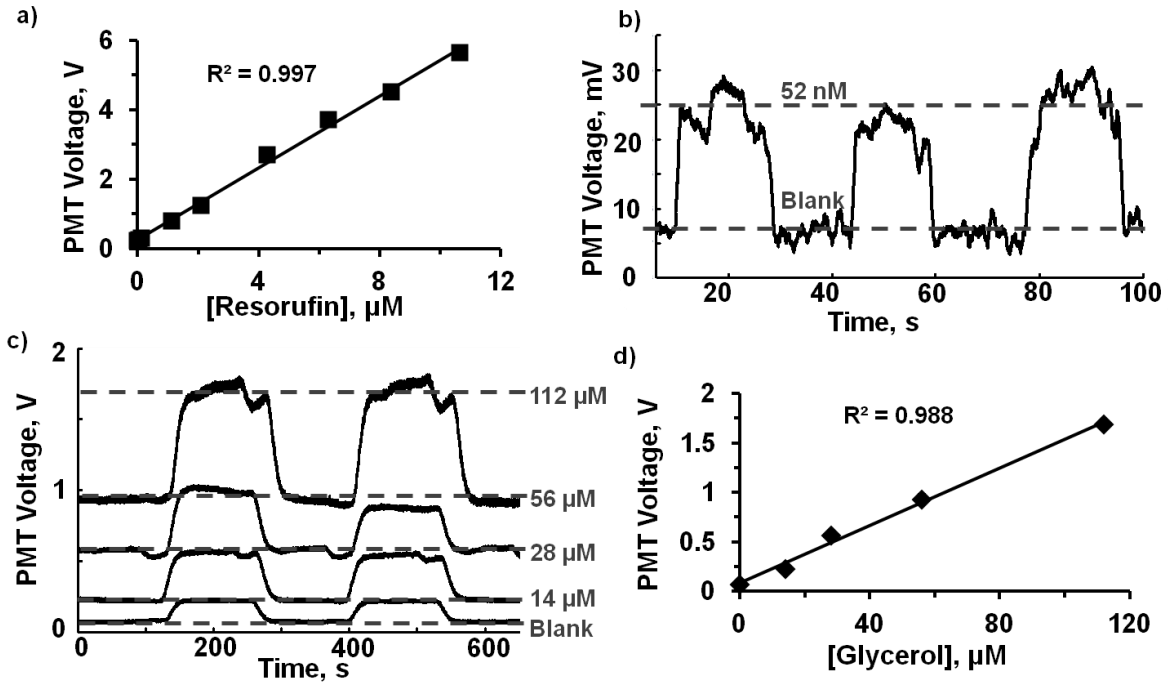

Figure A.4. Probe performance in 150 µm i.d. x 360 µm o.d. capillary (a,b) and the PDMS chip (c,d). a) Calibration curve of 0.05 to 10 µM resorufin, resulting in detection limit of 6 nM after 249 point boxcar smooth (acquisition rate of 250 samples/s). b) Trace of 52 nM resorufin switching with a blank. c) Probe detection of on-chip glycerol assay. Individual traces show alternating between low and high glycerol concentrations (0, 14, 28, 56, 112 µM, respectively). d) Linear range of glycerol assay corresponding to (c). Deviation from the line at 14 µM is inherent to the assay (38).

The probe was then coupled to a PDMS-based microfluidic chip for quantification of glycerol in an on-chip fluorescence enzyme assay. The signals of the fluorescent products from different glycerol concentrations are shown in Figure A.4c. Each trace represents the signals upon switching between low and high glycerol concentrations. The fluorescence assay, using the probe as a detector, resulted in a linear response with R^2 of 0.988 and RMSE of 3.81 (Figure A.4d). The calculated LOD was 0.7 µM for glycerol. The results demonstrated that the probe could be used to detect fluorophores with decent reproducibility and wide dynamic range. With probe detection, analytical performance of the on-chip assay was comparable to our previously reported on-line enzyme assay (39) and other commercial glycerol assay kits (38).

The results showed that our microfabricated probes are suitable for on-chip fluorescence applications with adequate sensitivity. The LODs were comparable to other microfabricated devices with integrated optics and optical fibers (17, 18, 23). Our probes had the advantage of being able to focus into small channels (down to 15 µm deep x 30 µm wide, results not included here), enabling their use for a wider variety of applications, such as electrophoresis, cytometry, and applications requiring high temporal resolution or low flow rates. Furthermore, the probes incorporated both excitation and emission fibers in parallel on the same side of the microfluidic device, which allowed for simplified fabrication and required less space for integration. Because our probes were standalone devices, they were also flexible, i.e. a single probe design could be used for many different applications on different chips. As the major microfluidic design characteristic is the coverslip material and thickness, a given design could be highly reusable. Individual probes could also be reusable, and low material costs could allow large numbers to be used simultaneously in parallel.

Conclusion

Microfabrication, soft lithography in particular, is a viable and cost-effective way to miniaturize spectroscopic probes. The potential for low cost through integrated molding of probe optics may enable disposable high performance probes. The materials selected for this probe are also compatible with autoclaving at 134 ºC or 121 ºC,

offering a unique potential compatibility with biomedical applications as compared to traditional assembled microprobes that require the use of adhesives and have materials with dissimilar thermal expansion coefficients. The microprobes were only slightly larger than the optical fibers on which they were molded. Our microfabricated probes were thus smaller than any commercial optical probes, enabling chemical measurements in tight sampling points which would require the probe to be less than a few mm in size. The probes' applications were accordingly versatile, including fluorescence measurements in both microfluidic and non-microfluidic systems.

A variety of further applications can be realized due to the size and configuration of the probes. Pairing a microfluidic device with the probes illustrates a simple approach for coupling fluorescence to a chip. Multiple probes can be placed on a single chip for monitoring several chemicals in real time; this was previously restricted because of microscope dimensions (40, 41). Another benefit of the probe design is its applicability to lab-on-a-chip applications. The probes can feasibly be coupled with more compact light sources (42, 43) and detectors (44) and other miniature optics (45, 46), resulting in highly-integrated and portable analytical devices. One issue to address is probe alignment to the chips, which is currently accomplished via a micropositioner and can be lengthy at times. Future iterations of the probes will contain alignment markers to aid during this process.

Sensitivity of the probe is currently not low enough to measure levels of FITC that would be relevant for an electrophoretic immunoassay, which limited the potential of applying this technology for multi-point fluorescent detection of $[Ca^{2+}]_i$ and insulin secretion on-chip. However, further improvements to the microprobe can improve the sensitivity to the level required for our assay. One simple improvement is to use glass-based photomasks rather than film. With higher quality masks, optical faces can be fabricated with less surface roughness, resulting in reduced backscattering. A second method for improving the detection limits is to integrate filters directly onto the tips of the fibers; this will reduce the effect of light scattering that occurs along the length of the fiber and thus reduce the fluorescent background.

References

1. J. R. Krogmeier, I. Schaefer, G. Seward, G. R. Yantz and J. W. Larson, *Lab. Chip*, 2007, **7**, 1767.
2. G. V. Kaigala, M. Bercovici, M. Behnam, D. Elliott, J. G. Santiago and C. J. Backhouse, *Lab. Chip*, 2010, **10**, 2242.
3. J. C. C. Day, R. Bennett, B. Smith, C. Kendall, J. Hutchings, G. M. Meaden, C. Born, S. Yu and N. Stone, *Phys. Med. Biol.*, 2009, **54**, 7077–7087.
4. M. C. M. Grimbergen, C. F. P. van Swol, R. O. P. Draga, P. van Diest, R. M. Verdaasdonk, N. Stone and J. H. L. R. Bosch, SPIE, 2009, pp. 716114–716114–6.
5. I. Latka, S. Dochow, C. Krafft, B. Dietzek, H. Bartelt and J. Popp, in *Clinical and Biomedical Spectroscopy and Imaging II*, ed. N. and P. Ramanujam, Optical Society of America, 2011, vol. 8087, p. 80872D.
6. M. A. Burns, B. N. Johnson, S. N. Brahmasandra, K. Handique, J. R. Webster, M. Krishnan, T. S. Sammarco, P. M. Man, D. Jones and D. Heldsinger, *Science*, 1998, **282**, 484–487.
7. J.-C. Roulet, R. Völkel, H. P. Herzig, E. Verpoorte, N. F. de Rooij and R. Dändliker, *Anal. Chem.*, 2002, **74**, 3400–3407.
8. E. Verpoorte, *Lab. Chip*, 2003, **3**, 42N.
9. G. T. Roman and R. T. Kennedy, *J. Chromatogr. A*, 2007, **1168**, 170–188.
10. K. B. Mogensen and J. P. Kutter, *Electrophoresis*, 2009, **30**, S92–S100.
11. X. Zeng and H. Jiang, *J. Phys. Appl. Phys.*, 2013, **46**, 323001.
12. J. Vieillard, R. Mazurczyk, C. Morin, B. Hannes, Y. Chevolot, P. Desbene and S. Krawczyk, *J. Chromatogr. B*, 2007, **845**, 218–225.
13. C. L. Bliss, J. N. McMullin and C. J. Backhouse, *Lab. Chip*, 2007, **7**, 1280.
14. J. Godin, C.-H. Chen, S. H. Cho, W. Qiao, F. Tsai and Y.-H. Lo, *J. Biophotonics*, 2008, **1**, 355–376.
15. H. Becker and C. Gärtner, *Anal. Bioanal. Chem.*, 2007, **390**, 89–111.
16. P. N. Nge, C. I. Rogers and A. T. Woolley, *Chem. Rev.*, 2013, **113**, 2550–2583.
17. M. L. Chabinyc, D. T. Chiu, J. C. McDonald, A. D. Stroock, J. F. Christian, A. M. Karger and G. M. Whitesides, *Anal. Chem.*, 2001, **73**, 4491–4498.
18. S. Qi, X. Liu, S. Ford, J. Barrows, G. Thomas, K. Kelly, A. McCandless, K. Lian, J. Goettert and S. A. Soper, *Lab. Chip*, 2002, **2**, 88.
19. M.-H. Wu, H. Cai, X. Xu, J. P. Urban, Z.-F. Cui and Z. Cui, *Biomed. Microdevices*, 2005, **7**, 323–329.
20. R. Mazurczyk, J. Vieillard, A. Bouchard, B. Hannes and S. Krawczyk, *Sens. Actuators B Chem.*, 2006, **118**, 11–19.
21. R. Irawan, S. C. Tjin, X. Fang and C. Y. Fu, *Biomed. Microdevices*, 2007, **9**, 413–419.
22. P. C. Ashok, G. P. Singh, H. A. Rendall, T. F. Krauss and K. Dholakia, *Lab. Chip*, 2011, **11**, 1262–1270.
23. S. Camou, H. Fujita and T. Fujii, *Lab. Chip*, 2003, **3**, 40.
24. J. Seo and L. P. Lee, *Sens. Actuators B Chem.*, 2004, **99**, 615–622.
25. L. Jiang and S. Pau, *Appl. Phys. Lett.*, 2007, **90**, 111108–111108.
26. B. R. Watts, Z. Zhang, C.-Q. Xu, X. Cao and M. Lin, *Biomed. Opt. Express*, 2012, **3**, 2784–2793.

27. D. A. Chang-Yen, R. K. Eich and B. K. Gale, *J. Light. Technol.*, 2005, **23**, 2088–2093.
28. Z. Cai, W. Qiu, G. Shao and W. Wang, *Sens. Actuators Phys.*, 2013, **204**, 44–47.
29. X. Mao, J. R. Waldeisen, B. K. Juluri and T. J. Huang, *Lab. Chip*, 2007, **7**, 1303.
30. S. K. Y. Tang, C. A. Stan and G. M. Whitesides, *Lab. Chip*, 2008, **8**, 395.
31. M. Rosenauer and M. J. Vellekoop, *Lab. Chip*, 2009, **9**, 1040–1042.
32. M. Rosenauer and M. J. Vellekoop, in *World Congress on Medical Physics and Biomedical Engineering, September 7-12, 2009, Munich, Germany*, Springer, 2010, pp. 185–188.
33. C. Song, N.-T. Nguyen, A. K. Asundi and C. L.-N. Low, *Opt. Lett.*, 2011, **36**, 1767–1769.
34. K.-S. Chao, M.-S. Lin and R.-J. Yang, *Lab. Chip*, 2013, **13**, 3886.
35. F. Sapuppo, F. Schembri, L. Fortuna, A. Llobera and M. Bucolo, *Microfluid. Nanofluidics*, 2011, **12**, 165–174.
36. S. M. Langelier, E. Livak-Dahl, A. J. Manzo, B. N. Johnson, N. G. Walter and M. A. Burns, *Lab. Chip*, 2011, **11**, 1679.
37. C. E. Dugan, W. P. Cawthorn, O. A. MacDougald and R. T. Kennedy, *Anal. Bioanal. Chem.*, 2014, **406**, 4851–4859.
38. A. M. Clark, K. M. Sousa, C. Jennings, O. A. MacDougald and R. T. Kennedy, *Anal. Chem.*, 2009, **81**, 2350–2356.
39. *Free Glycerol Colorimetric/Fluorometric Assay Kit*; Catalog #K630-100 [Online]; BioVision, Milpitas, CA, Feb 2013. http://www.biovision.com/manuals/K630.pdf (accessed Nov 3, 2014).
40. J. F. Dishinger, K. R. Reid and R. T. Kennedy, *Anal. Chem.*, 2009, **81**, 3119–3127.
41. C. S. Nunemaker, J. F. Dishinger, S. B. Dula, R. Wu, M. J. Merrins, K. R. Reid, A. Sherman, R. T. Kennedy and L. S. Satin, *PLoS ONE*, 2009, **4**, e8428.
42. S. Pagliara, A. Camposeo, A. Polini, R. Cingolani and D. Pisignano, *Lab. Chip*, 2009, **9**, 2851.
43. B. Yao, G. Luo, L. Wang, Y. Gao, G. Lei, K. Ren, L. Chen, Y. Wang, Y. Hu and Y. Qiu, *Lab. Chip*, 2005, **5**, 1041.
44. T. Kamei, B. M. Paegel, J. R. Scherer, A. M. Skelley, R. A. Street and R. A. Mathies, *Anal. Chem.*, 2003, **75**, 5300–5305.
45. L. Jiang and S. Pau, *Appl. Phys. Lett.*, 2007, **90**, 111108.
46. O. Hofmann, X. Wang, A. Cornwell, S. Beecher, A. Raja, D. D. C. Bradley, A. J. deMello and J. C. deMello, *Lab. Chip*, 2006, **6**, 981.

APPENDIX B

Application of Metabolomic Method to Study of Hypoxia in Islets

Introduction

Several types of stress can occur during islet isolation and diabetes pathogenesis in addition to oxidative stress. Because multiple stressors likely act on islets simultaneously, it is important to understand the effects of multiple types of stress on islet viability. Hypoxia occurs in isolated islets in culture due to limited diffusion of oxygen and nutrients within the islet (1). A previous study used ^{1}H NMR to investigate changes in metabolic markers in INS-1 cells during hypoxia-induced cell death. That study shows a decrease in creatine-containing compounds during early-stage hypoxia (2-6 h) and an increase in taurine-containing compounds during late-stage hypoxia (12-24 h) (1). Since our LC-MS method measures many different compounds than the published NMR method, we can potentially obtain complementary data that gives more insight into the particular pathways affected. Measuring responses to hypoxia is also interesting from the standpoint that islets preconditioned with intermittent hypoxia have been found to have improved insulin secretion under hypoxic condition as compared to control islets (2). Further exploration into the effects of hypoxia on islets can provide insights into the effects of islet preconditioning on islet function.

Experimental Procedures

Materials

Kreb's Ringer Buffer (KRB) consisted of 20 mM HEPES, 118 mM NaCl, 5.4 mM KCl, 1.2 mM $MgSO_4 \bullet 7H_2O$, 1.2 mM KH_2PO_4, and 2.4 mM $CaCl_2$, adjusted to pH 7.4.

Roswell Park Memorial Institute (RPMI) culture medium, fetal bovine serum, penicillin-streptomycin, collagenase, and fura-2 dye were purchased from Life Technologies (Carlsbad, CA). Acetonitrile, ammonium acetate, methanol, and chloroform were purchased from Sigma-Aldrich (St. Louis, MO). All other chemicals were purchased from Thermo Fisher Scientific (Waltham, MA).

Glass Microfluidic Chip Fabrication

Glass microfluidic chips were fabricated as previously described (3). Briefly, blank 2.5 cm x 7.6 cm x 1.1 mm glass slides coated with a 530 nm thick layer of AZ1518 positive photoresist over a 120 nm chrome layer (Telic Co., Santa Monica, CA) were exposed to collimated UV light through patterned photomasks for 5 s. The exposed slides were developed in AZ726 MIF Developer (Microchemicals) for 30 s, and the underlying chrome was removed using CEP-200 Chrome Etchant (Microchrome Technologies, Inc., San Jose, CA). The exposed glass was etched in a solution of 14:20:66 (v/v/v) HNO_3/HF/H_2O for variable times depending on desired channel depth. Carbide drill bits (Kyocera Precision Tools, Inc., Hendersonville, NC) were used to drill 360 µm diameter access holes. The remaining photoresist and chrome were then removed using acetone and CEP-200 chrome etchant, respectively, and the etched glass plates were cleaned in piranha solution (3:1 v/v H_2SO_4/H_2O_2) for 20 min followed by heated RCA solution (5:1:1 v/v/v H_2O/NH_4/H_2O_2) for 40 min. Chips were aligned under water, dried, and annealed at 640 ºC for 8 h. Microfluidic reservoirs (Upchurch Scientific, Oak Harbor, WA) were applied over access holes after bonding.

PDMS Hypoxia Chamber Fabrication

Multilayer PDMS microfluidic devices were fabricated using soft photolithography as previously described (4). The completed device consisted of three layers: the top layer contained a cell culture reservoir and gas inlet/outlets; the middle layer consisted of a 100 µm PDMS film for gas exchange with the cell chamber; and the bottom layer contained microfluidic channels for gas flow. An image of the assembled device is shown in Figure B.1.

Cell Culture and Hypoxia Treatment

Pancreatic islets were isolated from 20-30 g male CD-1 mice as previously described (5). Islets were cultured in RPMI-1640 media supplemented with 11 mM glucose, 10% fetal bovine serum, and 1% penicillin/streptomycin at 37 ºC and 5% CO_2 for 2-3 days prior to experimentation. Islets were then transferred to a hypoxia chamber in 500 μL of KRB supplemented with 3 mM glucose (for metabolomic experiments) or RPMI (for $[Ca^{2+}]_i$ experiments). A thin film resistor was taped to the bottom of the device to maintain a temperature of 37 ºC. Nitrogen gas was flowed through the microchannels to induce hypoxia in the islets. Using this method, oxygen concentrations in the media approached 0% (4). Islets were treated with hypoxia for 1 h. For $[Ca^{2+}]_i$ measurements, islets were then removed and either immediately inserted into a perfusion microfluidic chip for $[Ca^{2+}]_i$ measurements or allowed to recover in RPMI for 1 h prior to $[Ca^{2+}]_i$ measurements. For metabolomic experiments, glucose was spiked into the media to a final concentration of 16.7 mM. Islets (50 per sample) were then immediately collected into Eppendorf tubes, samples were centrifuged for 30 s, supernatant was removed, and metabolism was quenched via addition of 100 μL of 90% 9:1 methanol:chloroform/10% water at 75 ºC (stored on dry ice). This process was completed in 3-4 min.

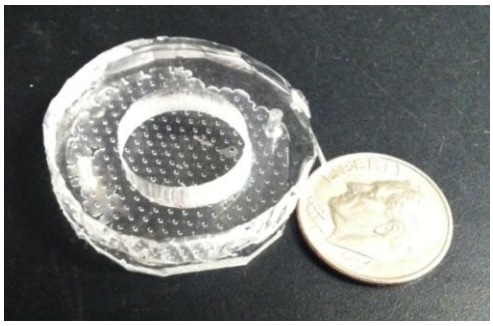

Figure B.1. Image of PDMS device used for inducing hypoxia in islets.

Calcium Flux Measurement

$[Ca^{2+}]_i$ was measured using fura-2 dye as previously described (6). Briefly, islets were loaded with 2 μM fura-2 via 45 min incubation. They were then rinsed with KRB and loaded into a microfluidic chamber, where they were perfused with KRB containing

basal (2.8 mM) and stimulatory (16.7 mM) levels of glucose. The dye was excited alternately with 340 nm (Ca^{2+}-complexed dye) and 380 nm (free dye) light and emission was collected at 510 nm. The ratio of complexed to free dye was calculated and converted to Ca^{2+} concentrations using calibration standards.

Metabolite Measurement

Immediately before analysis, islets were lysed using a probe sonicator. Samples were then centrifuged at 4 ºC for 5 min and the supernatant was transferred to LC vials. Analyses were performed using high performance liquid chromatography-time-of-flight-mass spectrometry (HPLC-TOF-MS). Chromatographic separations of polar compounds were carried out on a Phenomenex Luna NH_2 column (150 x 1 mm, 3 µm particle size). Mobile phase A consisted of acetonitrile and mobile phase B consisted of 5 mM ammonium acetate, adjusted to pH 9.9 with ammonium hydroxide. The gradient program was (time, %B, flow rate): 0 min, 20%, 70 µL min^{-1}; 25 min, 100%, 70 µL min^{-1}. Injection volume was 30 µL, column temperature was 25 ºC, and autosampler temperature was 6 ºC. An Agilent Technologies LC/MSD TOF equipped with a dual electrospray ionization (ESI) source was used for detection in negative ion mode.

Directed analysis was performed for a series of 87 metabolites previously identified in islets or in INS-1 cells. Of these, 62 were consistently measured in our samples. We have chosen to focus here on those that exhibited changes due to hypoxia treatment. Metabolites were identified using retention time compared to standards and accurate mass. Combined peak areas were reported for unresolved isomers, like citrate/isocitrate and glucose-6-phosphate/fructose-6-phosphate. For most metabolites, peak areas were measured from extracted ion chromatograms of $[M-H]^-$ metabolite ions with ±70 ppm detection windows centered on the theoretical mass. $[M-2H]^{2-}$ ions were used for acetyl-CoA (aCoA) and other CoAs to improve sensitivity.

To account for instrumental drift, samples were randomized prior to injection onto the columns. To account for variations in MS sensitivity from run-to-run, metabolite peak area fold changes as compared to the average metabolite peak areas measured from

control samples maintained at basal levels of glucose were calculated and used to compare results from separate runs rather than absolute peak areas.

Results

$[Ca^{2+}]_i$ Response to Hypoxia

Control islets showed an immediate rise in $[Ca^{2+}]_i$ in response to 16.7 mM glucose stimulation (Figure B.2). The $[Ca^{2+}]_i$ response tended to stay level after the initial increase. Immediately following hypoxia, islets exhibited two different trends. Baseline $[Ca^{2+}]_i$ was initially elevated ~2 fold in all islets, although in some of the islets, it decreased back to normal levels over ~4 min. The islets that returned to normal baseline exhibited lower 1st and 2nd phase $[Ca^{2+}]_i$ compared to control, whereas the islets that remained elevated had a continually increasing $[Ca^{2+}]_i$ response (similar to H_2O_2-treated islets). One hour post-hypoxia, there was no observed difference between hypoxia-treated islets and control.

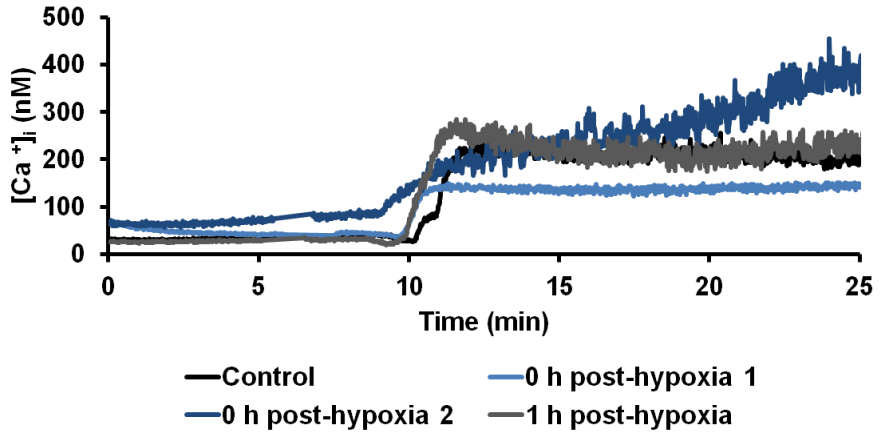

Figure B.2. $[Ca^{2+}]_i$ response to glucose stimulation following 1 h hypoxia. Islets were perfused with basal (2.8 mM) and stimulatory (16.7 mM) glucose in KRB. $[Ca^{2+}]_i$ was measured either immediately following removal of hypoxic conditions (0 h post-hypoxia) or 1 h post-hypoxia. Data represent the average response from multiple islets; n = 2-3 islets per condition.

Metabolic Response to Hypoxia

Several metabolites were found to be altered immediately following exposure to hypoxia, including increased fructose 1,6-bisphosphate (FBP) concentration, decreased

malonyl CoA (mCoA), nicotinamide adenine dinucleotide (NAD^+), CDP-ethanolamine (CDP-EA), and citicoline (CDP-choline) concentrations, and reduced long chain acyl CoA response to glucose stimulation, as shown in Figure B.3a-f.

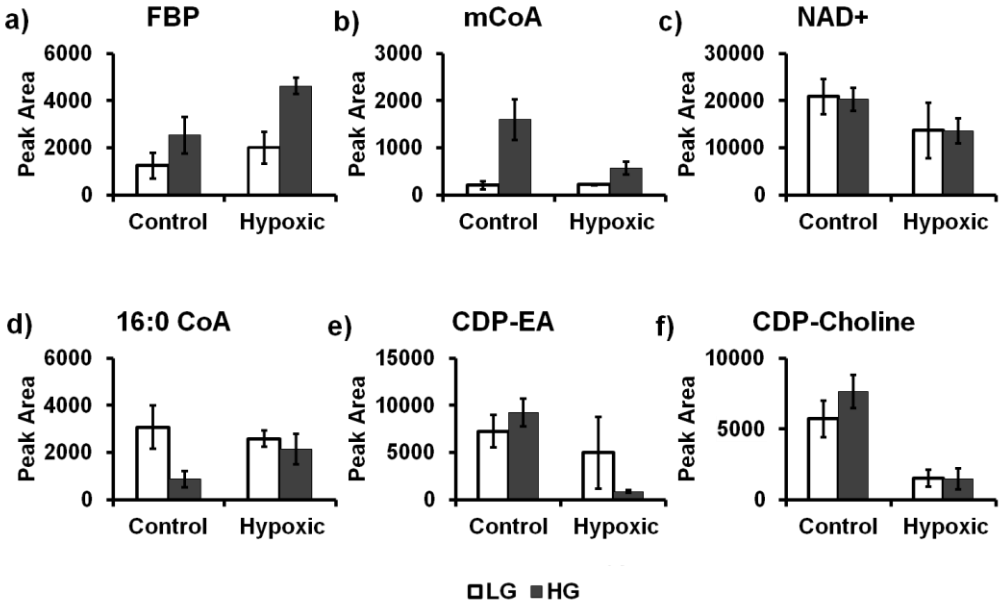

Figure B.3. Absolute metabolite peak areas immediately following 1 h hypoxia for a) FBP b) mCoA c) NAD^+ d) 16:0 CoA e) CDP-EA f) CDP-Choline. Metabolism was quenched 3-4 min following glucose stimulation. LG = low glucose (2.8 mM) , HG = high glucose (16.7 mM), n = 2 sets of 50 islets per conditions. Error bars represent SEM.

Discussion

Islets were made hypoxic for 1 h using hypoxia chambers kindly provided by Elizabeth Ferraz-Samar at the University of Illinois at Chicago. This treatment appeared to be more mild than the 100 μM H_2O_2 treatment discussed in Chapter 4. $[Ca^{2+}]_i$ was slightly elevated (~2 times) above control levels immediately following hypoxia treatment with a blunted response to glucose stimulation. In comparison, H_2O_2-treated samples exhibited 6.6-fold elevation in basal $[Ca^{2+}]_i$ immediately following treatment and only slow increases in response to glucose stimulation. Within 1 h of treatment, the hypoxia-treated samples were similar to control in both basal and glucose-stimulated $[Ca^{2+}]_i$.

Islet morphology appeared to be normal at this time, with no membrane blebbing observed.

Preliminary metabolomic studies showed several metabolites that appeared to be affected immediately following hypoxia treatment, as shown in Figure B.3. These changes in metabolites were similar to those affected by H_2O_2 treatment, with much greater decreases in CDP-choline and CDP-EA amounts with hypoxia treatment.

Conclusion

This work demonstrated the use of hypoxia chambers to effectively induce stress in islets, as determined by interference with $[Ca^{2+}]_i$ and perturbations in metabolite levels immediately following treatment. More replicates are needed to verify the results observed and delve into pathways involved in hypoxia-induced stress. Because this treatment was less severe than our previously used H_2O_2 treatment, it may not have as many long-term effects. Studying the effects of hypoxia on islet metabolism at various time points following treatment will provide insights into the effect of hypoxia on islet metabolic function, with possible implications for islet preservation for transplant and for islet evaluation.

References

1. Tian, L., Kim, H. S., Kim, H., Jin, X., Jung, H. S., Park, K. S., Cho, K. W., Park, S., and Moon, W. K. (2013) Changes in Metabolic Markers in Insulin-Producing β-Cells during Hypoxia-Induced Cell Death As Studied by NMR Metabolomics. *J. Proteome Res.* **12**, 3738–3745
2. Lo, J. F., Wang, Y., Blake, A., Yu, G., Harvat, T. A., Jeon, H., Oberholzer, J., and Eddington, D. T. (2012) Islet Preconditioning via Multimodal Microfluidic Modulation of Intermittent Hypoxia. *Anal. Chem.* **84**, 1987–1993
3. Roper, M. G., Shackman, J. G., Dahlgren, G. M., and Kennedy, R. T. (2003) Microfluidic Chip for Continuous Monitoring of Hormone Secretion from Live Cells Using an Electrophoresis-Based Immunoassay. *Anal. Chem.* **75**, 4711–4717
4. Lo, J. F., Sinkala, E., and Eddington, D. T. (2010) Oxygen gradients for open well cellular cultures via microfluidic substrates. *Lab. Chip*. **10**, 2394
5. Pralong, W. F., Bartley, C., and Wollheim, C. B. (1990) Single islet beta-cell stimulation by nutrients: relationship between pyridine nucleotides, cytosolic Ca2+ and secretion. *EMBO J.* **9**, 53
6. Grynkiewicz, G., Poenie, M., and Tsien, R. Y. (1985) A New Generation of Ca2+ Indicators with Greatly Improved Fluorescence Properties. *J. Biol. Chem.* **260**, 3440–3450
7. Lorenz, M. A., Burant, C. F., and Kennedy, R. T. (2011) Reducing Time and Increasing Sensitivity in Sample Preparation for Adherent Mammalian Cell Metabolomics. *Anal. Chem.* **83**, 3406–3414